Nonlinear Optics in Selectively Fluid-filled Photonic Crystal Fibers

Von der Fakultät Mathematik und Physik der Universität Stuttgart
zur Erlangung der Würde eines Doktors der
Naturwissenschaften (Dr. rer. nat.) genehmigte Abhandlung

vorgelegt von

Marius Vieweg
aus Siegburg

Hauptberichter:	Prof. Dr. Harald Giessen
Mitberichter:	Prof. Dr. Thomas Graf
Tag der mündlichen Prüfung:	29.06.2012

4. Physikalisches Institut der Universität Stuttgart
2012

Contents

Appendix

List of Figures

Abstract

Selective filling of photonic crystal fibers with different media enables a plethora of possibilities in linear and nonlinear optics. Using the two-photon direct laser writing technique we demonstrate full flexibility of individual closing and subsequent filling of photonic crystal fibers with highly nonlinear liquids.

We experimentally demonstrate a solitonic supercontinuum generation over 600 nm bandwidth using a compact femtosecond oscillator as pump source.

A nonlinear optofluidic coupler is built based on the developed technique that shows power dependent switching and all-optical control of the output. This device utilizes the ultrafast Kerr nonlinearity and hence switching times below 1 ps are feasible. Exploiting the thermo-optical properties of the liquids, the coupler can be tuned externally in its switching characteristics by temperature.

To demonstrate the capabilities of our fiber devices to spatially control the light, we present the formation of spatial solitons in a discrete optofluidic nonlinear waveguide array, entering the field of discrete optofluidics.

Our work is fundamentally important to the field of nonlinear effects and underpins new applications in sensing and communication technology. Selective filling of various materials will be the basis of new reconfigurable and versatile optical devices with unprecedented performance. Our devices allow tailoring of the dispersion, spatial coupling and spatial arrangement of a waveguide array, as well as the optical nonlinearity in a two-dimensional discrete system. Thus complete control is given of the optical properties of these here presented devices.

Zusammenfassung

Selektives Befüllen von photonischen Kristallfasern mit verschiedensten Materialien eröffnet neue Möglichkeiten im Feld der linearen und nichtlinearen Optik. Durch das Verfahren des Zwei-Photonen-Schreibens erreichen wir volle Flexibilität beim individuellen Schließen und nachfolgendem Befüllen der photonischen Kristallfaser mit hochnichtlinearen Flüssigkeiten.

Wir zeigen experimentell die Erzeugung eines solitonischen Supercontinuums mit einer Bandbreite von 600 nm, wobei ein kompakter Femtosekunden-Laseroszillator als Pumpquelle genutzt wurde.

Ein nichtlinearer optofluidischer Koppler wurde auf Grundlage derselben Technik hergestellt. Dieser zeigt intensitätsabhängiges Schalten und rein optische Kontrolle des Ausgangs. Der Koppler nutzt dabei die ultraschnelle Kerr-Nichtlinearität, die Schaltzeiten unter 1 ps erlaubt. Darüber hinaus können die thermo-optischen Eigenschaften der Flüssigkeiten genutzt werden, um die Schaltcharakteristik zu beeinflussen.

Die Möglichkeiten der räumlichen Kontrolle des Lichts in unseren Fasern zeigen wir durch die Erzeugung von räumlichen Solitonen in einem diskreten optofluidischen nichtlinearen Wellenleiterarray und betreten damit das Feld der diskreten Optofluidik.

Unsere Arbeit ist fundamental für das Feld der nichtlinearen Optik und bietet neue Möglichkeiten für Anwendungen im Bereich der Sensorik und der Kommunikationstechnik. Selektives Befüllen mit unterschiedlichen Materialien ist die Grundlage für neue und vielseitige optische Faserkomponenten mit noch nie dagewesenen Eigenschaften. Mit diesen Fasern ist es möglich die Dispersion, die räumliche Kopplung und Anordnung innerhalb eines Wellenleiterarrays genau den experimentellen Anforderungen anzupassen. Durch die Flüssigkeiten kann eine hohe optische Nichtlinearität in einem 2D diskreten optischen System erreicht werden. Daraus ergibt sich die komplette Kontrolle über die optischen Eigenschaften durch die hier vorgestellten Faserkomponenten.

Publications

The following papers have been published in the context of this thesis.

Scientific Journals:

[1] M. Vieweg, T. Gissibl, S. Pricking, B. T. Kuhlmey, D. C. Wu, B. J. Eggleton, and H. Giessen, "Ultrafast nonlinear optofluidics in selectively liquid-filled photonic crystal fibers," Optics Express **18,** 25232 (2010).

[2] M. Vieweg, T. Gissibl, H. Giessen, "Photonic-crystal fibers are selectively filled with nonlinear liquids," Laser Focus World **47,** 53 (2011).

[3] M. Vieweg, T. Gissibl, S. Pricking, Y. Kartashov, L. Torner, and H. Giessen, "Tunable ultrafast nonlinear optofluidic coupler," Optics Letters **37,** 1058 (2012).

[4] M. Vieweg, T. Gissibl, Y. Kartashov, L. Torner, and H. Giessen, "Spatial solitons in optofluidic waveguide arrays with focusing ultrafast Kerr nonlinearity," Optics Letters **37,** 2454 (2012).

[5] S. Pricking, M. Vieweg, H. Giessen "Influence of the retarded response on an ultrafast nonlinear optofluidic fiber coupler," Optics Express **19,** 21673 (2011).

[6] T. Gissibl, M. Vieweg, M. M. Vogel, M. Aboud Ahmed, T. Graf, and H. Giessen, "Preparation and characterization of a large mode area liquid-filled photonic crystal fiber: transition from isolated to coupled spatial modes," Applied Physics B **106,** 521 (2012).

[7] S. Kedenburg, M. Vieweg, T. Gissibl, and H. Giessen, "Linear refractive index and absorption of nonlinear optical liquids," Optical Materials Express, submitted (2012).

Conferences:

1. M. Vieweg, T. Gissibl, and H. Giessen, "Application of Selectively Filled Photonic Crystal Fibers," DPG Spring Meeting (Deutsche Physikalische Gesellschaft, 2010), paper Q60.2, Hannover, Germany.
2. M. Vieweg, T. Gissibl, and H. Giessen, "Selectively Filled Photonic Crystal Fibers," in Conference on Lasers and Electro-Optics, OSA Technical Digest (CD) (Optical Society of America, 2010), paper CThB2, San Jose, USA.
3. M. Vieweg, T. Gissibl, and H. Giessen, "Selectively Filled Photonic Crystal Fibers," in Nonlinear Photonics, OSA Technical Digest (CD) (Optical Society of America, 2010), paper NThA2, Karlsruhe, Germany.
4. M. Vieweg, T. Gissibl, S. Pricking, Y. Kartashov, L. Torner, and H. Giessen, "Selectively Fluid-filled Photonic Crystal Fibers," in Conference on "Nonlinear optics and complexity in photonic crystal fibers and nanostructures" 2011, Erice, Italy.
5. M.Vieweg, T. Gissibl, S. Pricking, Y. Kartashov, L. Torner, and H. Giessen, “Tunable ultrafast nonlinear optofluidic coupler,” in XVIII International Conference on Ultrafast Phenomena, 2012, Lausanne, Switzerland.

1. Introduction

In 1960 the field of nonlinear optics was founded by N. Bloembergen and co-workers with the investigation of second harmonic generation in crystals [8,9]. Several years later in 1981 he obtained the Nobel Prize for his work, recognizing this landmark in optical physics which enables numerous new insights into physics but also influences our personal lives.

Developing the field of nonlinear optics further, in 1967 Shimizu [10] demonstrated spectral broadening in liquids due to self-phase modulation [11]. This was the starting point of the generation of supercontinua. It is no surprise that first experiments were performed with liquids, since some of them provide a nonlinearity which is several times larger than that of fused silica. With the invention of pulsed laser systems with much higher peak power, these small nonlinear effects become more accessible.

However, the early experiments with liquids were limited, because the liquid cells could only provide a propagation length of a few centimeters. The situation changed with the advent of optical fibers, providing a nonlinear medium in which the light is confined over hundreds of meters, increasing the interaction length by orders of magnitude. This increase of interaction length was paid for by a decrease of the nonlinearity of the medium. This drawback could be counterbalanced by the development of mode locked lasers [12,13]. Thus a new field of physics arose: Nonlinear fiber optics [14]. Systematic research started revealing numerous new effects, such as self-phase modulation in fibers [15,16], parametric mixing processes [17,18] as well as solitons [19,20] and their dynamics [21–23]. These discoveries accumulated in the generation of supercontinua with ultrabroad spectra spanning across the complete visible spectrum of light [24,25].

Nevertheless, this was not the end of discoveries in the field of nonlinear fiber optics. In 1996 the invention of the photonic crystal fiber [26–30]

was a turning point in the field and reaccelerated the research. A photonic crystal fiber consists of a waveguide core surrounded by a photonic structure [31] which yields light confinement to the core [32,33]. Photonic crystal fibers are a versatile tool to investigate all kinds of optical phenomena, since the optical properties of these fibers are tailorable and offer a high degree of freedom to adjust them to the needs of the experiments. In particular the dispersion can be controlled very accurately in this system, which is crucial to generate a supercontinuum. In the year 2000 Ranka et al. [34] demonstrated the first supercontinuum in a photonic crystal fiber, benefiting from the capability of such devices to tailor their optical properties.

Photonic crystal fibers are ideally suited to be filled with liquids. The early fluid-filled fibers were completely filled with a specifically chosen liquid. Although a simple procedure, this concept was very useful and broadened the applicability of photonic crystal fibers even further. For instance, complete filled fibers were used to influence the band structure of the photonic structure and thus the dispersion properties [35] or were utilized to build narrow all-fiber filters [36].

An obligatory step was to fill these structures selectively. A first technique and application of a selectively fluid-filled fiber was presented by Kerbage et al. [37] in 2002. In this publication the concept was used to introduce tunable birefringence.

Under the impression of the first supercontinuum generation in photonic crystal fibers by Ranka et al., researchers went back to the beginnings of supercontinuum generation, where liquids were used as nonlinear medium. The idea of filling these fibers with highly nonlinear liquids would even further enhance their potential in the field of nonlinear fiber optics. First theoretical studies were published by Zhang et al. [38] in 2006 which showed tremendous potential of the combination of liquids and photonic crystal fibers for the generation of a supercontinuum and temporal solitons.

Several techniques were presented aiming toward the fabrication of selectively fluid-filled fibers [39,40]. Most of them were either not able to indeed produce arbitrary patterns but rather only simple and limited structures, or they could not be applied to different kinds of fibers.

Especially fibers with a photonic structure consisting of holes with a diameter close to the hole-to-hole distance present great difficulty for those techniques. Unfortunately this kind of fiber is very important for the generation of supercontinua.
In this thesis a new technique to selectively fill different kinds of fibers with liquids in an arbitrary pattern is presented by combining the direct laser writing technique [41–43] with the photonic crystal fiber. Subsequently this technique is applied to demonstrate the first supercontinuum generation enhanced by the nonlinearity of the infiltrated liquid, combined with the dispersion control provided by the photonic crystal fiber.
The presented technique here is also enabling the fabrication of structures with more than a single waveguide. Therefore it is used to build two coupled waveguides. These coupled structures benefit from the properties of the liquid, either by its nonlinearity or by the tunability due to the thermo-optical effect. In this coupled optofluidic devices switching becomes possible based on the ultrafast Kerr nonlinearity, which allows it to switch light on a time scale of picoseconds.

Parallel to the invention of the photonic crystal fiber, in 1988 a different field arose: the field of discrete optics [44, 45]. It deals with waveguide structures consisting of more than two coupled waveguides. These structures reveal special behavior by the propagation of light and show effects such as discrete diffraction [46, 47], nonlinear light localization (also known as spatial solitons) [48–51] as well as beam steering and routing [52–55]. These concepts can be transferred to the selectively fluid-filled fiber devices, which can incorporate several waveguides with enhanced nonlinearity by the liquids in a single photonic crystal fiber. This opens the gate to a new field of optics, namely the discrete optofluidics. First investigations have already been carried out, most of them in completely filled photonic crystal fibers [56–58]. Nevertheless, discrete optics also profits from the ability to selectively infiltrate single strands of a photonic crystal fiber in arbitrary spatial patterns. Here the complete two-dimensional photonic structure can be utilized for true two-dimensional discrete optics, which was not possible with previous concepts.

The combination of spatial effects with temporal control would be the next step. This will lead to the generation of optical bullets [59–61] in optofluidic systems. This is still an open problem which awaits realization. This thesis delivers the tools that are necessary for this step. Switching, routing, and nonlinearities are the key to future photonic networks. Nonlinear effects in the liquids utilize the ultrafast Kerr effect, which provides switching times in the order of a few picoseconds. This allows to build all-optical devices that are capable to work in future THz photonic networks. Further, controllable dispersion properties, enhanced interaction length, high nonlinearity, a large degree of freedom in the spatial arrangement, and tailorable coupling strength between the waveguides in two dimensions are the essential ingredients for versatile optical fiber devices with a broad applicability for future photonic circuits.

The possibility to construct such devices and the implementation of first functionalities will be demonstrated in this thesis. Furthermore, this thesis is devoted to discrete optofluidic devices, their fabrication and application, offering a new technology to serve as versatile devices for supercontinuum generation, tunable and ultrafast nonlinear switching, and the generation of spatial solitons.

The thesis is structured as follows:

Chapter 2 covers the theoretical introduction to the temporal propagation behavior in a nonlinear fiber with a single core and develops all important equations for the description of the following experimental sections.

Chapter 3 gives a theoretical introduction to the field of discrete optics. By following the path from simple to complex, the chapter starts with a description of the linear coupler and then extends this theory to the nonlinear waveguide arrays.

Chapter 4 presents all the materials which will be used in the experiments and lists all the parameters necessary for the experimental sections.

Chapter 5 is devoted to the fabrication process of the selectively fluid-

filled photonic crystal fibers. The setup and all major steps of this novel technique are introduced here followed by some examples of structured and selectively filled photonic crystal fibers.

Chapter 6 briefly describes the setup that is used for the characterization of the fluid-filled fibers. All aspects of the setups, which are common for all experiments, are presented here.

Chapter 7 is the first experimental chapter. It describes supercontinuum generation in a photonic crystal fiber selectively fluid-filled with a highly nonlinear liquid. Special focus is given to the dispersion control, which is a result of liquid choice and fiber geometry.

Chapter 8 enters the field of nonlinear discrete optics in fluid-filled fibers. The simplest structure consists of two waveguides forming a nonlinear optofluidic coupler. Ultrafast nonlinear switching will be demonstrated. Exploiting the thermal properties of the liquid, the coupler can be tuned, which is also shown therein.

Chapter 9 extends the situation of the two waveguides for the nonlinear coupler to a nonlinear waveguide array built by several nonlinear optofluidic waveguides within a single photonic crystal fiber. Nonlinear light localization which results in a spatial soliton is shown in this configuration.

2. Theory of light propagation in single core fibers

In this chapter the theory of propagating light in a single waveguide is described. It starts with the linear propagation in standard optical fibers. This description can be transferred to photonic crystal fibers (PCF) and the theory is extended to nonlinear propagation. Finally the important propagation equation, the nonlinear Schrödinger equation (NLSE), is developed and main effects covered by this equation are qualitatively described.

The following presentation is mainly restricted to issues which are necessary for the explanation of the experiments. In general this chapter is based on references [14], where a more detailed derivation can be found.

2.1. Linear propagation in optical fibers

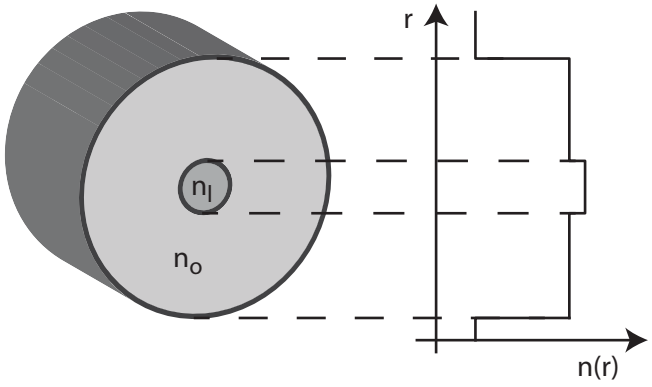

Figure 2.1.: Schematic fiber cross section and radial refractive index distribution.

An optical fiber consists at least of two parts which are illustrated in Fig. 2.1. Firstly the core region where most of the light is confined usually has a diameter of a few micrometers. Secondly, the enclosing cladding region has an overall diameter of 125 μm for standard fibers. Usually the core has a higher refractive index than the cladding as depicted in Fig. 2.1, and the light is guided by total internal reflection. One exception is given by the PCF, where the core and cladding material possess the same refractive index. Just the photonic structure of the cladding made from glass provides confining properties. These fibers are presented in more detail in Section 2.3. The differences in the guiding mechanism and the similarities in the description of light propagation are explained there as well.

As all light phenomena, the description of light propagation in all sorts of fibers starts from Maxwell's equations, here given in the mks-system:

$$\nabla \times \mathbf{E} = -\frac{\partial \mathbf{B}}{\partial t}, \tag{2.1}$$

$$\nabla \times \mathbf{H} = \mathbf{J} + \frac{\partial \mathbf{D}}{\partial t}, \tag{2.2}$$

$$\nabla \cdot \mathbf{D} = \rho_\mathrm{f}, \tag{2.3}$$

$$\nabla \cdot \mathbf{B} = 0, \tag{2.4}$$

where $\mathbf{E}$ and $\mathbf{H}$ are the electric and magnetic field vectors, respectively, and $\mathbf{D}$ and $\mathbf{B}$ are their corresponding electric and magnetic flux density vectors. The current density vector $\mathbf{J}$ and the charge density ρ_f are the sources of the electro-magnetic fields. In optical fibers made from non-metallic materials such as fused silica, no free charges exist and therefore $\mathbf{J} = 0$ and $\rho_\mathrm{f} = 0$ is valid.

The electric and magnetic fields are connected to the properties of the material, the polarizability $\mathbf{P}$, and the magnetization $\mathbf{M}$, by the equations

$$\mathbf{D} = \varepsilon_0 \mathbf{E} + \mathbf{P}, \tag{2.5}$$

$$\mathbf{B} = \mu_0 \mathbf{H} + \mathbf{M}. \tag{2.6}$$

Here, ε_0 denotes the dielectric constant and μ_0 the magnetic perme-

ability. In non-magnetic materials such as fused silica $\mathbf{M}$ is equal to zero.
To obtain the so-called wave equation, the curl operator is applied to Eq. (2.1) and subsequently Eq. (2.2) is inserted. The resulting wave equation reads as follows:

$$\nabla \times \nabla \times \mathbf{E} = -\frac{1}{c^2}\frac{\partial^2 \mathbf{E}}{\partial \mathbf{t}^2} - \mu_0 \frac{\partial^2 \mathbf{P}}{\partial \mathbf{t}^2} \tag{2.7}$$

with c being the vacuum speed of light. For a complete description it is necessary to find a relationship between the polarizability $\mathbf{P}$ and the electric field $\mathbf{E}$. This is only possible in a classical framework in the absence of any material resonance in the considered frequency range. Throughout this thesis this assumption is well justified because all investigated materials are transparent for wavelengths between 400 nm and 2000 nm (for more details on the absorption spectrum of the used liquid see Appendix A). The polarizability can be split up into a part linear to $\mathbf{E}$ and a nonlinear part:

$$\mathbf{P}(\mathbf{r}, t) = \mathbf{P}_{\mathrm{L}}(\mathbf{r}, t) + \mathbf{P}_{\mathrm{NL}}(\mathbf{r}, t). \tag{2.8}$$

Thus both parts of the polarizability are connected to the electrical field $\mathbf{E}$ via

$$\mathbf{P}_{\mathrm{L}}(\mathbf{r}, t) = \varepsilon_0 \int_{-\infty}^{\infty} \chi^{(1)}(t - t') \cdot \mathbf{E}(\mathbf{r}, t')\mathrm{d}t' = \left(\chi^{(1)} * \mathbf{E}\right) \tag{2.9}$$

$$\begin{aligned} \mathbf{P}_{\mathrm{NL}}(\mathbf{r}, t) =& \varepsilon_0 \int_{-\infty}^{\infty} \chi^{(3)}(t - t_1, t - t_2, t - t_3) \ldots \\ & \ldots \vdots \mathbf{E}(\mathbf{r}, t_1)\mathbf{E}(\mathbf{r}, t_2)\mathbf{E}(\mathbf{r}, t_3)\mathrm{d}t_1\mathrm{d}t_2\mathrm{d}t_3. \end{aligned} \tag{2.10}$$

In these equations the susceptibilities $\chi^{(1)}$ and $\chi^{(3)}$ are introduced. They are tensors and for isotropic materials $\chi^{(1)}$ have only one independent element unequal to zero. From the 21 elements of $\chi^{(3)}$, which are unequal to zero, just three are independent from each other. Furthermore, from symmetry considerations it follows that for isotropic materials such as glasses and liquids, the formally expected $\chi^{(2)}$ term vanishes [62]. Higher orders of the polarizability χ are not taken into

account.

For linear propagation in optical fibers $\mathbf{P}_{\mathrm{NL}} = 0$. For this case $\mathbf{P}$ is linear in $\mathbf{E}$ and Eq. (2.7) can be rewritten with Eq. (2.9) to

$$\nabla \times \nabla \times \mathbf{E} = -\frac{1}{c^2}\frac{\partial^2 \mathbf{E}}{\partial \mathbf{t}^2} - \mu_0 \frac{\partial^2}{\partial \mathbf{t}^2}\left(\chi^{(1)} * \mathbf{E}\right). \tag{2.11}$$

Using the operator relation $\nabla \times \nabla \times \tilde{\mathbf{E}} = \nabla(\nabla \cdot \tilde{\mathbf{E}}) - \nabla^2 \tilde{\mathbf{E}}$ together with the Maxwell Eq. (2.3), Eq. (2.11) yields

$$\nabla^2 \tilde{\mathbf{E}}(\mathbf{r}, \omega) = -\varepsilon(\omega)\frac{\omega^2}{c^2}\tilde{\mathbf{E}}(\mathbf{r}, \omega) \tag{2.12}$$

which is known as the Helmholtz equation. The tilde ($\tilde{}$) denotes the Fourier transform of the quantities. The change to Fourier space allows to write the convolution of Eq. (2.9) as normal product. In the absence of absorption, the real part of the dielectric function is connected to the refractive index via

$$\varepsilon(\omega) := 1 + \tilde{\chi}^{(1)}(\omega) = n_0(\omega)^2. \tag{2.13}$$

For the solution of the Helmholtz equation it is advantageous to use the cylindrical coordinates ρ, ϕ, and z. It follows:

$$\frac{\partial^2 \tilde{\mathbf{E}}}{\partial \rho^2} + \frac{1}{\rho}\frac{\partial \tilde{\mathbf{E}}}{\partial \rho} + \frac{1}{\rho^2}\frac{\partial^2 \tilde{\mathbf{E}}}{\partial \phi^2} + \frac{\partial^2 \tilde{\mathbf{E}}}{\partial z^2} + n_0^2(\omega) k_0^2 \tilde{\mathbf{E}} = 0 \tag{2.14}$$

with $k_0 = \omega / c$.

A similar equation can be found for the Fourier transformed magnetic field $\tilde{\mathbf{H}}$. Due to the Maxwell equations only two components are independent and all other components can then be calculated via Eq. (2.3) to Eq. (2.2). It is common to choose E_z and H_z as the independent components. In the following only the solution for the electric field component is presented. H_z can be deduced analogously.

To solve this equation an ansatz is chosen to separate the variables:

$$E_z(\rho, \phi, z, \omega) = A(z, \omega) F(\rho) \exp(im\phi) \exp(i\beta z). \tag{2.15}$$

Here, $A(\omega)$ is a normalization function only dependent on ω, $F(\rho)$ is the radial distribution of the electric field, m is an integer and β is the propagation constant, which has to be determined. By inserting this ansatz into the Helmholtz equation the Bessel differential equation for the radial part $F(\rho)$ is obtained:

$$\frac{\mathrm{d}^2F}{\mathrm{d}\rho^2} + \frac{1}{\rho}\frac{\mathrm{d}F}{\mathrm{d}\rho} + \left(n_0^2k_0^2 - \beta^2 - \frac{m^2}{\rho^2}\right)F = 0 \tag{2.16}$$

whose solutions are given by the Bessel functions. Depending on the sign of $\kappa^2 = n_0^2k_0^2 - \beta^2$ the solutions read as

$$F(\rho) = \begin{cases} A\mathrm{J}_m\left(\rho\sqrt{n_0^2k_0^2 - \beta^2}\right) + B\mathrm{Y}_m\left(\rho\sqrt{n_0^2k_0^2 - \beta^2}\right) & \kappa^2 > 0 \\ C\mathrm{I}_m\left(\rho\sqrt{\beta^2 - n_0^2k_0^2}\right) + D\mathrm{K}_m\left(\rho\sqrt{\beta^2 - n_0^2k_0^2}\right) & \kappa^2 < 0 \end{cases} \tag{2.17}$$

with J_m and Y_m denoting the Bessel function of the first and second kind, whereas I_m and K_m are the corresponding modified Bessel functions. A,B,C, and D are constants.

For an optical fiber with a core radius a, two sets of solutions are obtained separated at the radial distance $\rho = a$: One is for the inner core region with the refractive index n_I and a second one is for the outer cladding region with the refractive index n_O. Due to the requirement that for $\rho = 0$ the field remains finite and drops sufficiently fast for large ρ, the terms including the Bessel functions Y and I vanish and become

$$F(\rho) = \begin{cases} A\mathrm{J}_m(\rho\kappa_1) & \rho \leq a \\ D\mathrm{K}_m(\rho\kappa_2) & \rho > a \end{cases} \tag{2.18}$$

with $\kappa_1^2 = n_\mathrm{I}^2k_0^2 - \beta^2$ and $\kappa_2^2 = \beta - n_\mathrm{O}^2k_0^2$.

From the continuity conditions of the two sets of solutions at the intersection point $\rho = a$ an eigenvalue equation is obtained for the

determination of the propagation constant β:

$$\left(\frac{\mathrm{J}'_m(\kappa_1 a)}{\kappa_1 \mathrm{J}_m(\kappa_1 a)} + \frac{\mathrm{K}'_m(\kappa_2 a)}{\kappa_2 \mathrm{K}_m(\kappa_2 a)}\right)\left(\frac{\mathrm{J}'_m(\kappa_1 a)}{\kappa_1 \mathrm{J}_m(\kappa_1 a)} + \frac{n_\mathrm{I}^2}{n_\mathrm{O}^2}\frac{\mathrm{K}'_m(\kappa_2 a)}{\kappa_2 \mathrm{K}_m(\kappa_2 a)}\right) = \ldots$$
$$\ldots \left(\frac{m\beta k_0 (n_\mathrm{I}^2 - n_\mathrm{O}^2)}{a\kappa_1^2 \kappa_2^2 n_\mathrm{I}}\right)^2 . \quad (2.19)$$

A prime (′) denotes the derivative regarding the argument. Every eigenvalue of $\beta(\omega)$ corresponds to a propagating mode of the fiber. In general Eq. (2.19) has more than one eigenvalue of $\beta(\omega)$ as a solution for a certain m due to the degeneracy of several modes.

Eq. (2.19) and its solution describe the full problem of light propagating in an optical fiber. With the propagation constant β the radial electric field distribution $F(\rho)$ is given (except a constant factor), and therefore the z-component of the electric field E_z is also known. All other field components can easily be deduced with the help of Maxwell's equation.

There are several other computational possibilities to access the modes of an optical fiber. Most of them are solving the Helmholtz Eq. (2.12) directly by a finite-difference [63–65] or a finite-element [65, 66] scheme. These methods are not more accurate and they are very memory intense and slow. For single strand fibers it is easier to solve the eigenvalue Eq. (2.19) on a desktop computer. For more complex structures different numerical techniques have to be applied.

2.2. Group-velocity dispersion

For very short pulses, even if nonlinear effects can be neglected, several wavelengths are propagating in the fiber simultaneously. For different wavelengths Eq. (2.19) has different solutions. The wavelength dependence of the propagation constant $\beta(\omega)$ is called dispersion. Developing $\beta(\omega)$ in a Taylor series yields

$$\beta(\omega) = \beta_0 + \beta_1(\omega - \omega_0) + \frac{1}{2}\beta_2(\omega - \omega_0)^2 + \ldots \quad (2.20)$$

with

$$\beta_k := \left(\frac{\mathrm{d}^k \beta(\omega)}{\mathrm{d}\omega^k} \right)_{\omega=\omega_0} \qquad (k = 0, 1, 2, \ldots). \tag{2.21}$$

Here, β_1 is equal to the inverse of the group velocity v_g. Together with the definition of β_2 it becomes

$$\beta_2(\omega) = \frac{\mathrm{d}\beta_1}{\mathrm{d}\omega} = \frac{\mathrm{d}}{\mathrm{d}\omega} \frac{1}{v_\mathrm{g}(\omega)} = -\frac{1}{v_\mathrm{g}^2} \frac{\mathrm{d}v_\mathrm{g}}{\mathrm{d}\omega}. \tag{2.22}$$

This indicates that the group velocity dispersion (GVD) is the change of the group velocity with frequency. It is important to distinguish two different dispersion regions. For $\beta_2 > 0$ in the so-called normal dispersion regime, the red components travel faster than the blue. The opposite holds for the region with $\beta_2 < 0$ in the anomalous dispersion regime. The wavelength at which β_2 is zero is called zero-dispersion wavelength (ZDW). In the following experiments it will be crucial to tailor the GVD for the different applications. Throughout the description another definition of the GVD is also used:

$$D = -\frac{2\pi c}{\lambda^2} \beta_2 \tag{2.23}$$

with λ denoting the wavelength. Higher orders have to be considered when the pulses are very short (i. e., the pulses are spectrally broad) or the central wavelength is very close to the ZDW.

2.3. Propagation in photonic crystal fibers

The photonic crystal fibers schematically depicted in Fig. 2.2 are a special kind of fibers. As already mentioned in the introduction their core region is surrounded by a photonic structure that is running along the complete length of the fiber [26, 27, 30, 67]. This photonic structure consists of a mostly hexagonal pattern of air channels inside the host medium fused silica with a diameter of usually a few micrometers (up to about 10 μm). Other types of a PCF with different photonic

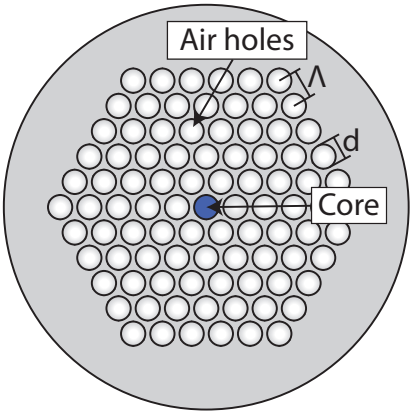

Figure 2.2.: Schematic picture of a photonic crystal fiber with hole diameter d and pitch Λ. The blue circle indicates the lattice defect acting as core for the propagation.

structures [29,32] and whose photonic structure consists of high index glasses, polymers, or other materials are possible as well and have been presented in literature [68–71].

Depending on the photonic structure and the core, two guiding mechanisms are possible in the PCF to maintain light confinement to the core. First, especially important for hollow-core fibers with an air strand as core, photonic band gap guiding can take place [29,72]. For a specific wavelength within a narrow wavelength band the outer photonic structure possesses a photonic band gap. The core acts as a defect within the photonic crystal. All the light is reflected back into the core region and no light can escape, resulting in the confinement of light inside the core.

The second mechanism is called modified internal reflection. The air channels reduce the average refractive index in the holey region. The solid glass core then possesses a higher refractive index compared to the average of the surrounding structure, and total internal reflection can take place. All the fibers used in the experiments of this thesis rely on the modified internal reflection.

Based on this comparison of a PCF with a standard optical fiber [73,74], an effective refractive index of the cladding can be calculated depending on the hole-to-hole distance of next neighboring holes Λ, also referred

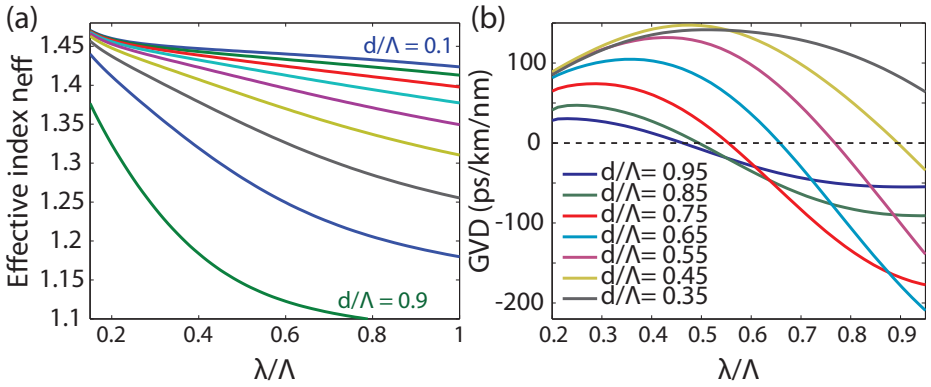

Figure 2.3.: Effective refractive index of the cladding of a PCF and dispersion relation for different wavelengths. - (a) The averaged refractive index of the photonic structure of a PCF calculated with Eq. (2.24) for different d/Λ combinations. (b) Group velocity dispersion of a PCF with varying d/Λ parameter. It can be clearly seen that the zero dispersion wavelength can be tailored by adjusting the structural geometry.

to as pitch, and the hole diameter d. An eigenvalue equation for the effective index n_{eff} was derived in [75–77], which is here given for the fundamental mode:

$$-\frac{\mathrm{I}_2(w)}{\mathrm{I}_1(w)} = \frac{1}{w} + \frac{w}{2}p(u)\left(1+\frac{n_{\mathrm{S}}^2}{n_{\mathrm{H}}^2}\right) - \ldots \\ \ldots w\sqrt{\frac{1}{4}p(u)^2\left(1-\frac{n_{\mathrm{S}}^2}{n_{\mathrm{H}}^2}\right)^2 + \frac{f(u,w)}{n_{\mathrm{H}}^2}}, \quad (2.24)$$

with the dimensionless fiber parameters u and w given by

$$4u^2 = k_0^2 d^2 (n_{\mathrm{S}}^2 - n_{\text{eff}}^2) \quad (2.25)$$

$$4w^2 = k_0^2 d^2 (n_{\text{eff}}^2 - n_{\mathrm{H}}^2). \quad (2.26)$$

Here, n_{S} is the refractive index of the scaffold material and n_{H} the refractive index of the material inside the holes. The functions $p(u)$ and

$f(u,w)$ incorporated in Eq. (2.24) read as follows:

$$p(u) = \frac{1}{u}\frac{(\mathrm{J}_0(u) - \frac{1}{u}\mathrm{J}_1(u))\mathrm{Y}_1(\frac{\Lambda}{d}u) - (\mathrm{Y}_0(u) - \frac{1}{u}\mathrm{Y}_1(u))\mathrm{J}_1(\frac{\Lambda}{d}u)}{\mathrm{J}_1(u)\mathrm{Y}_1(\frac{\Lambda}{d}u) - \mathrm{Y}_1(u)\mathrm{J}_1(\frac{\Lambda}{d}u)} \tag{2.27}$$

$$f(u,w) = \left(\frac{1}{u^2} + \frac{1}{w^2}\right)\left(\frac{n_\mathrm{S}^2}{u^2} + \frac{n_\mathrm{H}^2}{w^2}\right). \tag{2.28}$$

In all equations J and Y stand for the Bessel functions of the first and second kind, respectively, and I for the modified Bessel functions of the first kind. With this formula the average effective refractive index of the cladding region can be calculated as depicted in Fig. 2.3(a). Together with Eq. (2.19) the propagation characteristics of a PCF can be reduced to the problem of a standard optical fiber. In Fig. 2.3(b) different dispersion curves are simulated with the described method. It is clearly visible that the dispersion can be tuned over a wide range and thus can be adjusted to the application. It is mandatory for nonlinear experiments that the ZDW of a fiber is suited to the wavelength of the laser. The reason for this will be explained in the next sections.

2.4. Nonlinear propagation and supercontinuum generation

For the linear propagation it was assumed in the former chapter that $\mathbf{P}_\mathrm{NL} = 0$. From now on nonlinearities will be included and their influence on propagation will be described. Starting from the wave Eq. (2.7), in combination with the already mentioned operator relation, one obtains

$$\mathbf{E} - \frac{1}{c^2}\frac{\partial^2 \mathbf{E}}{\partial t^2} = \mu_0 \frac{\partial^2 \mathbf{P}_\mathrm{L}}{\partial t^2} + \mu_0 \frac{\partial^2 \mathbf{P}_\mathrm{NL}}{\partial t^2} \tag{2.29}$$

where the relationships of polarization and the E-field given in Eq. (2.9) and Eq. (2.10).
To solve Eq. (2.29) some assumptions and simplifications are useful:

- The nonlinear part of the polarization $\mathbf{P}_{\mathrm{NL}}$ has to be small to be treated as perturbation of $\mathbf{P}_{\mathrm{L}}$.
- The slowly varying envelope approximation (SVEA) is applied to separate the fast oscillating part of the field from the slowly varying envelope.
- The electric field should be polarized along a certain axis. Without loss of generality the electric field is in the following chosen to be constantly polarized along the x-axis. This allows a scalar approach for the solution.

With these assumptions the electric field and the linear and nonlinear polarization read as

$$\mathbf{E}(\mathbf{r},t) = \frac{1}{2}\hat{x}\left(E(\mathbf{r},t)\mathrm{e}^{i\omega_0 t} + c.c.\right) \tag{2.30}$$

$$\mathbf{P}_{\mathrm{L}}(\mathbf{r},t) = \frac{1}{2}\hat{x}\left(P_{\mathrm{L}}(\mathbf{r},t)\mathrm{e}^{i\omega_0 t} + c.c.\right) \tag{2.31}$$

$$\mathbf{P}_{\mathrm{NL}}(\mathbf{r},t) = \frac{1}{2}\hat{x}\left(P_{\mathrm{NL}}(\mathbf{r},t)\mathrm{e}^{i\omega_0 t} + c.c.\right) \tag{2.32}$$

with $c.c.$ for the complex conjugated. The linear polarization can then be written in the Fourier domain as:

$$\tilde{P}_{\mathrm{L}} = \varepsilon_0 \tilde{\chi}^{(1)}_{xx}(\omega)\tilde{E}(\omega) \tag{2.33}$$

For the determination of P_{NL} the response of the material is regarded as instantaneous. This assumption is valid only for nonlinearity caused by fast electron oscillations and will be relaxed later. Slower processes causing nonlinearities are neglected. With this assumption the nonlinear polarization is obtained as follows:

$$P_{\mathrm{NL}} = \frac{3}{4}\varepsilon_0 \chi^{(3)}_{xxxx}\left|E(\mathbf{r},t)\right|^2 E(\mathbf{r},t) \tag{2.34}$$

$$= \varepsilon_0 \varepsilon_{\mathrm{NL}} E(\mathbf{r},t) \tag{2.35}$$

defining the nonlinear dielectric function $\varepsilon_{\mathrm{NL}} = \frac{3}{4}\chi^{(3)}_{xxxx}\left|E(\mathbf{r},t)\right|^2$.
All these results allow transforming Eq. (2.29) into the Fourier domain

and the Helmholtz Eq. (2.12) is obtained again. Now for the nonlinear case, the complete dielectric function reads as

$$\varepsilon(\omega) = 1 + \tilde{\chi}_{xx}^{(1)} + \varepsilon_{\mathrm{NL}} = \left(n_0(\omega) + n_2^{\mathrm{E}} \left|E(\mathbf{r}, t)\right|^2\right)^2 \tag{2.36}$$

with the relation for the linear and nonlinear refractive index result from a comparison with Eq. (2.13). Both refractive indices can then be extracted to

$$n_0^2(\omega) = 1 + \tilde{\chi}_{xx}^{(1)} \tag{2.37}$$

$$n_2^{\mathrm{E}} = \frac{3}{8n_0}\chi_{xxxx}^{(3)}, \tag{2.38}$$

assuming $n_2^{\mathrm{E}} \ll n_0$. In terms of the intensity Eq. (2.36) can be rewritten as

$$\tilde{n}(\omega) = n_0 + n_2^I I. \tag{2.39}$$

For the solution of the Helmholtz equation the following ansatz is chosen:

$$\tilde{E}(\mathbf{r}, \omega - \omega_0) = MF(x, y)\tilde{A}(z, \omega - \omega_0)\exp(i\beta_0 z). \tag{2.40}$$

Here, β_0 is the first Taylor coefficient of the propagation constant, $F(x, y)$ is the radial distribution of the field, M is a normalization constant, and $\tilde{A}$ is the slowly varying envelope along the fiber depending on the frequency ω. This ansatz provides the ability to decouple the differential equation resulting in

$$\frac{\partial^2 F}{\partial x^2} + \frac{\partial^2 F}{\partial y^2} + \left(\varepsilon(\omega)k_0^2 - \bar{\beta}^2\right) F = 0 \tag{2.41}$$

for the radial components and

$$2i\beta_0\frac{\partial\tilde{A}}{\partial z}+\left(\bar{\beta}^2-\beta_0^2\right)\tilde{A}=0 \tag{2.42}$$

$$\Rightarrow\quad 2i\beta_0\frac{\partial\tilde{A}}{\partial z}+2\beta_0\left(\bar{\beta}-\beta_0\right)\tilde{A}\approx 0 \tag{2.43}$$

$$\Rightarrow\quad \frac{\partial\tilde{A}}{\partial z}-i\left(\bar{\beta}-\beta_0\right)\tilde{A}=0 \tag{2.44}$$

for the z-component. Because A is a slowly varying function, the second derivative with respect to z is neglected. For the linear case β must be equal to $\bar{\beta}$. For the nonlinear case $\bar{\beta}$ is identified as the propagation constant β plus a small perturbation:

$$\bar{\beta}(\omega)=\beta(\omega)+\Delta\beta. \tag{2.45}$$

First order perturbation theory gives an expression for $\Delta\beta$:

$$\Delta\beta=\frac{\omega n_2^{\mathrm{E}}|M|^2\iint_{-\infty}^{\infty}|F(x,y)|^4\mathrm{d}x\mathrm{d}y}{c\iint_{-\infty}^{\infty}|F(x,y)|^2\mathrm{d}x\mathrm{d}y}|A|^2. \tag{2.46}$$

The radial field distribution $F(x,y)$ remains unchanged in first order perturbation theory, and Eq. (2.44) can be rewritten to

$$\frac{\partial\tilde{A}}{\partial z}=i\left(\sum_{k=1}^{\infty}\frac{\beta_k}{k!}(\omega-\omega_0)^k+\Delta\beta\right)\tilde{A}, \tag{2.47}$$

where the expansion of the propagation constant into a Taylor series (Eq. (2.20)) is used. After back transformation with the inverse Fourier transformation and inserting Eq. (2.46) and Eq. (2.36), the so-called Nonlinear Schrödinger Equation is obtained:

$$\frac{\partial A}{\partial z}-i\sum_{k=1}^{\infty}i^k\frac{\beta_k}{k!}\frac{\partial^k A}{\partial t^k}=i\gamma|A|^2A. \tag{2.48}$$

Here the nonlinear parameter γ is introduced as:

$$\gamma = \frac{n_2^{\mathrm{I}} \omega_0}{c A_{\mathrm{eff}}} \tag{2.49}$$

with n_2^{I} as nonlinear refractive index. The effective mode area A_{eff} is defined as

$$A_{\mathrm{eff}} = \frac{\left(\iint_{-\infty}^{\infty} |F|^2 \mathrm{d}x\mathrm{d}y \right)^2}{\iint_{-\infty}^{\infty} |F|^4 \mathrm{d}x\mathrm{d}y}, \tag{2.50}$$

depending on the refractive index difference between core and cladding. Hence for a PCF the effective mode area which influences the nonlinearity γ is connected to the fiber parameters pitch and hole diameter [78,79]. The value of the mode area can be simply approximated by a variational approach with a Gaussian approximation of the fundamental mode [80,81] that is used in the simulations and calculations of this thesis.

Two different kinds of nonlinear refractive indices n_2^{I} and n_2^{E} are used throughout this derivation. They are connected via:

$$n_2^{\mathrm{E}} = \frac{\varepsilon_0 c n_0}{2} n_2^{\mathrm{I}}. \tag{2.51}$$

The remaining unknown normalization constant M can be determined from these results to be

$$\frac{1}{M^2} = \frac{1}{2} \varepsilon_0 c n_0 \iint_{-\infty}^{\infty} |F(x,y)|^2 \mathrm{d}x\mathrm{d}y, \tag{2.52}$$

such that the quantity $|A|^2$ represents the optical power in units of Watts.

The name of the NLSE originates from the equality with the Schrödinger equation of quantum mechanics with a nonlinearity in the potential (also known as Gross-Pitaevskii equation). Only the time and space coordinates are interchanged.

For the deviation of the NLSE the response of the material was taken to be instantaneous. This omits the effect of Raman scattering. The

effect describes the stimulated inelastic scattering of photons on optical phonons. In a spectrally broader pulse this effect transfers energy from shorter wavelength to longer wavelength, causing the pulse to shift towards the red. The effect can be included into the NLSE by allowing a non-instantaneous response. Eq. (2.34) has to be modified to

$$P_{\mathrm{NL}} = \frac{3}{4}\varepsilon_0 \chi^{(3)}_{xxxx} E(\mathbf{r},t) \int_{-\infty}^{t} R(t-t')|E(\mathbf{r},t)|^2 \mathrm{d}t' \tag{2.53}$$

with $R(t)$ denoting the retarded response of the material normalized such that $\int R(t)\mathrm{d}t = 1$. This function has to be measured separately or can be looked up for few materials in literature [14, 82–84].

While the assumption of an instantaneous response is justified for solids and not too short optical pulses, it cannot be applied to liquids. Here it is very important to take the retarded response into account to obtain simulation results in good agreement to the experimental data. The reason for the retarded response in liquids is the topic of Section 2.6.

Without any further derivation the generalized nonlinear Schrödinger equation (GNLSE) is given, including Raman effects and also the effect of self-steepening [14]:

$$\begin{aligned} &\frac{\partial}{\partial z}A(z,T) - i\sum_{k=2}^{\infty} i^k \frac{\beta_k}{k!}\frac{\partial^k A}{\partial T^k} = \dots \\ &\qquad \dots i\gamma\left(1+\frac{i}{\omega_0}\frac{\partial}{\partial T}\right)\left(A(z,T)\int_{-\infty}^{\infty} R(t')|A(z,T-t')|^2\mathrm{d}t'\right) \end{aligned} \tag{2.54}$$

in a co-propagating time frame with $T = t - z/v_{\mathrm{g}}$. This Eq. (2.54) is being used in this thesis to simulate the propagation in the selectively filled PCF. It is solved numerically with a split-step Fourier method by plugging in all the parameters of the fibers used in the experiments such as the calculated dispersion coefficients β_k, retarded response $R(t)$ of the liquids as well as the nonlinearity γ. The simulations show good agreement with experiments for optical fibers and, as shown in Chapter 7, also for propagation in single liquid strands scaffolded by a PCF.

The simulation tool for solving the GNLSE was provided by S. Pricking

[85].
In the following the nonlinear refractive index regarding the intensity n_2^I is used. For simplicity the nonlinear refractive index is then just called n_2.

2.5. Qualitative explanation of supercontinuum generation

The generalized nonlinear Schrödinger equation (2.54) describes the complete problem of nonlinear propagation of light through a fiber. It is also suitable to explain the mechanism underlying the generation of a supercontinuum. In the following the effects which contribute to the broadening of the spectrum are qualitatively explained.
A fundamental consequence of the dependence of the refractive index on intensity is the influence on the phase ϕ of the light wave by the light itself. Therefore this effect is called self-phase modulation (SPM). The phase of a propagating wave inside a medium is dependent on the refractive index. Together with the nonlinear part of the refractive index given by Eq. (2.39) the complete expression for the phase yields

$$\phi = nk_0z = (n_0 + n_2I)k_0z. \tag{2.55}$$

With the relation between phase and frequency

$$\omega = \omega_0 - \frac{\partial\phi}{\partial t} \tag{2.56}$$

the frequency shift due to SPM is obtained to:

$$\Delta\omega = -\frac{\partial\phi}{\partial t} \propto -k_0n_2\frac{\partial I}{\partial t}z. \tag{2.57}$$

New frequencies are generated by temporal change of the intensity. For $n_2 > 0$ it follows that for a rising intensity red-shifted frequency components are generated, whereas for a declining intensity blue-shifted components are generated.

If only the GVD is considered in Eq. (2.48) a stable solution of Eq. (2.48) can be found. In the anomalous dispersion regime effects of SPM and GVD can be balanced out. In this case a fundamental soliton has formed, propagating temporally and spectrally unchanged along the fiber. Solitons were first discovered by Mollenauer et al. [19]. Different orders of solitons can be generated with the order given by

$$N = \sqrt{\frac{\gamma P_0 \tau_0^2}{|\beta_2|}}, \tag{2.58}$$

with τ_0 denoting the initial pulse length and P_0 the peak power. These higher order solitons undergo a temporal and spectral oscillation during their propagation.

If now higher order terms of the dispersion, Raman processes, or simply noise are included into considerations, the higher N-order solitons can break up into N fundamental solitons [21,86]. First fundamental solitons generated by fission possess higher peak power and, due to Eq. (2.58), a shorter temporal duration τ, and propagate with a higher group velocity [20]. These solitons become red-shifted by the soliton self-frequency shift proportional to τ^{-4} [22,23]. Simultaneously non-solitonic radiation (NSR) is emitted in the blue wavelength regime. Analogously to Cerenkov radiation, this serves as channel to lose energy to fulfill the phase-matching conditions for the red-shifting solitons [87].

Several other effects such as four-wave mixing and cross-phase modulation are able to fill the remaining gaps in the spectrum. Thus with the correct fiber parameters a flat and ultra-broad spectrum can be achieved, spanning from deep blue wavelengths (400 nm) to the infrared (about 2000 nm). The superposition of these wavelength appears as white light.

In a closer view it turns out that different spectral components are generated at different times or travel through the fiber with different group velocities. To measure this temporal behavior the so-called frequency-resolved optical gating (FROG) [88] or cross-correlated frequency-resolved optical gating (XROG) [89] have to be used.

The conditions for an efficient supercontinuum generation in optical fibers, PCFs, or liquid-filled fibers are recapitulated in the following

points:

- Short pulses are desired. For longer pulses the maximum peak power is too small to cause nonlinear effects.
- The central wavelength should be in the anomalous dispersion regime and close to the ZDW. SPM can then easily compensate for the effects caused by the dispersion. Also for small GVD higher order terms play a significant role, mandatory for soliton fission and subsequent supercontiuum generation.
- The length of the fiber must not be shorter than a minimum length, as mixing processes need to fill up the gaps in the spectrum. Also solitons require a minimum length to form and subsequently break up.
- The effective mode area A_{eff} should be as small as possible to achieve a maximum nonlinearity γ. This can be influenced by the refractive index difference between cladding and core size. These parameters also affect the dispersion curve and a trade-off has to be found.
- The core should consist of a material with a high nonlinear refractive index n_2.

All these requirements can be fulfilled by liquid-filled photonic crystal fibers. In comparison to standard optical fibers and PCFs, the liquid-filled PCF fibers are ideal for the very efficient generation of a broad supercontinuum. This is provided by the much higher nonlinear refractive index n_2 in the liquid core, very small mode areas by strong light confinement to the core, and the correct dispersion characteristics due to the fiber structure.

2.6. Nonlinearities in liquids

The retarded response of the nonlinear material is described by the function $R(t)$ in the generalized nonlinear Schrödinger Eq. (2.54). Several physical effects contribute to the response function $R(t)$ and for

the main constituents the function can be written as [90,91]:

$$R(t) = f_e\delta(t) + f_R h_R(t) + f_m h_m(t). \tag{2.59}$$

The first contribution results from the electron motion caused by the incoming light. Since the electrons are tightly bound, the response follows within a few femtoseconds. For the illumination of the material with pulses of the length of several hundred femtoseconds, this effect can be taken as instantaneous and the temporal dependence can be written as δ-function.

The second part is given by Raman effects. The function $h_R(t)$ describes the temporal response. It is a property of the material as well and in [92] a general form of $h_R(t)$ is suggested as

$$h_R(t) = \frac{\tau_1^2 + \tau_2^2}{\tau_1 \tau_2^2} \exp(-t/\tau_2) \sin(t/\tau_1), \tag{2.60}$$

with the parameters τ_1 and τ_2 given by the Raman line shift and line width, respectively.

The third part is caused by the molecular reorientation. This effect can only happen in gases and liquids. The thermally oriented molecules in the medium are aligned by the incoming light and then provide a much higher polarizability [93,94]. For different liquids the delay varies from several femtoseconds to a few picoseconds [90,95–98].

The coefficients f_e, f_R, and f_m give the ratio of these effects. In liquids the reorientational effect dominates and, for example, in CS_2 has a ratio of about 90% [96,97]. This huge influence of the molecular reorientation explains the high nonlinearity of some liquids compared to solids, where only the electronic part contributes. The dynamics of the molecular motion depend on the molecular structure. The resulting nonlinear refractive index can be 10 to 100 times higher than that of fused silica.

The influence of the retarded response of liquids in fluid-filled fibers to the soliton dynamics has been investigated in more detail in [99].

3. Theory of linear and nonlinear fiber arrays

In the former chapter the temporal behavior of light propagating through a waveguide has been described, resulting in the nonlinear Schrödinger equation. Only the effective mode area has a minor spatial influence on the propagation. The light is confined by the surrounding structure and stays constant for a given input power over the propagation length.

This situation changes dramatically when a second waveguide is placed in close proximity. Light can now propagate in both waveguides individually. For an asymmetrical excitation of this structure, the light can escape from one waveguide to the other. Coupling occurs and for longer propagation length a back and forth switching of the light can be observed in this coupler device [80, 100–106]. The explanation and description of this effect including the main parameters will be the first part of this chapter.

The situation can be extended and nonlinear effects can be included into the description. This leads to a device called the nonlinear coupler (NLC) and will be demonstrated theoretically in the following section [107–111] as well.

A more general approach is given by adding more waveguides to the investigated system. This opens the road to a completely new field of optics, namely discrete optics with a plethora new phenomena [44, 45, 50, 112]. Some aspects of discrete optics will be shown in the last part of this chapter to provide the basis for the following experiments.

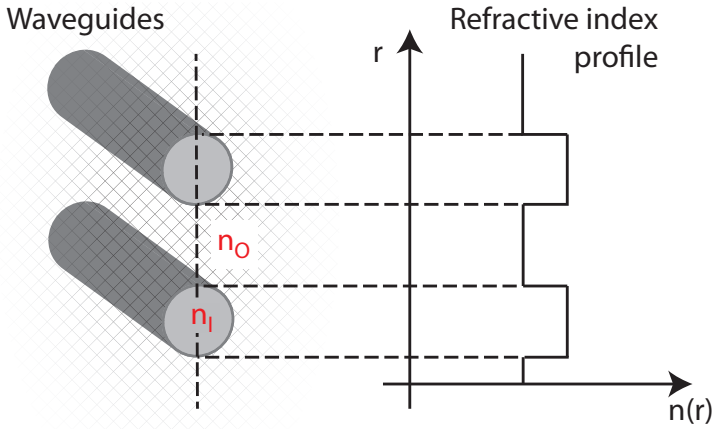

Figure 3.1.: Refractive index profile of an optical coupler. Two waveguides with the core index n_I represent a coupled waveguide system with a conjoint cladding with refractive index n_O.

3.1. Linear coupler

The linear optical coupler consists of two waveguides surrounded by a conjoint cladding as depicted in Fig. 3.1. The distance of the two waveguide cores is about several micrometers, but of course strongly depends on the cladding's structure.

The formal description of an optical coupler can be deduced from coupled mode theory [80, 104]. For two independent waveguides infinitely far away from each other, the amplitudes a_1 and a_2 of the modes propagate along the z direction unperturbed and independently with their propagation constants β_1 and β_2. They obey the equations

$$\begin{aligned} \frac{\mathrm{d}}{\mathrm{d}z} a_1(z) &= i\beta_1 a_1(z) \quad \text{and} \\ \frac{\mathrm{d}}{\mathrm{d}z} a_2(z) &= i\beta_2 a_2(z). \end{aligned} \tag{3.1}$$

When the waveguides are brought together they interact via their evanescent field. The mode amplitude of one waveguide is influenced by the presence of the other waveguide and the modes couple. For weak

coupling, the coupled equations can be written as [102–105, 113, 114]

$$\begin{aligned} \frac{\mathrm{d}}{\mathrm{d}z}a_1(z) &= i\beta_1 a_1(z) + \kappa_{12}a_2(z) \quad \text{and} \\ \frac{\mathrm{d}}{\mathrm{d}z}a_2(z) &= i\beta_2 a_2(z) + \kappa_{21}a_1(z), \end{aligned} \tag{3.2}$$

with κ_{ij} as coupling strength defined by the modal overlap of the two waveguides. This coupling strength can be written [115]

$$\kappa_{12} = \frac{k_0^2}{2\beta}\iint_{-\infty}^{\infty}(n_\mathrm{I}^2 - n_\mathrm{O}^2)F_1^*(x,y)F_2(x,y)\mathrm{d}x\mathrm{d}y, \tag{3.3}$$

with $F_i(x,y)$ $(i = 1,2)$ denoting the radial distribution of the mode, n_O the refractive index of the background material, and n_I the refractive index of the waveguide core medium. Here β stands for the average of the individual propagation constants, i. e., $\beta = \frac{1}{2}(\beta_1 + \beta_2)$. The expression for κ_{21} can be derived by interchanging the waveguide indices.

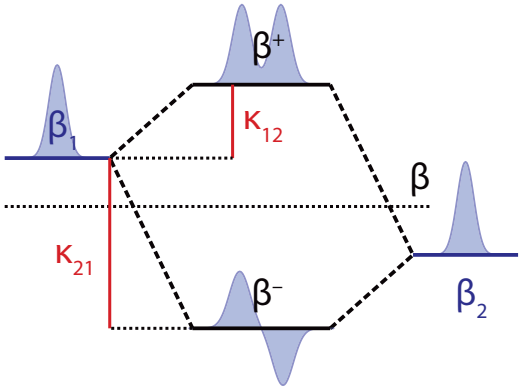

Figure 3.2.: Schematic picture of mode splitting in the supermode formalism. $\beta_{1,2}$ denote the individual modes, β their average, $\beta^{\pm}$ the symmetric and the anti-symmetric collective mode. κ_{ij} is the coupling constant.

Another interpretation of the coupling is given in the frame of supermode theory. The two individual modes together form a symmetric and an anti-symmetric collective supermode. The mode is hybridized

as shown in Fig. 3.2. The coupling strength κ is then interpreted as a perturbation of the individual modes and gives the value for the mode splitting. This offers an easy way to determine the coupling strength, simply by numerically calculating the two supermodes and their corresponding propagation constants β^+ and β^-. This can be carried out using a commercial finite element mode solver (FEM, Comsol). The coupling strength is then simply given by the equation

$$\kappa = \frac{1}{2}\left(\beta^+ - \beta^-\right) \tag{3.4}$$

obtained from Fig. 3.2. Here and in the following description two identical waveguides are assumed leading to $\beta_1 = \beta_2 = \beta$ and $\kappa_{12} = \kappa_{21} = \kappa$.

Eqs. (3.2) can be solved analytically. The power of each waveguide is given by $|a_1(z)|^2 = P_1(z)$ and $|a_2(z)|^2 = P_2(z)$. It is common to illuminate only the input of one waveguide, i. e., $P_1(z = 0) = P_0$ and $P_2(z = 0) = 0$. Thus the solution for the power transfer of the linear coupler consisting of two identical waveguides coupled together with the coupling strength of κ has the form

$$\begin{aligned} P_1(z) &= P_0 \cos^2(\kappa z) \quad \text{and} \\ P_2(z) &= P_0 \sin^2(\kappa z). \end{aligned} \tag{3.5}$$

A visualization of this solution is given in Fig. 3.3. The sinusoidal back and forth coupling of the light between the two cores is obvious. The propagation distance is given in units of the coupling length L_c which defines the length for a complete power transfer from one core to the other. Mathematically speaking, L_c is defined as

$$L_c = \frac{\pi}{2\kappa}. \tag{3.6}$$

The linear coupler can be used as fiber-based beamsplitter. The splitting ratio depends on the parameters κ and the length of the coupler L.

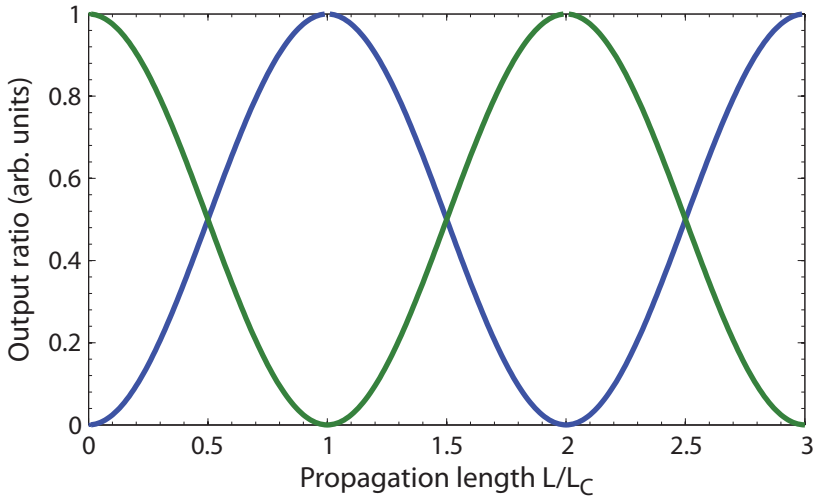

Figure 3.3.: Solution for the linear coupler given in Eq. (3.5) over propagation distance in units of the coupling length L_c.

3.2. Directional nonlinear coupler

For the linear coupler the output ratio is determined only by the length of the coupler and the coupling strength. The coupling strength itself is a function of the difference of the refractive index between the core medium and the surrounding cladding (see Eq. (3.3)). For the description of the linear case, all included refractive indices were taken as constant. No nonlinearity is included. If the power of the incoupled light is increased, nonlinear effects have to be considered. The refractive index then changes accordingly to Eq. (2.39), and an additional phase term has to be added to the coupler Eq. (3.2) to take the nonlinear effects into account [44, 107]:

$$\begin{aligned}\frac{\mathrm{d}}{\mathrm{d}z}a_1(z) &= i\beta a_1(z) + \kappa a_2(z) + \gamma|a_1(z)|^2 a_1(z) + \mu|a_2(z)|^2 a_1(z) \quad \text{and} \\ \frac{\mathrm{d}}{\mathrm{d}z}a_2(z) &= i\beta a_2(z) + \kappa a_1(z) + \gamma|a_2(z)|^2 a_2(z) + \mu|a_1(z)|^2 a_2(z). \end{aligned} \tag{3.7}$$

The nonlinear coefficient γ is defined in Eq. (2.49), and μ describes the induced phase by the nonlinear interaction of one mode with the mode

in the adjacent waveguide [107]. The dominating nonlinear influence is given by the self-induced nonlinear phase. Hence we can set $\mu = 0$ from now on.

The Eqs. (3.7) can be solved analytically, which was carried out by Jensen [107] for the approximation shown here, i. e., for weak coupling considering only the amplitudes. The solution for the case that only one input channel is illuminated, as was already described for the linear solution, reads as

$$P_1(z) = P_1(z=0)\frac{1}{2}\left(1 + \mathrm{cn}(2\kappa z|m)\right) \tag{3.8}$$

with

$$m = \frac{P(0)^2}{P_c^2} \tag{3.9}$$

and cn denoting a Jacobi elliptical function [116]. The critical power P_c is defined in this model by

$$P_c = \frac{4\kappa}{\gamma}. \tag{3.10}$$

In Fig. 3.4 the three different regimes of the nonlinear coupler are shown. For low powers the solution (3.8) evolves into the solution of the linear coupler. Hence sinusoidal coupling characteristics appear (blue line in Fig. 3.4). For increased power the parameter m is also increased. This results in a slightly longer coupling length and the solution starts to deviate from the linear case (see the green and red lines in Fig. 3.4). If the incoupled power $P(0)$ is equal to the critical power P_c, the coupling length becomes infinite and the coupler ends up in a fifty-fifty distribution of the light (see the bright blue line in Fig. 3.4). If more light is brought into the coupler, the two waveguides cannot couple anymore because of the large phase-mismatch due to the induced phase by the nonlinear effects. The light does not couple completely from one waveguide to the other, but remains mainly in the core in which it is launched initially into (i. e., pink and yellow lines in Fig. 3.4).

Another more elucidating presentation is given by the plot of the solu-

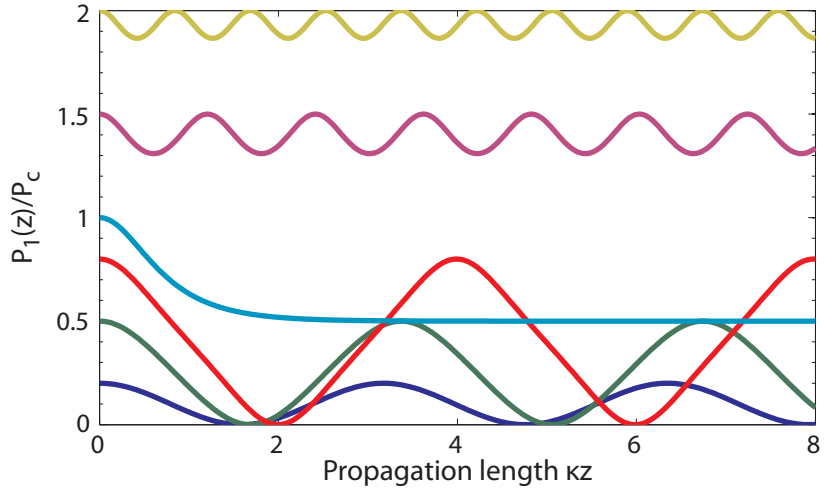

Figure 3.4.: Plot of the solution for one strand given in Eq. (3.8) for different input power in units of the critical power over the propagation length z given in multiples of the coupling strength κ.

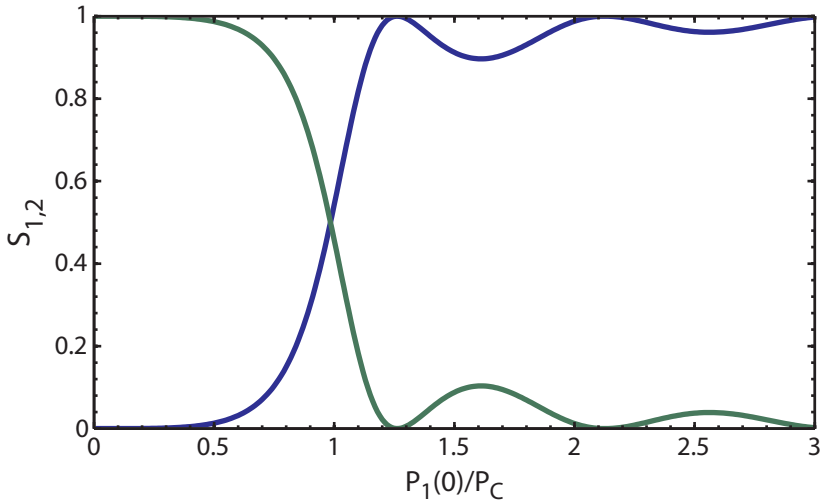

Figure 3.5.: Solution of the nonlinear coupler for a fixed length as function of power for the two strands S_1 and S_2.

tion versus power for a certain coupler length, because this corresponds to the data which are accessible by the measurements. In Fig. 3.5 such a representation is displayed. It becomes obvious that the output ratio for such a nonlinear coupler can be controlled by the incoupled light power. This offers the possibility to use a nonlinear coupler as an all-optical switch in photonic circuits. The three regimes of linear coupling, the critical power, and the nonlinear detuning or nonlinear decoupling are visible in this simulation.

As stated before, the Jensen model deals only with the amplitudes in the waveguides. A more precise solution is given by the solution of the complete two-dimensional spatial Schrödinger equation, that takes into account the whole spatial landscape of the linear and nonlinear refractive index. The equation reads as [3, 59, 61, 117]

$$i\frac{\partial A}{\partial z} = -\frac{\lambda}{4\pi}\left(\frac{\partial^2 A}{\partial x^2} + \frac{\partial^2 A}{\partial y^2}\right) - \frac{2\pi}{\lambda n_O} n_2(x,y)A|A|^2 - \frac{2\pi}{\lambda n_O} G(x,y)A, \tag{3.11}$$

with x, y being the transverse coordinates, z being the propagation coordinate, and A being the amplitude. λ denotes the wavelength as usual, and n_O is the background linear refractive index. The nonlinear refractive index $n_2(x,y)$ is a function of the transverse coordinates, as well as the local linear refractive index perturbation $G(x,y)$, which accounts for the complete photonic structure (in terms of the deviation from the background index n_O). This becomes more important if the cladding is not homogeneous anymore, but possesses a complex structure as in the case for PCFs (see Chapter 8).

Because in Eq. 3.11 the complete photonic structure is incorporated, the equation is also valid for more complex systems like nonlinear waveguide arrays, which are the topic of the next section.

All equations describing the nonlinear coupler as well as the nonlinearity itself incorporated here do not include any time dependence. If the time is included numerous further effects appear. First, the formation of temporal solitons becomes possible. This would have a strong influence on the coupling dynamics [108, 118–120]. Also the Kerr nonlinearity exhibits time dependence. For the complete model this retarded material response has to be included as well. This can influence the required

critical power P_c [5] and thus changes the coupler characteristics [121]. The spatial nonlinear Schrödinger Eq. (3.11) can be easily extended to include all kinds of temporal effects [5, 14] similar to the GNLSE. The numerical calculation then becomes then very difficult if the time dependence as well as the two-dimensional spatial dependence are considered.

3.3. Nonlinear waveguide arrays and effects of discreteness

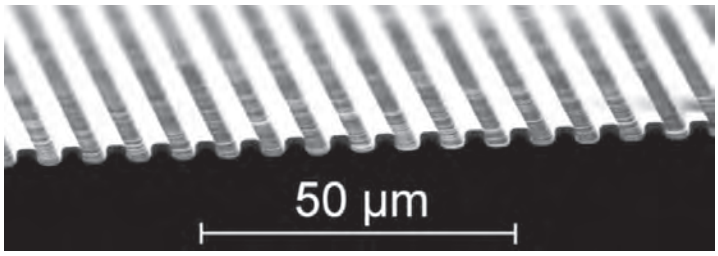

Figure 3.6.: Etched waveguide array on a substrate [47].

For the directional coupler in the previous sections the coupling device consisted of only two waveguides. This is the simplest case for observing coupling between waveguides. The situation can be extended to several waveguides next to each other, forming a waveguide array. In Fig. 3.6 such an array is shown where the waveguides are arranged along a line. The waveguides are coupled to each other. In the following description it is assumed that only next neighbors couple together. Then the formalism presented for the 2-waveguide coupler can be applied to this new configuration by including the newly added waveguides.
For the linear case the coupled equation for $2N+1$ waveguides can be written as

$$\frac{\mathrm{d}}{\mathrm{d}z}a_n(z) = i\beta a_n(z) + \kappa\left(a_{n+1}(z) + a_{n-1}(z)\right), \tag{3.12}$$

where n is the waveguide number running from $-N$ to N. For this

equation it is assumed that all waveguides are identical and the coupling strength κ is constant in the complete waveguide array. In the formalism of the supermode theory new hybridization states occur. For an array with $2N+1$ waveguides, $2N+1$ supermodes also exist (neglecting the degenerate ones). This leads to a complex behavior of the linear modes of such an array, but it can be determined by the solution of the mode amplitude coupling Eq. (3.12) [122–125].

Analogous to the derivation of Eq. (3.7), the nonlinear term can also be added in the case of the waveguide array. The nonlinear influence of one waveguide to the next neighbor is neglected. The equation then reads as [44, 48, 126]

$$\frac{\mathrm{d}}{\mathrm{d}z}a_n(z) = \ldots \\ \ldots i\beta a_n(z) + \kappa\left(a_{n+1}(z) + a_{n-1}(z)\right) + \gamma|a_n(z)|^2 a_n(z) \quad (3.13)$$

with the same notation as before. This equation is also known as Discrete Nonlinear Schrödinger Equation (DNLSE) [48, 127, 128].

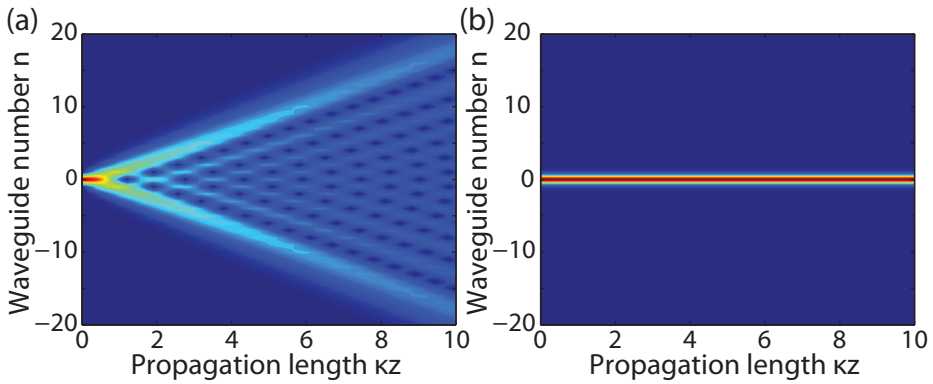

Figure 3.7.: Solution of the discrete nonlinear Schrödinger equation for the waveguide array - (a) Linear case and (b) nonlinear case, where a spatial soliton has formed.

The solution for the linear waveguide array can be calculated in the special case where the initial condition obeys the condition that $a_0(z = 0) = A_0$ and $a_m(z = 0) = 0$ with $m \neq 0$. For the linear case the solution

is [48]

$$a_n(z) = A_0 i^n \exp(i\beta z) \mathrm{J}_n(2\kappa z) \tag{3.14}$$

which is depicted in Fig. 3.7(a). Nonlinearity does not play a role. The two side lobes which appear in the solution are a direct result of the discreteness of the waveguide structure. This effect is therefore called "discrete diffraction" [46, 47]. The two side wings are only visible in the case of an array with no reflection at its side boundaries ($a_N = a_{-N} = 0$ for all z). Otherwise this clear signature of discrete diffraction is washed out.

If the incoupled power is increased, nonlinear effects start to affect the propagation pattern. Above a certain power threshold a stable solution for Eq. (3.13) can be found. The solution has the form [48]

$$a_n(z) = A_0 \exp(i(2\kappa + \beta)z) \mathrm{sech}\left(\frac{X_n}{X_0}\right) \tag{3.15}$$

with X_n being the position of the n^{th} waveguide and X_0 being the characteristic spatial soliton width. An example is plotted in Fig. 3.7(b). The power along the waveguides remains constant over the complete propagation distance. This effect is called a "spatial soliton" and is the result of balancing the discrete diffraction and nonlinear self-focusing effects [45, 50, 129]. For the formation of spatial solitons it is not necessary to use several tens of waveguides. The effect also occurs in a nonlinear array with only three waveguides [44].

The complete description so far only regards linear spatially arranged waveguide arrays. The situation becomes much more complex if the waveguides are arranged in a 2D pattern. The physical realization of these structures require new fabrication methods. Fibers and especially PCFs provide a perfect platform to enter this field and make new physics and novel effects accessible. A lot of theoretical work has already been invested to these new structures [130–134], and recently also experiments have been conducted in this area [60].

3.4. Numerical methods

To calculate the amplitudes in each waveguide of an array, Eq. (3.13) has to be solved. Therefore the equation can be rewritten as

$$\frac{\mathrm{d}}{\mathrm{d}z}a_n(z) = i(\beta + \gamma|a_n(z)|^2)a_n(z) + \kappa\left(a_{n+1}(z) + a_{n-1}(z)\right) \tag{3.16}$$

where the nonlinear phase term including γ is regarded as a perturbation of the individual waveguide. Then the equation can be transformed into a matrix equation as

$$\frac{\mathrm{d}}{\mathrm{d}z}\mathbf{a}(z) = i\mathbf{M}\mathbf{a} \tag{3.17}$$

with $\beta + \gamma|a_n(z)|^2 = \hat{\beta}$, $\mathbf{a}$ as amplitude vector and $\mathbf{M}$ as the $(2N+1) \times (2N+1)$ coupling matrix. The form of the matrix $\mathbf{M}$ depends on the structure of the array. For a linear array the matrix reads as

$$\mathbf{M}_{\text{linear}} = \begin{pmatrix} \hat{\beta}_{-N} & \kappa & 0 & \dots & 0 \\ \kappa & \hat{\beta}_{-N+1} & \kappa & \dots & 0 \\ 0 & \kappa & \hat{\beta}_{-N+2} & \dots & 0 \\ \vdots & & & \ddots & \vdots \\ 0 & \dots & \dots & \kappa & \hat{\beta}_N \end{pmatrix}.$$

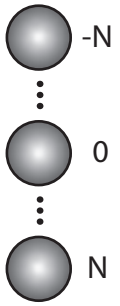

However, not only linear distributions can be treated with this method. For example, for three waveguides arranged in a triangle the matrix looks like

$$\mathbf{M}_{\text{triangular}} = \begin{pmatrix} \hat{\beta}_1 & \kappa & \kappa \\ \kappa & \hat{\beta}_2 & \kappa \\ \kappa & \kappa & \hat{\beta}_3 \end{pmatrix}.$$

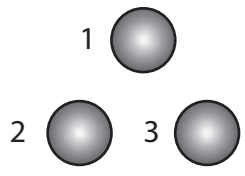

All other kinds of spatial arrangement of waveguides can also be included into this formalism by adapting the coupling matrix **M** to the particular problem.

The numerical solution of matrix Eq. (3.17) at the position z is found iteratively. First, all unperturbed propagation constants β are calculated. In a next step γ_n is determined. In the first step the excited waveguide is used as the initial condition for $z = 0$. With this all $\hat{\beta}_n$ are known and the differential Eq. (3.17) is solved using the standard method by finding the eigenvalue of the matrix **M**. The amplitudes **a** are used in the next spatial step along z for the new calculation of γ_n. For sufficiently small spatial steps along z and small changes of the amplitude from one spatial step to the next, the solution converges to the exact solution of the problem.

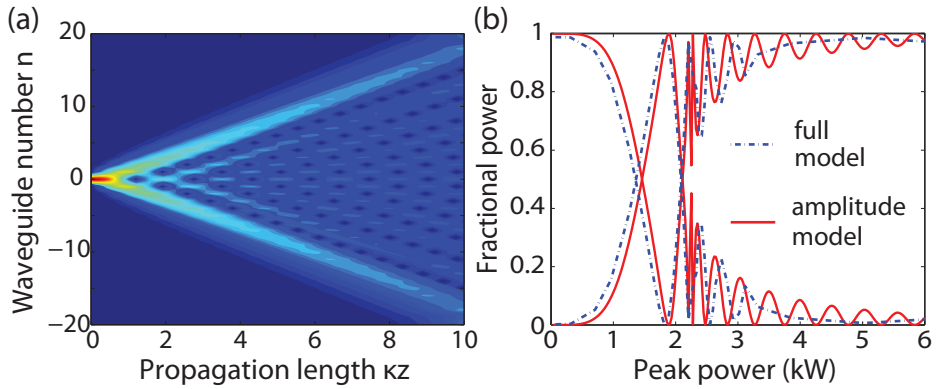

Figure 3.8.: Simulation results (a) for a linear waveguide array with 41 waveguides showing discrete diffraction and (b) comparison for a nonlinear coupler simulation between the full model and amplitude model.

In Fig. 3.8(a) a linear waveguide array consisting of 41 waveguides is simulated. The result is in excellent agreement with the analytical solution of Eq. (3.12) which is shown in Fig. 3.7(a). For 10000 spatial steps the algorithm requires 70 sec in Matlab on a desktop computer.

The simulation of the amplitude model of a nonlinear coupler is shown in Fig. 3.8(b) in comparison to the results of the full model described by Eq. (3.11). This simulation takes 150 sec for 3600 spatial steps and

300 power steps. An excellent agreement with the complete model also for the nonlinear case could be achieved. Only for input powers above the critical power, oscillations appear in the amplitude approximation. However, the approximation reproduces the results of the full model in good accordance.

The scheme presented here for calculating the amplitudes of each waveguide in an array cannot include any time dependence. Further, it does not contain the complete spatial structure. The cladding has to be taken as average material determined by Eq. (2.24) with all disadvantages arising from that fact. Especially no information can be deduced about the appearance of the modes themselves except of course their amplitude.

On the other hand this method is very fast, easy to implement, and very accurate with respect to the mode amplitudes. Main parts of the program can be found in Appendix B.

The solution of the full model given by Eq. (3.11) and the simulation technique presented here are both used throughout the following chapters. Which method is specifically used will be stated in the text as appropriate. The numerical calculation of Eq. (3.11) has been carried out by Y. Kartashov at ICFO Barcelona, using a finite-difference solver.

4. Materials

This chapter is devoted to the different materials used in the experiments. Two different applications will be demonstrated experimentally; the supercontinuum generation in a single strand and nonlinear spatial coupling either in two strands or in a waveguide array. In the previous chapter a variety of prerequisites were theoretically deduced, which have to be fulfilled regarding the individual application of the fiber and the liquids used.

In the following chapter possible candidates of photonic crystal fibers and highly nonlinear liquids will be demonstrated and their properties will be explained and compared with each other.

4.1. Photonic crystal fibers

While photonic crystal fibers exist in a huge number of different forms and structures, it is important to choose the parameters such that the resulting optical properties are well suited to the experimental purpose. The main influence on the optical properties of PCFs are given by the hole diameter d and the hole-to-hole distance Λ as already mentioned in Section 2.3.

To observe nonlinear effects, the intensity inside the core medium has to be as high as possible. To reduce the demands on the pump laser source, it is feasible to engineer the difference of the refractive index between core and cladding such that the light is mainly confined inside the nonlinear medium of the core to achieve a small effective mode area A_{eff}. To increase the intensity inside the core further, the core size can be decreased to reduce the effective mode area. This is only valid down to a value, below which the mode area starts to increase with decreasing core size [135, 136].

Unfortunately the refractive index difference also affects the GVD as

well as the coupling strength in the nonlinear coupling experiments. Here a trade-off has to be found resulting in the use of two kinds of fibers for the different experiments. The choice of the fibers is restricted to commercially available fibers.

For the generation of a supercontinuum, it is crucial to tailor the dispersion. For an efficient generation it is necessary to be in the anomalous dispersion regime and to have a low $|\beta_2|$ value to easily generate solitons and provide conditions where they can break up again. As shown in Fig. 2.3(b) and mentioned above, PCFs allow it to shift the ZDW substantially by tailoring the structural parameter d and Λ.

4.1.1. NL-2.3-790

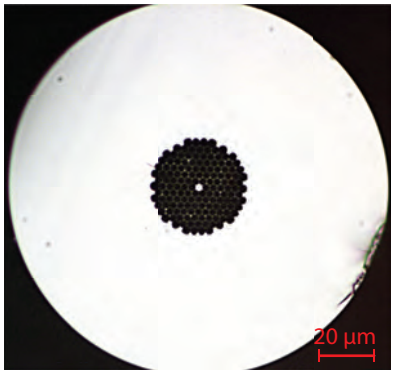

Figure 4.1.: Microscope image of an NL-2.3-790 fiber from NKT Photonics with a hole diameter of $d = 2.5\,\mu$m and a pitch of $\Lambda = 2.6\,\mu$m.

For the experiments the fiber NL-2.3-790 from NKT Photonics has been used with a hole diameter of $d = 2.5\,\mu$m and a pitch of $\Lambda = 2.6\,\mu$m [137]. A microscopic picture of the fiber is shown in Fig. 4.1. The core diameter is not important for the application presented here because the liquid filled strands take over this function and hence the liquid core has the size of a fiber hole. The number of rings is also not influential. The confinement loss decreases exponentially with the number of surrounding rings. Only for fibers with small d/Λ values, the leakage has to be considered [74, 138].

The NL-2.3-790 fiber is usually used as highly nonlinear fiber for the supercontinuum generation, suited for pumping at a wavelength of 800 nm (the common wavelength of Ti:Sapphire oscillators). The d/Λ value is close to one and strong light confinement to the core is achieved. Hence the intensity inside the fiber core is increased (or alternatively the effective mode area is decreased, increasing the nonlinearity γ).

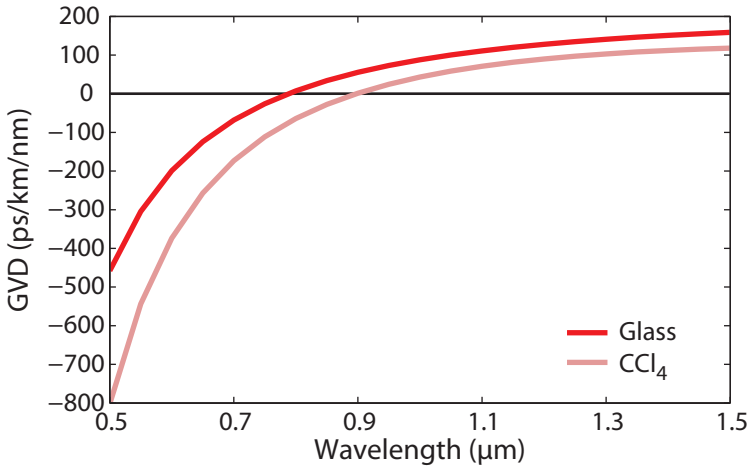

Figure 4.2.: GVD curve of the NL-2.3-790 photonic crystal fiber with a hole diameter of $d = 2.5\,\mu$m and a pitch of $\Lambda = 2.6\,\mu$m under propagation through the glass core. As comparison the GVD curve of a single strand infiltrated with CCl_4 is also plotted here with a liquid core diameter of $2.5\,\mu$m.

In Fig. 4.2 the dispersion curve of the NL-2.3-790 fiber is shown. The ZDW for this configuration is approximately 790 nm. Pumping the fiber with a wavelength above this value provides an anomalous dispersion. Also shown in Fig. 4.2 is the GVD curve for the NL-2.3-790 filled with a single strand of CCl_4 as comparison. For this combination the ZDW shifts to longer wavelengths.

The fiber length for the supercontinuum generation has been extracted from numerical simulations. A length of 10 to 20 cm should be sufficient to generate white light. However, the fiber should be as long as possible. If the fiber is too short, i. e., shorter than the soliton fission length, no supercontinuum will be generated [99].

4.1.2. LMA-8

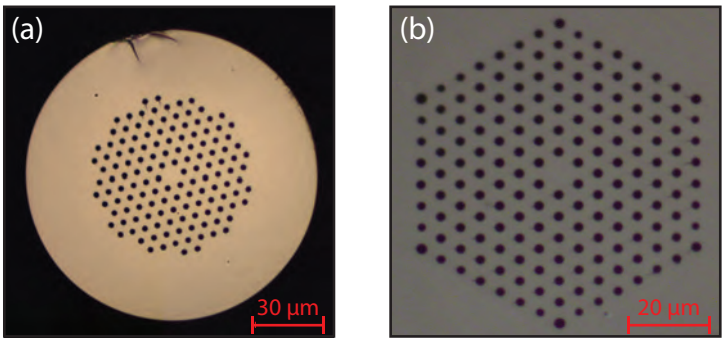

Figure 4.3.: Microscope image of an LMA-8 fiber from NKT Photonics with a hole diameter of $d = 2.7\,\mu$m and a pitch of $\Lambda = 5.6\,\mu$m. The glass core has a diameter of $d_0 = 8\,\mu$m. (a) and (b) show different realizations of the same fiber.

The LMA-8 fiber is not suitable for supercontinuum generation at a wavelength of 1000 nm because the ZDW is shifted due to the geometry of the fiber to longer wavelength deeper in the IR-region. The LMA-8 fiber is usually used as a large-mode area fiber to deliver high powers without exceeding the damage threshold of glass. The guiding mechanism is modified internal reflection. In Fig. 4.3 two microscopic images of the LMA-8 fiber are shown. The holes of the fiber have a diameter of $d = 2.7\,\mu$m and a hole-to-hole distance of $\Lambda = 5.6\,\mu$m [139]. The diameter of the core itself is $d_0 = 8\,\mu$m. The mode properties of the fiber allow it to have only the fundamental mode propagating over a broad spectral region [28].

The LMA-8 exists in two types, differing only in the number of hole rings and formation of the outer ring. Fig. 4.3 shows both types. For the experiments it is not important which type of LMA-8 is being used. The positioning of the liquid waveguides within the fiber structure might differ, but without any physical effect.

In the following experimental sections the LMA-8 fiber is used for the spatial and coupling experiments because it turns out that the coupling strength of two coupled waveguides within the photonic structure can give a coupling length (see Eq. (3.6)) which is in the range of a few

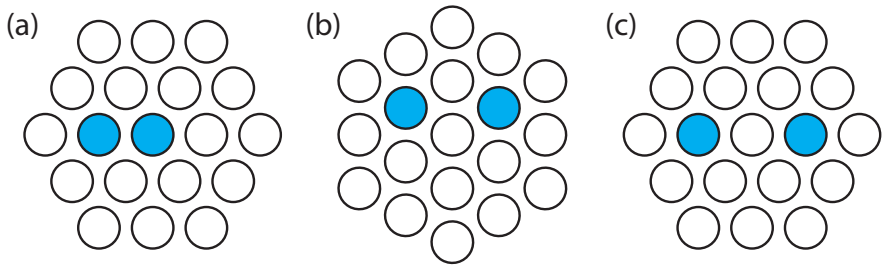

Figure 4.4.: Different coupler geometries within the same fiber with reducing the coupling strength from (a) to (c).

centimeters. This value differs for different infiltrated liquids but, as shown in Fig. 4.4, various possibilities exist to control the coupling strength by a reasonable choice of the waveguide separation. It can be shown by integration of Eq. (3.3) that the coupling strength depends exponentially on the distance between the waveguides. Thus the coupling strength can be tuned by the three different configurations plotted in Fig. 4.4 over a wide region and it will be possible to find a combination with a liquid which is suitable for the setup and experiment.

In contrast to that, if one would try to use the NL-2.3-790 fiber for the coupling experiments, it would be found that two next neighboring filled holes would give a way too strong coupling or simply a collective mode. However, the corresponding structure to Fig. 4.4(b) or (c) in a NL-2.3-790 would give a way too weak coupling due to the very good mode confinement in the NL-2.3-790. This would require very long device lengths because of very long coupling lengths.

4.2. Liquids

The second part besides the fibers of the optofluidic fiber device are liquids. The liquids used in these experiments must possess some specific properties to allow the observation of nonlinear effects. In addition to being highly nonlinear of course, they also have to be transparent in the wavelength region of interest. A last point important especially for the experiments is that these liquids should not be too

toxic since necessary safety measures would increase the experimental effort unreasonable. These requirements will exclude some candidates from the list.

A wide variety of liquids provide a high nonlinear refractive index [140, 141]. Most of them have in common that they are organic solvents and transparent [142]. Because they do not have any oxygen in the molecule, no OH-overtones can absorb the pump light in the NIR.

An incomplete list of highly nonlinear liquids can be found in Tab. 4.1. Also included as comparison is fused silica. The material with the highest nonlinear refractive index, salol ($C_{13}H_{10}O_3$), has several OH-groups and therefore strong absorption will occur in the NIR, which makes this liquid not usable for optical experiments. Also nitrobenzene, chloroform and toluene show absorption directly around the pump wavelength. Only CCl_4 and CS_2 are almost perfectly transparent in the complete wavelength range of interest.

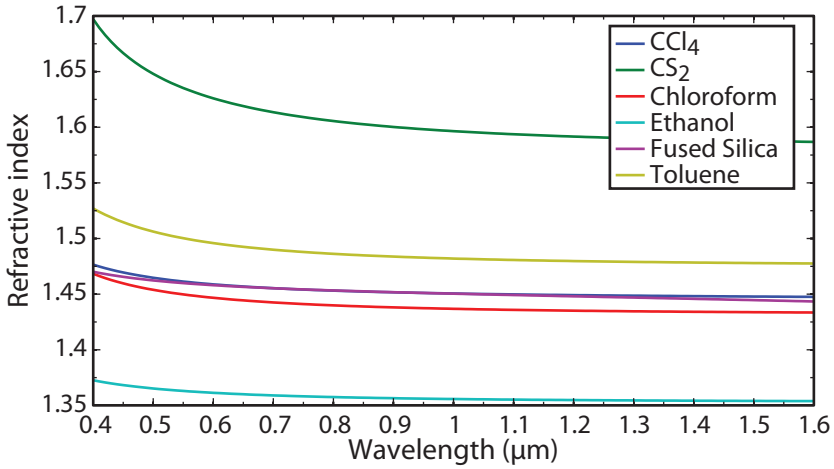

Figure 4.5.: Refractive index of different selected liquids and of fused silica as function of the wavelength (see Tab. 4.1 for references).

Besides the nonlinear properties, the linear refractive index plays an important role for the waveguiding and of course for the dispersion properties, which are essential for the supercontinuum generation. Therefore, in Tab. 4.1 the linear refractive indices are also listed and plotted over the wavelength in Fig. 4.5. If the waveguide should only

support the fundamental mode, it is crucial to have liquids with a linear refractive index close to the value of fused silica. This is also important for the coupling of two waveguides. A huge difference of the refractive index between core and cladding region confines the light very strongly to the core region and hence the coupling strength will be lowered.

It should be mentioned that one major advantage of liquids is their possibility for them to be mixed and thus to control the linear properties [143,144]. Suitable combination of liquids can adjust the linear refractive index to the demands of the individual experiments and even spread their applicability further.

Several liquids were tested in different experiments, but it turned out that especially CCl_4 seems to be a good starting point for the investigations of the nonlinear properties of these novel optofluidic devices. CCl_4 has only a 5 times larger nonlinear refractive index n_2 [91, 98, 141] than fused silica but it is almost transparent up to a wavelength of about 1.4 μm (see Appendix A) and it is not as toxic as CS_2, which would be the best alternative.

As stated in Section 2.6 different molecular properties are described with the delayed response function in Eq. (2.54) resulting in different optical nonlinear behaviors. A detailed overview of the effects caused by the different molecular responses of the liquids is presented in [85, 99] and in the references therein. Also included there is the influence on the soliton dynamics and the switching behavior in two-waveguide coupled systems. The molecular properties of the liquid CCl_4, which is used in the following, can be found in the references [82, 84, 95].

For a measured dispersion curve as well as an absorption spectrum of CCl_4, see Appendix A.

Another intriguing feature of liquids is their thermo-optical properties. The thermo-optical coefficients of the selected liquids are also listed in Tab. 4.1 together with the value for fused silica. The dependence of the refractive index of the liquid on the temperature can be two orders of magnitude stronger than in fused silica. This effect can be used to control *in situ* the difference between the glass cladding and the liquid core and allows adjusting the guiding properties by influencing the guided mode. Hence in the case of coupled systems, the coupling

Name	Chem. formula	Linear refractive index n_0 at 1040 nm	Nonlinear refractive index n_2 in $(10^{-20}\,\mathrm{m}^2/\mathrm{W})$	Thermo-optical effect in $10^{-4}\,\mathrm{K}^{-1}$
Water	H_2O	1.3266 [145]	1.3 [141]	-1.00 [140]
Ethanol	C_2H_6O	1.3556 [146]	7.6 [141]	-4.00 [140]
Toluene	$C_6H_5CH_3$	1.4816 [147]	170 [96,141,148]	-5.51 [140]
Nitrobenzene	$C_6H_5NO_2$	1.5292 [38]	685 [141]	-4.60 [140]
Carbon tetrachloride	CCl_4	1.4503 [149,150]	15 [82,141]	-5.40 [140]
Chloroform	$CHCl_3$	1.4365 [147]	31 [141]	-5.30 [140]
Carbon disulfid	CS_2	1.5956 [147,150]	514 [141,148]	-7.80 [140]
Fused Silica	SiO_2	1.4500 [14,151]	2.6 [14,15]	0.11 [140]
Salol	$C_{13}H_{10}O_3$	1.2500 [152]	1540 [141]	- -

Table 4.1.: Linear and nonlinear optical properties of selected liquids in comparison to fused silica.

strength can be altered by the temperature that will be utilized in the following chapters.

5. Fabrication of selectively filled photonic crystal fibers

The present chapter is dedicated to the fabrication process of the selectively fluid-filled fibers. In the first two sections two methods for the selective closing of single holes are described. Examples of what becomes possible with the technique developed here are given throughout the following chapters. In the last section the filling procedure is briefly described. This chapter is limited to the main results and steps of this process. A detailed explanation of the complete procedure is given in [153,154].

With the invention of the PCF in 1996 [26] a system was developed which was ideally suited to be filled with liquids. Four years later first publications became available which presented the combination of liquids and PCF [35]. Several experiments utilized complete filled fibers for different applications such as anti-resonant high index inclusion photonic crystal fiber (ARROW-fiber) [155], influencing the band gap [156,157], photochemistry [158] and discrete optics [58,117,159]. However, it was an obvious step to try to fill only single holes selectively to broaden further the applicability of photonic crystal fibers and create novel devices. Not so obvious was how to do it. First ideas used large fiber structures that were partially tapered down but still had nozzles to fill the device [36,37]. The most promising approach without tapering the fiber down was demonstrated by [39,40] and used a fusion splicer to collapse and seal holes. The structures possible were limited to only concentric patterns, because the holey structure collapses from the outer to the inner region. Nevertheless, single strand structures could be fabricated. To overcome the limitation of concentric patterns, lateral access to the capillaries was intended to solve this problem either

by the fusion splicer or by micro-machining with a femtosecond laser source [160, 161].
All present techniques are unable to fabricate the desired structures with single selected holes within a complex spatial arrangement. Thus the following procedures are a major step forward and they fulfill all demands to really make this new family of optofluidic devices applicable.

5.1. Structuring of a selectively closed photonic crystal fiber

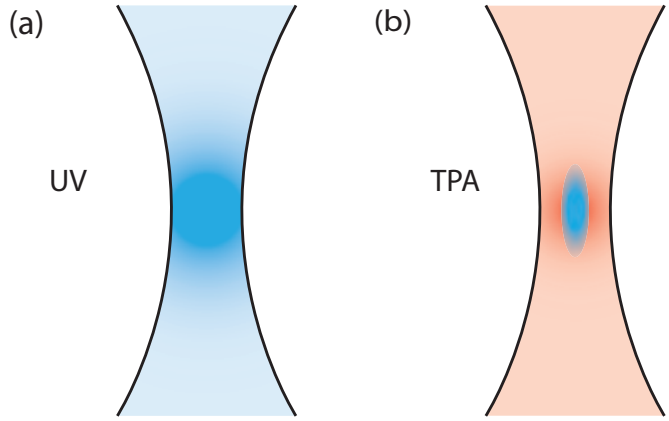

Figure 5.1.: Cross section of a the laser beam. The blue color indicates the region where the polymer is polymerized (a) for the UV technique and (b) for the two-photon absorption technique.

Historically the development of the structuring of a selectively closed photonic crystal fiber starts with the simple approach of covering a cleaved end of a fiber with a UV-curable polymer and illuminating it locally with a spot of a focused UV laser [153]. The situation is illustrated in Fig. 5.1(a). Unfortunately the doses in the polymer next to the desired holes accumulate and hence the polymerization also starts in these holes after exposure of several neighboring holes. The fiber cannot be structured and therefore a selectively filled PCF cannot be

fabricated with this method. Of course there might be special conditions where this method works out well, but it is not a general approach.

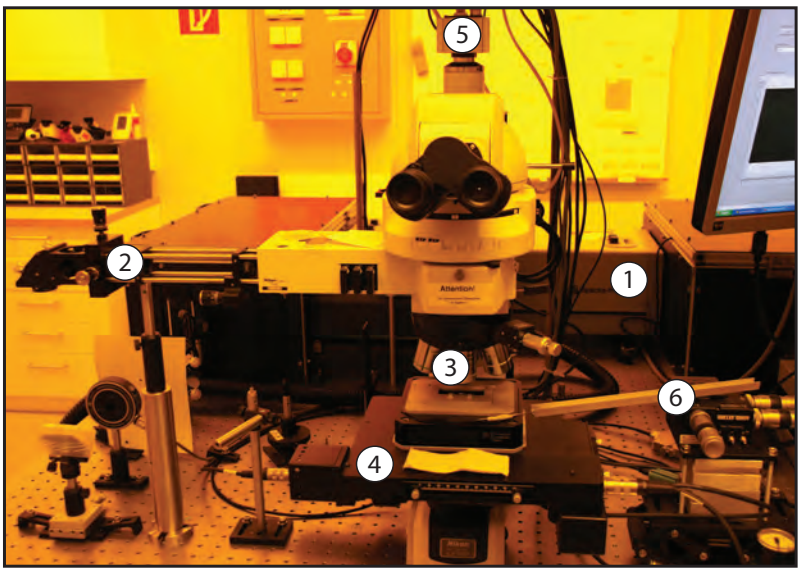

Figure 5.2.: Image of the fabrication setup - 1 Laser source, 2 incoupling of the laser beam into the microscope, 3 focusing optics, 4 motorized stage to move the fiber, 5 camera to observe and control the process, 6 setup for the needle method.

Starting from this, two techniques are presented in the following which are able to fabricate arbitrary patterns of selectively filled strands within a PCF. Both of them use the setup depicted in Fig. 5.2.

5.1.1. The two-photon absorption method

The general technique uses the two-photon absorption in the UV-curable polymer [41, 42, 162]. Thus the curing volume is determined by the laser power and the focus size and it can be controlled spatially in all three dimensions. The region in which the polymer is polymerized is illustrated in Fig. 5.1(b). This technique is called the direct laser writing technique and is used to produce very small optical structures and metamaterials e.g. in [163, 164], but it has never been used before in combination with fibers and photonic crystal fibers [1, 6].

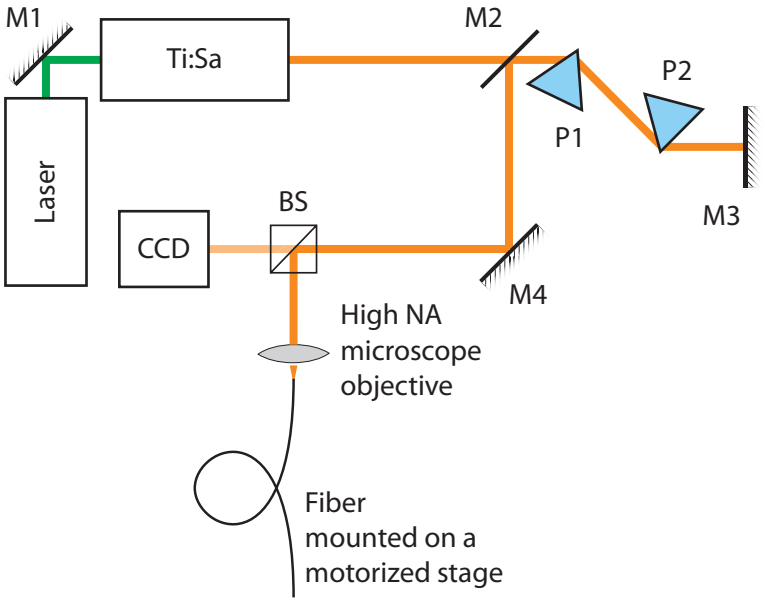

Figure 5.3.: Illustration of the fabrication setup. M - mirrors, P - prisms, BS - beam splitter.

The setup is shown in Fig. 5.2 and schematically drawn in Fig. 5.3. It uses 8 W laser light from a Nd:YVO_4 diode pumped cw Verdi [165] from Coherent Ltd. to pump a Tsunami Ti:Sapphire laser [166] that produces pulses with a duration of 190 fs, a repetition rate of 82 MHz, and 1 W average power. The polymer has its sensitivity peak at around 385 nm, therefore the Ti:Sapphire oscillator is tuned to the doubled wavelength of about 770 nm. The laser light is attenuated to a reasonable value by a filter. For the writing process only a low power of about 35 mW is needed. The remaining light is coupled into the microscope, focused down by the microscope objectives (usually a 100x objective with a numerical aperture (NA) of 0.85) and illuminates the cleaved end of the fiber, which is covered by the polymer. The fiber and the illumination are observed and controlled by a CCD camera. The fiber is moved by a piezostage. The whole writing process is automated and stabilized [154].

The standard photoresist SU-8 is used [167] as polymer. The SU-8 is applied by simply dipping the fiber into a drop of the polymer and

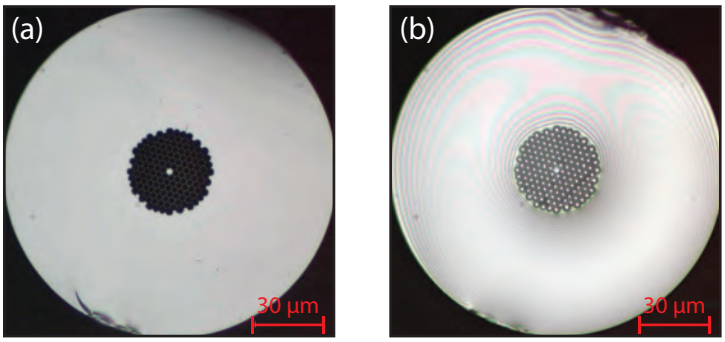

Figure 5.4.: (a) Clean cleaved NL-2.3-790 fiber. (b) Coated fiber with SU-8.

then carefully tipping the fiber against a clean glass plate. In Fig. 5.4 the result of this method is shown. The fiber is homogeneously covered with a thin layer of polymer. The thickness of this layer can be estimated by the fringes (see Fig. 5.4(b)). Typically a thickness of below 5 μm can be achieved.

The coated fiber is then illuminated hole by hole to selectively close them. The beam is moved vertically at each hole for a distance of about 75 μm around the fiber surface with a velocity of 100 μm/s to make sure to seal the holes properly. After illumination, the polymer is treated in the standard way which means that it is hard backed for 2 min and then developed. In the last step all unexposed SU-8 is washed away. Finally the desired structure is written into the fiber and the fiber is ready to be filled in a subsequent step.

Typical results are shown in Fig. 5.5. This method also works for fibers with a hole to pitch ratio close to one. The checkerboard pattern is the most challenging pattern, but also for this structure the two-photon absorption technique presented here works well.

The drawback of this technique is that there are sometimes plugged holes, which could not be opened during the developing process. Further, the technique has high demands on the stability of the setup and on the precision of the hole addressing which could be solved by a stabilization by image recognition [6, 154].

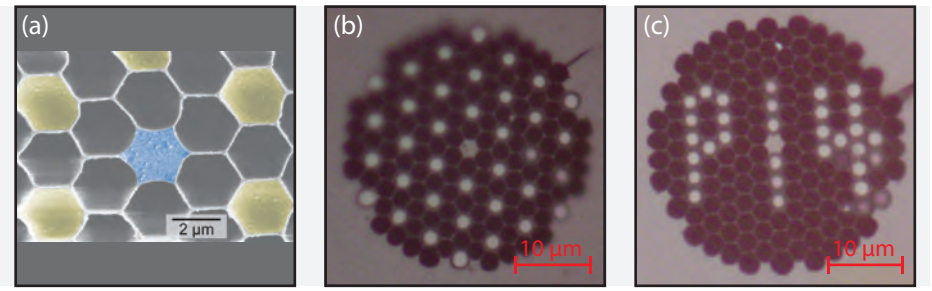

Figure 5.5.: Typical results of the two-photon technique - (a) Scanning electron microscope image of the checkerboard pattern (blue - glass core, yellow - sealed air voids). (b) Checkerboard pattern image. (c) Name of the institute written as structure.

5.1.2. The needle method

In addition to the two-photon absorption technique, another way to selectively close single holes of a PCF was developed. This technique uses a thin glass needle which has a diameter at its end of about 10 μm, usually used in biology for the artificial insemination of egg cells. With this needle little drops of UV curable polymer are positioned manually under the observation by a microscope on top of the fiber end. Thus the holey structure of the fiber is partially covered with the polymer. With a UV lamp the polymer is polymerized and the holes are sealed. These steps are repeated until all holes are closed except the desired structure. This procedure is described in more detail in [157, 168]. It is inherently limited to simple structures consisting of connected hole areas. These hole areas themselves can of course have arbitrary shapes.

In Fig. 5.6(a) an image of the needle together with the end of a fiber is shown as a microscope image. Also visible in this image is a large drop of polymer. As polymer the commercially available UV-glue Dymax OP-4-20632 is usually used, but the process works as well with different polymers. Fig. 5.6(b) shows a typical result achieved with the presented method. A single hole is left open. All other holes are covered and hence sealed by cured polymer.

This technique is a low cost and fast alternative to the two-photon absorption technique presented above. For simple structures, within

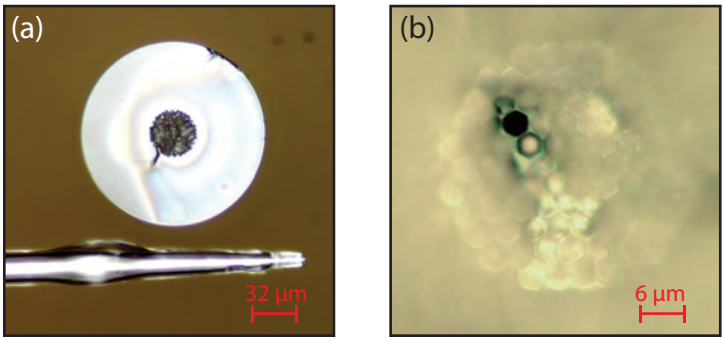

Figure 5.6.: Needle method - (a) Size comparison between the fiber cross-section and the needle. (b) Result of a single strand structure made with the needle method at a NL-2.3-790 photonic crystal fiber.

the limitations of the method, it is the preferable technique to fabricate selectively closed PCF which can be filled with a liquid in a subsequent step.

5.2. Filling of a selectively closed photonic crystal fiber

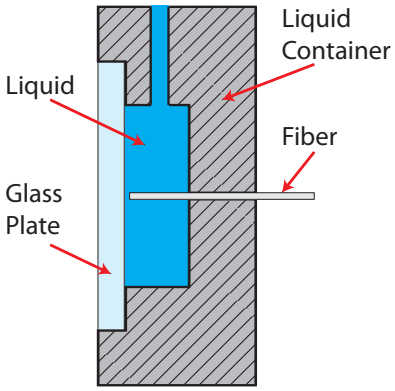

Figure 5.7.: Schematic drawing of the liquid container in a cross section.

After the structuring process described in the former sections, the fiber can be filled with the nonlinear liquids. Therefore the fiber is put into

the liquid with the structured end.

The fiber is filled by the capillary force [169]. For very short pieces of fiber in the range of a few centimeters, it takes less than a minute. For the fiber used for the supercontinuum generation with a length of 26 cm, it took 30 min until the liquid appears on the opposite side. The maximum filling height can be determined by

$$h_\infty = \frac{2\sigma \cos\Theta}{\rho g r} \tag{5.1}$$

with σ being the surface tension of the liquid, Θ being the contact angle, ρ its density, and g being the gravitational acceleration. With typical parameters of the liquids used and a capillary diameter r of 2.7 μm, the maximum filling height determines to be in the order of a few meters.

The liquid is stored in a specially designed liquid container in which the fiber is kept during the experiments. A cross section of the container is illustrated in Fig. 5.7. The fiber is not sealed to the container. The hole where the fiber fits through has a diameter of about 250 μm. Almost no liquid leaks out and the fiber is stable over several days (if the evaporated liquid is refilled, much longer times can be achieved). The light coming out at the end of the fiber leaves the liquid container through the glass window and is collected by a microscope objective (see Chapter 6). This method has the advantage that the incoupling of the light in the experiment can be done through a clean cleaved end of the fiber.

In Fig. 5.8 an example is shown for the filling of a complex structure – a ring structure. In Fig. 5.8(a) the structured side after the two-photon absorption writing process is shown. In Fig. 5.8(b) the opposite end of the fiber is imaged, where the filled strands are clearly visible.

In conclusion the methods presented here are very versatile and all possible patterns can be written to all kinds of fibers. The key to this versatility is the combination of the direct laser writing technique to the PCF. Due to the incorporated two-photon absorption process the cured volume can be controlled in a very accurate way, such that selective writing becomes possible.

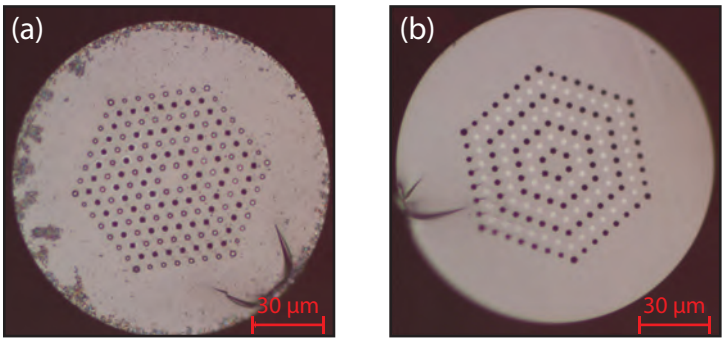

Figure 5.8.: Ring structure - (a) The written side fabricated by the two-photon absorption method. (b) Opposite end with the liquid in the open strands.

Since the development of the direct laser writing technique presented here, several new and different techniques were invented for different purposes. All of them suffer either from a lack of versatility because they can not be applied to all kinds of fibers (such as the femtosecond laser-assisted infiltration of PCF [160,170,171] or a technique based on a UV-laser source [172]), or from their practicability when they use costly ion beam techniques [173].

The filling of the structured fiber then is an easy step and the solution is provided by nature itself with the capillary force.

Of course structures of selectively closed fibers can not only be filled with nonlinear liquids but also with different kinds of materials, such as gases [174,175], semiconductors [172,176], liquid crystals [177,178], as well as other materials.

6. Experimental setup

In this chapter the experimental setup for the characterization of the selectively fluid-filled fibers is presented. It is, at first glance, a standard setup for incoupling light into fibers. The challenge arises here from the precision which is needed to address single holes exclusively with the laser light. Hence special focus lies on techniques to control the incoupling condition and to keep position and temperature constant.

6.1. Propagation and characterization setup

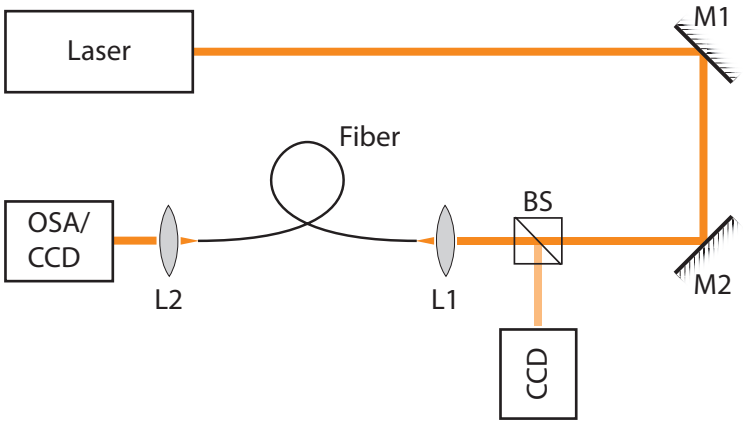

Figure 6.1.: Illustration of the setup - M1 and M2 are mirrors, BS is a beam splitter, L1 and L2 are the incoupling and outcoupling lenses respectively. OSA stands for optical spectrum analyzer.

In Fig. 6.1 a schematic illustration of the setup is shown. As light source a homebuilt pulsed laser oscillator is used. Two different types of lasers are used [179, 180] in the following experiments. The parameters are listed in the table below. The laser used is explicitly named in the description of each experiment.

Parameter	Laser 1	Laser 2
medium	Yb:KGW	Yb:Glass
wavelength	1026 nm	1040 nm
pulse duration	250 fs	180 fs
max peak power	60 kW	110 kW
max avg. power	1.2 W	0.8 W
rep. rate	42 MHz	20 MHz

Table 6.1.: Laser parameter of the two laser oscillators used.

From the laser the light is guided by mirrors to the 3D fiber launch stage manufactured by Elliot Scientific Ltd. [181] that provides position control with micrometer accuracy. Depending on the length of the fiber device a second fiber stage is used for the outcoupling.

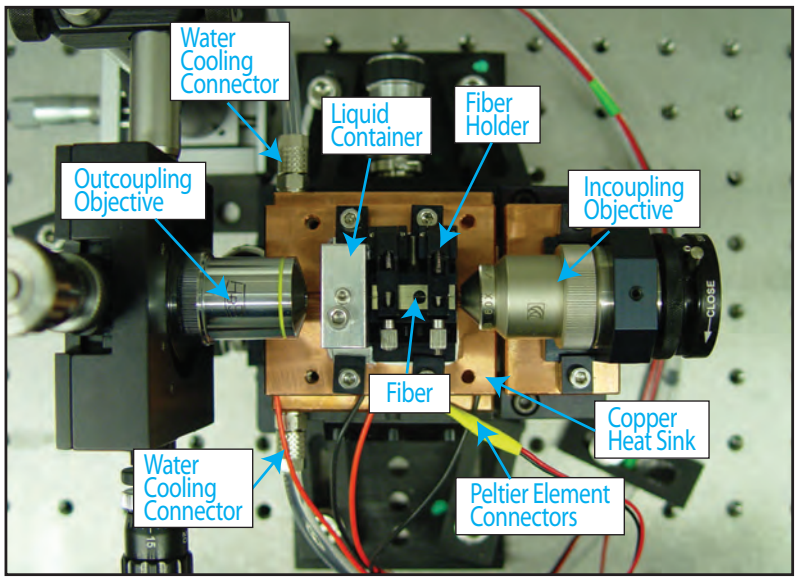

Figure 6.2.: Picture of the experimental setup with the fiber holder and the incoupling and outcoupling optics. The complete fiber with the liquid container is located on a Peltier element for the temperature control.

Fig. 6.2 shows a picture of the experiment. In this image a very short fiber is used which is held by the fiber holder. Therefore no additional outcoupling stage is used and the end of the fiber enclosed in the liquid

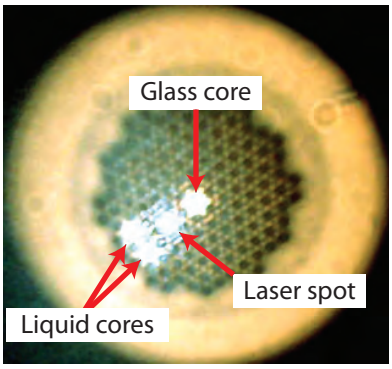

Figure 6.3.: Image recorded by the incoupling observation to maintain the right incoupling conditions, showing the glass core, the two liquid waveguides and the laser spot.

container is also located on the fiber stage. Only the outcoupling lens (L2) is mounted separately. With this lens (L2) the light is recollimated from the fiber end and is imaged by a CCD camera. To avoid overexposure of the camera, suitable neutral density filters are used to attenuate the intensity appropriately. The camera is read out by a computer controlled by the program MatLab.

For all following experiments it is crucial to couple most of the light into a single liquid waveguide. This requires an incoupling lens (L1) which is capable of focusing the laser beam to a spot with a size close to the hole diameter, but not larger than the hole-to-hole distance of the fiber. This is especially important if several waveguides are present. The disadvantage is that it introduces an NA mismatch and some power is lost at the incoupling. If only a single waveguide is used, a trade-off between focus size and NA mismatch has to be found. It turned out that a 20x (NA $= 0.5$) microscope objective for the single strand experiments and a 60x (NA $= 0.65$) microscope objective for the other experiments are the best choices.

Not only the correct spot size has to be assured. Also the correct position is of importance to guarantee the correct incoupling. Therefore a beam splitter (BS) is placed on the incoupling side of the fiber setup. The light reflected back from the fiber surface is reflected by the beam splitter and recorded by a CCD camera. If the fiber is illuminated

by a lamp from the backside, both the laser spot as well as the fiber structure can be observed simultaneously. By careful control of the fiber position, the laser spot is placed at the desired liquid waveguide. Thus the correct incoupling condition is maintained. A picture recorded by the incoupling observation camera is shown in Fig. 6.3. For the measurement the beam splitter is removed to achieve the highest possible power at the fiber.

Due to the optical elements, which are necessary to guide the laser beam, losses add up. The main loss is induced by the obligatory Faraday isolator. At the incoupling position, right before the incoupling objective (L1), only a fraction of the initial peak power is provided. For the Yb:KGW laser an average power of 600 mW is made available. Because of several improvements of the setup, the maximum average power that can be used for incoupling with the Yb:Glass laser is around 540 mW.

The power is controlled by a $\lambda/2$-waveplate in front of the Faraday isolator. In the experiments with the Yb:KGW laser, 4% of the beam is reflected at a glass plate and this 4% of laser light is measured and can be connected to the light which is coupled into the fiber device.

In the case of the Yb:Glass laser being used, the losses due to the glass plate are avoided. The end cap of the Faraday isolator has been removed and the outcoming light from the entrance polarizer of the isolator is measured. The thus measured power can be connected to the power at the incoupling stage.

The transmission through the fiber is limited by the losses stemming from the incoupling, the material, and the confinement inside the fiber. Particularly the incoupling is influenced by the fact that the liquid at the liquid-air transition forms a meniscus. This non-uniform incoupling surface leads to large losses. Thus the resulting transmission is usually at about 15-20%, but might differ for different samples. The material losses are diminished by the choice of the liquid.

6.2. Temperature setup

In the following experiments the temperature will be used to exploit the huge thermo-optical effect of the liquids inside the fiber (see Chapter 4). Thus the setup has to be temperature controllable. For a good thermal conductivity the mounting plate is made from copper and the fiber holder and the liquid container are thermally connected to the copper base plate by heat-transfer paste.

For a stable temperature two different techniques for cooling and heating are combined in the setup (see Fig. 6.2). For the rough temperature setting, the mounting plate of the fiber holder and the liquid container is water-cooled by a chiller. Because the temperature of the chiller varies within few degrees over time, two Peltier elements are added with a thermal power of 38 W each. The temperature is controlled by a resistive thermal sensor (PT100) in combination with a thermo-controller LDT-5910B from ILXLightwave. This controller can quickly adjust the temperature and can thus balance out the oscillations of the chiller. The combination of these two systems provides a tuning range from 3 °C up to 45 °C with a precision of ± 0.03°C.

Even for measurement at a single temperature, this system is used to compensate variations of the temperature caused by an inappropriate climate system in the laboratory.

7. Supercontinuum generation in selectively filled photonic crystal fibers

In Chapter 2 it is shown how the light propagates in a nonlinear fiber and the pulse is temporally and spectrally altered by the interaction of the light with the nonlinear medium. The following section demonstrates how to utilize this knowledge to tailor a nonlinear system consisting of a photonic crystal fiber selectively filled with a highly nonlinear liquid to gain spectral broadening at very low powers.

The generation of a broadened spectrum is well known since the 1960's. As already mentioned in the introduction, first investigations were made in liquids such as CS_2 [10]. With the advent of the optical fiber, it was a relatively short step to use simple quartz fibers as a system to observe spectral broadening [15, 18] because they can compensate the reduced nonlinearity by a much longer interaction length. The development underwent another boost by the invention of the mode-coupling technique, which suddenly provided femtosecond pulses with high peak power. On the fiber side, in 1996 the PCF was invented [26] and in the year 2000 supercontinuum generation in such a fiber was presented [34]. The development went on and in the meantime white-light laser sources became commercially available and have become a big market [24].

Looking at the beginning of this historical way of the supercontinuum, it seems to be straight forward to use highly nonlinear liquids as a medium for the supercontinuum generation and marry them to the fiber technology. A first theoretical investigation of this topic was published in 2006 by R. Zhang et al. [38] showing the tremendous possibilities for these novel nonlinear devices. Besides some single experiments which show broadening of the spectrum by enhanced Raman scattering in

toluene and chloroform [182], the first supercontinuum in a liquid-filled fiber was generated in water as nonlinear medium [183, 184]. This neglects the fact that water has a lower nonlinear refractive index than fused silica, throwing away all advantages of the combination of a highly nonlinear liquid and a PCF.

The first supercontinuum that was enhanced by the nonlinearity of the liquid inside a fiber will be presented in the following section. It has already been published [1] and was followed by a group of publications suggesting alternative liquids [185–187], novel effects due to the optical properties of the liquids [99, 188], and further application of this optofluidic device e. g. [189, 190].

The following chapter starts first with the investigation of the linear propagation and the dispersion properties, which are crucial in the case of nonlinear propagation. Here a choice for the fiber geometry is justified in addition to the selected liquid.

Starting from this point, in the second part of this chapter, the power is increased and nonlinear effects are observed that are gained by the highly nonlinear properties of the liquid. The interplay of fiber geometry and liquids leads to a broad spectrum for very low pump powers.

7.1. Dispersion and linear propagation

First the linear propagation properties of the fluid-filled fiber device are investigated. The simplest pattern is the single strand structure. Just a single hole is left open during the fabrication process and thus one liquid waveguide is created inside the structure of the PCF. The filled fiber is shown in Fig. 7.1(a). The linear mode image of this structure filled with CCl_4 is given in Fig. 7.1(b), which shows the fundamental mode. The mode image is superimposed with the fiber structure. The fiber chosen for this example, NL-2.3-790 (see Section 4.1), has a hole-to-hole distance of $\Lambda = 2.6\,\mu$m and a hole diameter of $d = 2.5\,\mu$m [137].

For these fibers filled with CCl_4 or another liquid, the guiding mechanism is the modified total internal reflection because the refractive

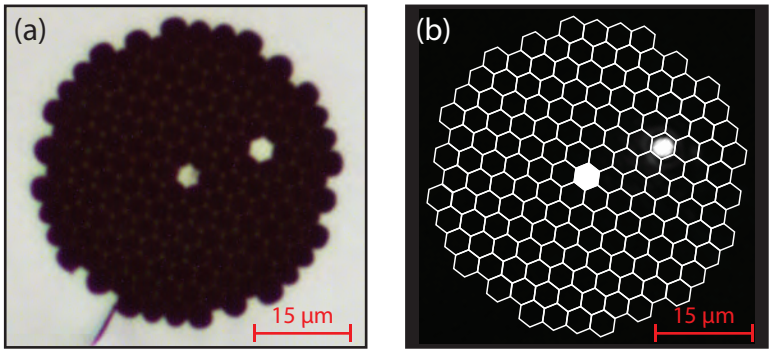

Figure 7.1.: Single strand structure - (a) Microscope image of the single liquid filled strand. (b) Mode image superimposed with the photonic structure of the fiber.

index of CCl_4 ($n = 1.4503$ at a wavelength of $1.03\,\mu$m [149]) and of toluene, nitrobenzene, or CS_2 is slightly higher than that of fused silica ($n = 1.4497$ at a wavelength of $1.03\,\mu$m). The filled liquid strand acts as the core and the surrounding photonic structure as the cladding. Even for chloroform with a refractive index below the refractive index of fused silica ($n = 1.4365$ at a wavelength of $1.03\,\mu$m [147]) guiding is preserved in this structure because of the high air filling fraction in the cladding. This reduces the effective refractive index of the holey region to close to one. Guiding is therefore possible due to modified internal reflection for all kinds of liquids.

For large differences of the refractive index between the core region and the cladding, the normalized frequency V [78, 191, 192] exceeds with $V = 2.57$ the criteria for propagation in the fundamental mode. Although this would lead to multimode propagation, straight incoupling and a straight fiber, support the fundamental mode as shown in the structure presented here.

By changing the filled strand medium or the geometry of the fiber, the dispersion properties of the fiber device can be tailored. If an additional temperature change or mixtures of different liquids are allowed, another degree of freedom is added to engineer the dispersion properties almost continuously. Just by replacing the liquid in a single filled strand of the NL-2.3-790 fiber, one can shift the ZDW from 900 nm for CCl_4 to

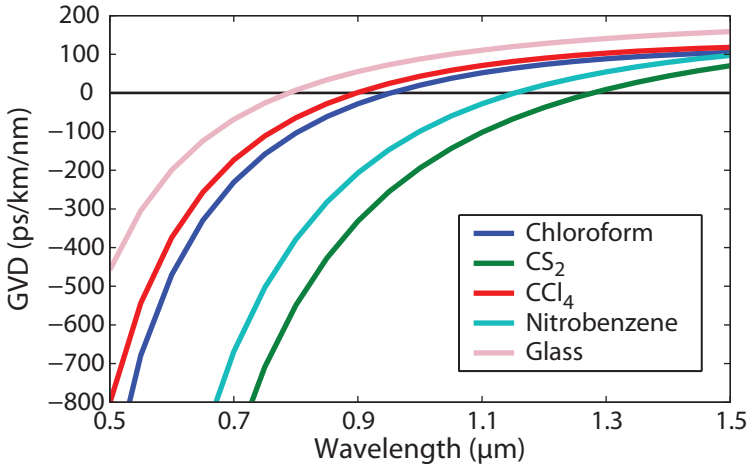

Figure 7.2.: Group velocity dispersion curves for the NL-2.3-790 fiber filled with different liquids. The zero dispersion point shifts from about 900 nm for CCl_4 up to 1300 nm for CS_2. For a comparison the dispersion curve of the original fiber structure is also included in the graph. The curves are obtained by numerically solving Eq.(2.19).

1300 nm for CS_2 over almost 400 nm. The dispersion curves for different liquids inside the NL-2.3-790 fiber are plotted in Fig. 7.2. Apart from the linear propagation regime, this high degree of freedom in dispersion engineering is crucial when entering the nonlinear propagation domain, as is well known [20]. The combination of the NL-2.3-790 fiber with a liquid as waveguide medium should be pumped in the anomalous dispersion region, which is essential for the formation of solitons in the nonlinear propagation regime. With a pump wavelength of 1026 nm, chloroform and CCl_4 are possible candidates for this purpose. Although CCl_4 has a lower nonlinear refractive index than chloroform, CCl_4 is selected as the nonlinear medium because it possesses much less pronounced absorption in the wavelength region of interest.

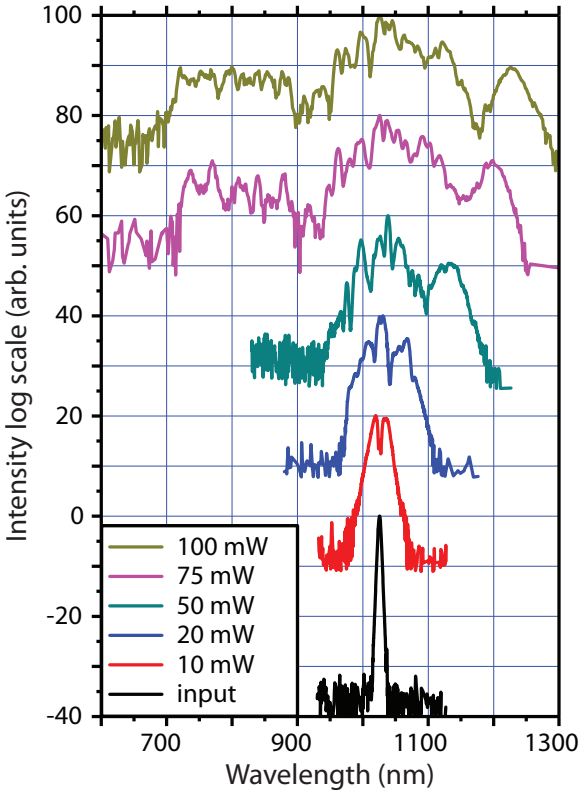

Figure 7.3.: Spectral evolution for different input powers of a 26 cm long fiber with a single strand filled with CCl_4 and with a core diameter of 2.5 μm. The pump power was increased from 10 mW to 100 mW, while spectral broadening could be observed. For the highest incoupled power of 100 mW a 600 nm wide spectrum could be obtained. Because the fiber is pumped in the anomalous dispersion regime, solitons form. The red shifting soliton in the near infrared wavelength regime, as well as the corresponding non-solitonic radiation in the blue wavelength regime [87], could be measured.

7.2. Nonlinear propagation and supercontinuum generation

Filling our devices with highly nonlinear liquids and managing the dispersion, nonlinear effects can be demonstrated including self-phase modulation (SPM), soliton formation and fission [20,21] resulting in an octave-wide spectral broadening.

CCl_4 was selected as the nonlinear medium. CCl_4 is almost transparent in the visible as well as in the infrared wavelength region and has a high nonlinear refractive index of $n_2 = 15 \cdot 10^{-20}\,\mathrm{m}^2/\mathrm{W}$ [141], five times that of fused silica. The underlying process for this high Kerr-nonlinearity is the molecular reorientation [38,93,94] described in Chapter 2.6, which takes place within several hundreds of femtoseconds, in contrast to the almost instantaneous nonlinearity of fused silica [14,92].

The optofluidic device (the single strand structure embedded in an NL-2.3-790 fiber filled with CCl_4) is pumped with the Yb:KGW femtosecond oscillator [179] with a repetition rate of 44 MHz which provides 210 fs long pulses (FWHM) at a center wavelength of 1026 nm.

Numerical simulations (Fig. 7.2) indicate that the ZDW of our device is at 900 nm with a GVD parameter at 1026 nm of $D = 51\,\mathrm{ps/km/nm}$; hence the pump wavelength of 1026 nm lies in the anomalous dispersion regime, which allows soliton formation.

The counterpart of the dispersion is the nonlinearity, which can be calculated for the given optofluidic device for the fundamental mode. According to Eq. (2.49), the nonlinearity is calculated to be $\gamma = 0.38\,\mathrm{m}^{-1}\mathrm{W}^{-1}$, which is up to five times larger than for standard PCF with a core made of fused silica.

Fig. 7.3 shows the spectral evolution in a 26 cm long filled single strand for increasing input powers. For low input powers, spectral broadening occurs due to SPM. For higher input powers soliton formation and the Raman-shift of solitons become clearly observable [20,21]. For an input power of 100 mW a spectral broadening of 600 nm is obtained, covering the spectral region from 700 nm to 1300 nm. The spectrum reveals the red-shifting soliton as well as the NSR in the blue [20,87].

With an overall throughput of 10-15 % including losses due to incou-

pling, material, and confinement, the corresponding peak power inside the fiber with less than 2 kW is extremely low compared to previous results in optofluidic supercontinuum generation experiments, where peak powers of MW were required [183, 184, 189]. Even for supercontiuum generation in a standard PCF with a fused silica core, this tremendous spectral broadening could not be reached for this low input power level.

Managing the dispersion, the nonlinearity of our device could be increased even further by using a liquid like chloroform or CS_2, with a higher nonlinear refractive index of $n_2 = 31 \cdot 10^{-20}\,\mathrm{m^2/W}$ [141] for chloroform and $n_2 = 514 \cdot 10^{-20}\,\mathrm{m^2/W}$ [141] for CS_2. The disadvantage of chloroform is, as already stated, that it shows higher absorption. This can negatively influence the spectral broadening and lowers the damage threshold of the device. Although CS_2 does not show any significant absorption in the NIR region, the high linear refractive index requires very small structures to push the ZDW below the pump wavelength (compare Fig. 7.2 for the ZDW of an NL-2.3-790 fiber filled with CS_2 at about 1300 nm). Thus the choice for the combination of CCl_4 with the NL-2.3-790 fiber is well justified.

7.3. Simulation results

By solving Eq. (2.54) numerically, theoretical predictions can be made about the spectral evolution in the system presented in the former section; i. e., an NL-2.3-790 fiber with a single strand filled with CCl_4. It is important to include the temporal dynamics of the liquid by taking into account the delayed response of the medium. In Fig. 7.4 an experiment with a 19 cm long fiber is compared to the simulation. In this experiment 330 mW average power is coupled into the fiber. A reduced incoupling efficiency makes it necessary to use higher pump powers compared to the results presented in Section 7.2 to generate a supercontinuum. However, for 330 mW average power the spectrum spans from 900 nm up to 1400 nm showing a red-shifting soliton at around 1.3 μm as well as NSR in the blue.

Neglecting all kinds of losses in the simulation, an average pump power

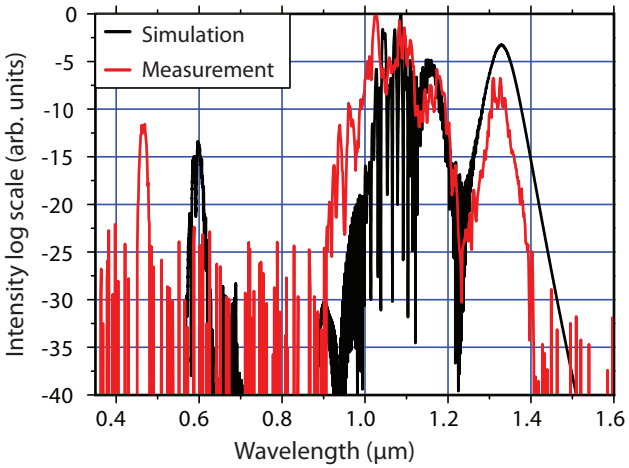

Figure 7.4.: Comparison between measurement and simulation of a 19 cm long fiber with a single strand filled with CCl_4 and a core diameter of 2.5 μm, pumped with an input power of 330 mW.

of 25 mW is used to achieve the best matching between simulation and experiment which corresponds to a peak power of 1.3 kW. In comparison to the experiment, the simulation shows all the features of the measurement; namely the soliton at 1.3 μm and also the peak in the blue caused by the NSR. Only the position of the NSR peak is slightly shifted. This can be addressed to an inaccuracy of the linear refractive index of CCl_4 which is given in [149].

The very good agreement between experiment and simulation makes it reasonable to interpolate the spectral evolution inside the fiber over the propagation length. The corresponding simulation is shown in Fig. 7.5(a) where the spectral intensity is plotted along the fiber length. The simulation is made with an average input power of 25 mW. At the beginning only SPM slowly broadens the spectrum. After a certain length, called the soliton fission length, a soliton forms and starts to red-shift by the Raman effect. In the current system this occurs after a propagation length of 6 cm. Starting from the same point NSR appears for the momentum conservation. The spectrum broadens drastically. In Fig. 7.5(a) one can also see the beating of the higher order solitons oscillation at the beginning of the soliton dynamics. This effect is

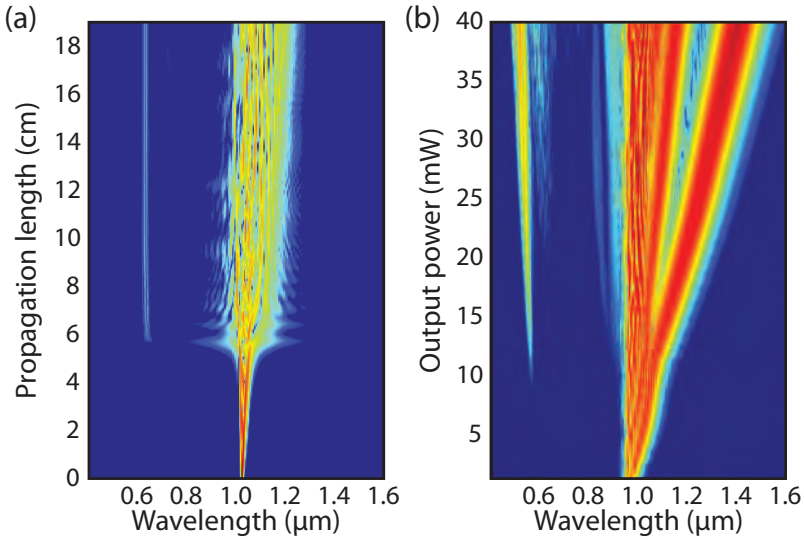

Figure 7.5.: Spectral evolution of a CCl_4 filled NL-2.3-790 single strand fiber - (a) Spectral evolution over the propagation length. (b) Spectral evolution for increasing input power.

washed out by other effects in the further propagation. If the fiber would be much longer, mixing effects would successively fill up the gap between the main part of the spectrum and the non-solitonic part in the blue.

In Fig. 7.5(b) the spectral evolution with increasing input power is depicted. All the effects described above and in Chapter 2.5 are also apparent here. Besides that, the total spectral width of course increases with increased input power. For higher powers a second soliton becomes visible in the spectrum, which also shifts to the red.

With the simulation it is also possible to demonstrate the tremendous influence of the nonlinear refractive index on the generated spectrum. In Fig. 7.6 a comparison of the output spectrum of a 20 cm long NL-2.3-790 fiber is presented for different core materials. The blue curve corresponds to the simulation of the CCl_4 filled single strand structure which has already been shown before. By artificially changing the nonlinear refractive index of the core material from $15 \cdot 10^{-20} m^2 W^{-1}$ for CCl_4 to $2.6 \cdot 10^{-20} m^2 W^{-1}$ for glass (red curve), the spectral broadening

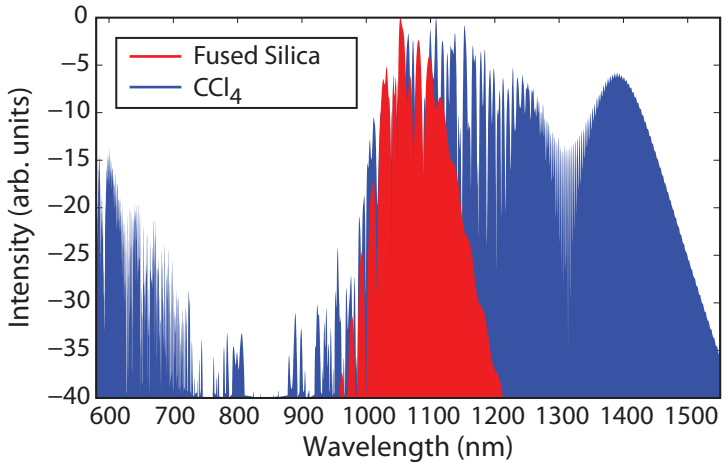

Figure 7.6.: Comparison of the spectral broadening for the same fiber with a glass core (red curve) and a CCl_4 core (blue curve). For comparison the linear refractive index as well as the dispersion properties are artificially set to be identically.

is significantly reduced. In the simulation the temporal dynamics of the material as well as the linear dispersion relation are unmodified and thus only the influence of the nonlinear refractive index n_2 can be demonstrated.

In conclusion this chapter presents an application of the selectively fluid-filled fiber. The remarkably high nonlinearity of CCl_4 is combined with the possibility to tailor the dispersion properties of the device resulting in a broad supercontinuum spanning over 600 nm, starting at 700 nm going up to 1300 nm. This tremendous effect is achieved for very low pump powers, where solitons already form in this system. Single strands filled with slowly responding liquids can also give rise to new propagation effects, such as the existence of so-called linearons [188] or they can strongly influence the soliton dynamics [99].

Single strands seem to be a simple structure but they are very versatile for applications: Not only can a supercontinuum be generated by this structure as presented here. Also, it is possible to built a laser by filling the single strand with an active medium. Another possibility would be the usage of the single strand fiber for sensing [193].

8. Nonlinear optofluidic coupler in selectively fluid-filled fibers

In 1982 Jensen [107] proposed an all-optical switch using the material Kerr nonlinearity to control the switching behavior.

Two waveguides placed in close proximity to each other couple together. This results in a sinusoidal back and forth switching of the light between both waveguides in the linear case. The spatial frequency of this process is determined by the overlap of modal fields of the two waveguides. The ratio of output powers is then given by the length of the coupling device (see Section 3.1). A schematic picture of a coupler is depicted in Fig. 8.1(a). The linear coupler device is very common for building fiber based beam splitters.

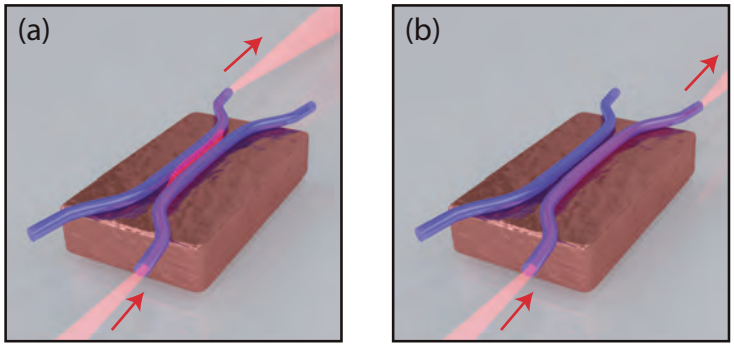

Figure 8.1.: Schematic nonlinear coupler device - (a) For a certain low power the light switches from one waveguide to the other. (b) For a power above the critical power the light remains in the initial waveguide.

In the linear regime one cannot control the output power ratio for a fixed

length of the device. The situation changes for the nonlinear coupler. Here the output becomes dependent on the incoupled intensity and can be tuned to different output power ratios for a fixed length. A variety of examples of quartz fiber couplers have been presented [109,110]. They all show the nonlinear dependence of the output ratio. This situation is depicted in Fig. 8.1(b) where the output can be changed without changing length and waveguide separation of the coupler device.

For fused silica fiber couplers [109,110] as well as for twin-core PCFs [194–196], the nonlinear coupling is limited by the nonlinear refractive index n_2 of the host material. With the presented fabrication technique of selectively filled PCFs [1] (Chapter 5), it becomes feasible to overcome this limitation by using highly nonlinear liquids such as CCl_4.

Furthermore, liquids have a large thermo optical effect which can be up to two orders of magnitude larger than for fused silica. Thus the refractive index of the liquid can be tuned which enables it to control the coupling strength of the coupler by temperature.

In the following chapter an optofluidic nonlinear coupler will be presented which benefits from the enhanced nonlinear properties of the liquids used [3]. It is also demonstrated how to utilize the thermo-optical effect to achieve a tunable optofluidic nonlinear coupler. Because the underlying process for this device is the ultrafast Kerr effect, this tunable coupler could be used for ultrafast all-optical switching with switching times below 1 ps.

8.1. Concept and parameter trade-off

The high Kerr nonlinearity of liquids offers the possibility to build nonlinear couplers, acting as all-optical switches. The liquid is scaffolded by the PCF and forms two waveguides in close proximity to each other. In Fig. 8.2(a) an example is illustrated. The glass core of the fiber itself is neglected and two holes are infiltrated by the desired liquid. These two liquid strands act as coupler. The waveguide distance of the coupler is then given by the hole-to-hole spacing of the PCF used and, therefore, has a strong influence on the coupling strength κ (see Eq. (3.3)). For

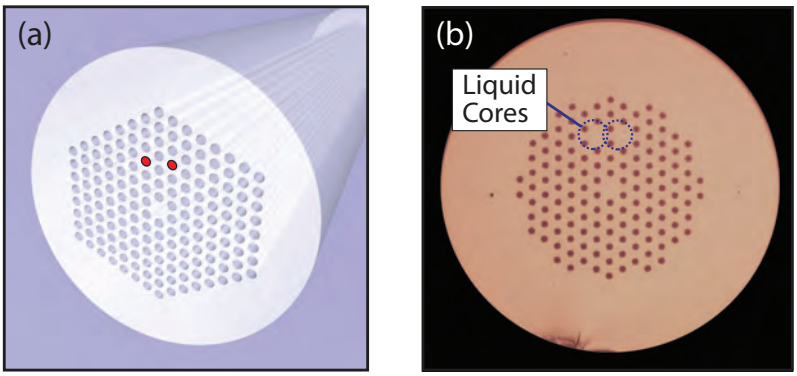

Figure 8.2.: (a) Illustration of a coupler structure inside the photonic crystal fiber. (b) Microscope image of a coupler in a LMA-8 fiber with two CCl_4 filled strands.

one specific fiber the coupling strength can be controlled by the choice of the separation of the holes filled (see Section 4.1.2).

Another influence on the coupler characteristics is given by the refractive index of the liquid. The refractive index determines the mode inside each waveguide and hence, for a given separation of the waveguides, also the mode overlap. In the following experiments all parameters are chosen such that the devices strongly prefer the fundamental mode.

In summary, all coupler parameters are determined by the geometry of the fiber and by the refractive index of the liquid.

It is favorable that the device length L_d is in the range of few multiples of the coupling length L_c [197]. Thus for the experiments presented here the LMA-8 fiber (see section 4.1) is chosen with a hole diameter of 2.7 μm and a pitch of 5.6 μm. The nonlinear liquid CCl_4 is used with a refractive index of 1.4503 at room temperature at a wavelength of about 1.04 μm. With a waveguide separation of only 5.6 μm the coupling length is calculated (see Section 3) to be about 500 μm. This is much too short for the experimental setup because it can only handle fibers down to a minimum length of 2.9 cm. By changing the spatial arrangement of the waveguide within the photonic structure, the coupling strength can be lowered and hence the coupling length increased. One empty row of holes between the two filled strands gives a coupling length of 9 mm and then the requirement for the device length can be fulfilled. Now

the two waveguides are $\sqrt{3}\Lambda = 9.6\,\mu$m apart. The final arrangement of the fluid-filled strands is shown in Fig. 8.2(b).

8.2. Measurement of the nonlinear optofluidic coupler

For the measurement of the nonlinear optofluidic coupler the same setup is used as described in Chapter 6. The Yb:Glass oscillator is used as the pump laser source at a wavelength of 1040 nm, a repetition rate of 20 MHz, and a pulse width of 180 fs [179]. The laser light is coupled into the liquid core S_1 focused with a microscope objective (60x with NA $= 0.65$). The incoupling condition is observed by a CCD camera to make sure that the laser light is coupled only to one liquid core.

The output is recorded by another CCD camera. In order to measure the output power ratio a Gaussian function is fitted to the mode image and the ratio of the amplitudes has been extracted from this fit.

In Fig. 8.3(a) the result for the NLC is shown for room temperature. In this measurement the fiber has a length of 3.6 cm. This corresponds to a length which is four times the coupling length.

The measurement clearly shows a power dependent behavior of the output. Superimposed on the measured data is the solution given by Eq. (3.8) with the critical power set to be 22 kW and a coupling strength of 180 m^{-1}. The measured data and the solution of the Jensen Model agree very well despite the discrepancy of the critical power values stemming from all kinds of losses in the device. In Fig. 8.3(b) three intensity patterns from three distinct power values are shown which are marked with the letters “A”, “B”, and “C” in Fig. 8.3.

The amplitude difference here is about 60%. This value is dependent on the sample and values of up to 90% separation are achieved. Thus, with the nonlinear optofluidic coupler device, the output ratio can be controlled by the incoupled light.

To avoid thermal effects, the fiber is sitting on a temperature stabilized copper block. This would not avoid thermal effects due to two photon absorption, but fortunately liquids have a very small two photon

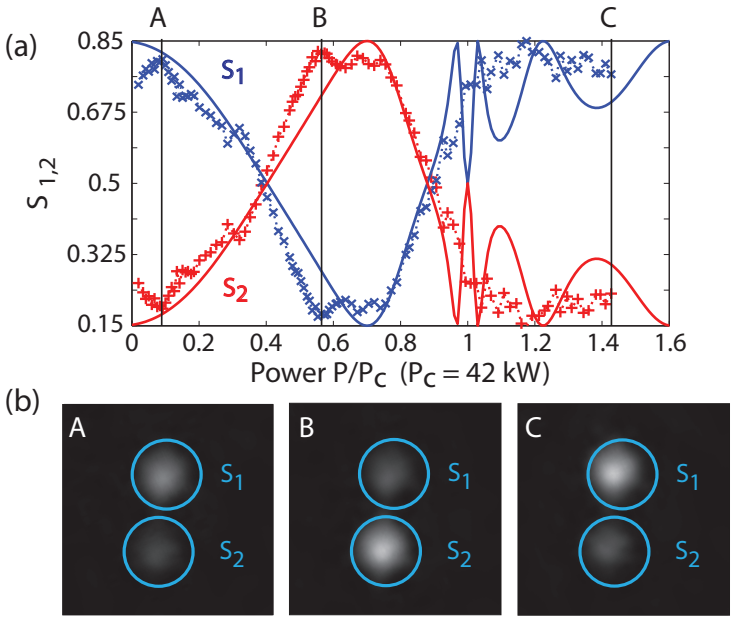

Figure 8.3.: (a) Experimentally measured and normalized power distribution between the two channels S1 (blue) and S2 (red) of the optofluidic coupler versus input power. Also plotted the theoretically calculated dependencies of the power distribution by the Jensen model. Three selected power values are indicated with the letters "A", "B", and "C". (b) Measured intensity distributions at the output of the optofluidic coupler at (A) 3.5 kW, (B) 24.2 kW, and (C) 58.7 kW.

absorption cross-section [198].

8.2.1. Simulation

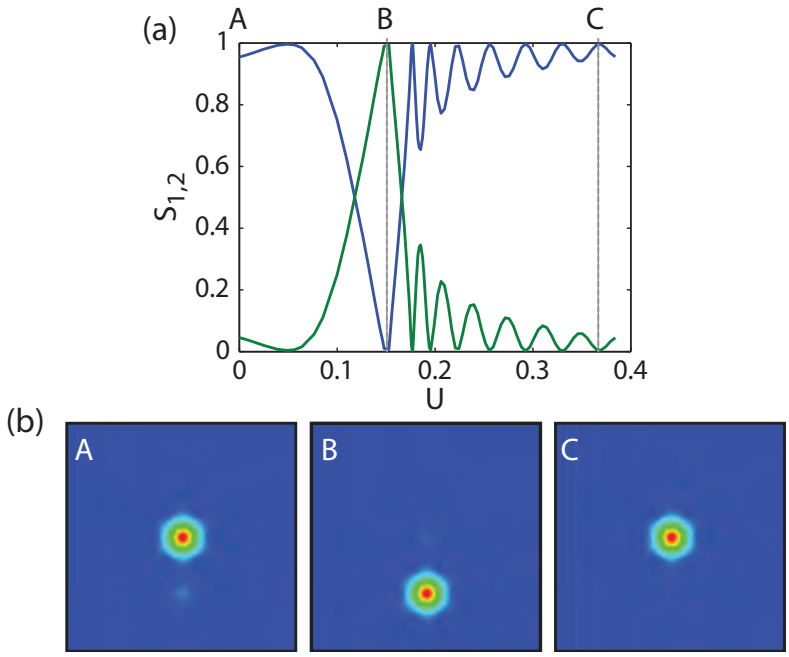

Figure 8.4.: Solution of the complete model for the case of a CCl_4 filled optofluidic coupler with the length of 3.6 cm - (a) Power distribution between the two channels S_1 and S_2 with increasing power. (b) Mode pattern at specific power values marked with the letters "A", "B", and "C".

So far only the simplified solution is fitted to the results. In Fig. 8.4(a) the complete model is calculated for the nonlinear optofluidic coupler filled with CCl_4 and a length of 3.6 cm. The power in the graph is given in dimensionless units with U as incoupled peak power. It is connected via

$$P_0 = \frac{U\lambda^2}{4\pi^2 n_0 n_2} \tag{8.1}$$

with the input peak power. The critical power can be estimated to be around 22 kW. This is below the value given by the measurement of

42 kW. The deviation results from all kinds of losses originating from the incoupling, outcoupling, confinement, and the material itself. The value is in very good agreement to the numerically evaluated value of the Jensen model. Three specific powers are selected analogously to Fig. 8.3 and the corresponding intensity patterns are shown in Fig. 8.4(b).

The dynamics of the simulated data and the measured data agree very well. Also the simulation shows power dependent switching.

8.3. Temperature tuning of the nonlinear optofluidic coupler

The large thermo-optical coefficient of $\mathrm{d}n/\mathrm{d}T = -5.5 \cdot 10^{-4}\mathrm{K}^{-1}$ of the used liquid CCl_4, which is about two orders of magnitude larger than that of fused silica, enables tuning the mode overlap of the two adjacent waveguides. Changing the temperature of the device causes considerable modifications in the refractive index contrast between infiltrated holes and silica cladding. Thus the coupling strength κ can be tailored according to the demands of applications. The following experiments will demonstrate the influence of the thermo-optical effect on the switching dynamics of the optofluidic NLC.

First, the output power ratio of a 2.9 cm long LMA-8 fiber filled with CCl_4 in the linear regime is measured as a function of temperature. In Fig. 8.5(a) the sinusoidal output of the coupler is shown for different temperatures. A sine function is fitted to the measured curve, also plotted in Fig. 8.5(a). The coupling strength is extracted as shown in Fig. 8.5(b) from the measurement (line 1) as well as from the fit function (line 2). The extracted values are in very good agreement to FEM simulations with Comsol, also presented in Fig. 8.5(b) (line 3). It is clearly visible that for increasing temperature the coupling strength also increases. Thus the coupling strength of the optofluidic NLC filled with CCl_4 can be tuned in this experiment by the thermo-optical effect from $\kappa = 150\,\mathrm{m}^{-1}$ for 15 °C up to $\kappa = 300\,\mathrm{m}^{-1}$ for 30 °C.

Three temperatures were chosen for the nonlinear measurements. All temperature dependent measurements were made with the same fiber,

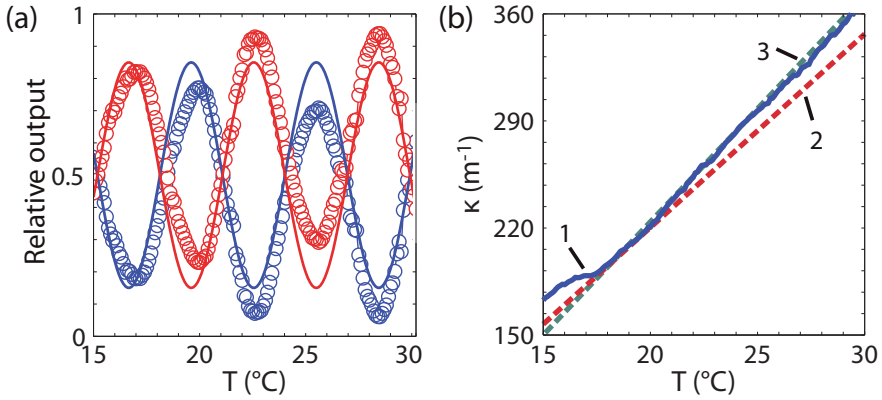

Figure 8.5.: (a) Measurement of the linear coupler output as a function of the temperature. (b) Extracted coupling strength from the measurement (blue, solid, 1) in comparison to Comsol simulations (dashed, red, 2). Also plotted is the coupling strength extracted from the sine-fit of (a) (dashed, green, 3).

a 2.9 cm long LMA-8 fiber selectively filled with CCl_4, where the liquid strands with a diameter of 2.7 μm each are separated by 9.6 μm as it was for the experiment at room temperature as well. As pump source the same laser oscillator is used as in the experiments of the former section, the Yb:Glass oscillator at a wavelength of 1040 nm. For all three temperatures the input power is increased and the power of the two output channels is recorded. The results are shown in Fig. 8.6 for the different temperatures. In these cases a light discrimination of about 90% could be realized.

According to [107] and Eq. (3.10), the critical power of the NLC is increased for increased coupling strength and hence also for higher temperatures. Therefore, only in the case of 16 °C, the regime of the nonlinear decoupling is reached. In the other cases this threshold lies beyond the limits of the pump laser. Apart from this, it is obvious from Fig. 8.6(a)-(c) that nonlinear coupling occurs and the output can be controlled by the incoupled power. The difference of these three measurements is due to the thermo-optical effect of the liquid and underlines the versatility of the presented optofluidic NLC device. The characteristic behavior of the coupler can be altered dramatically by

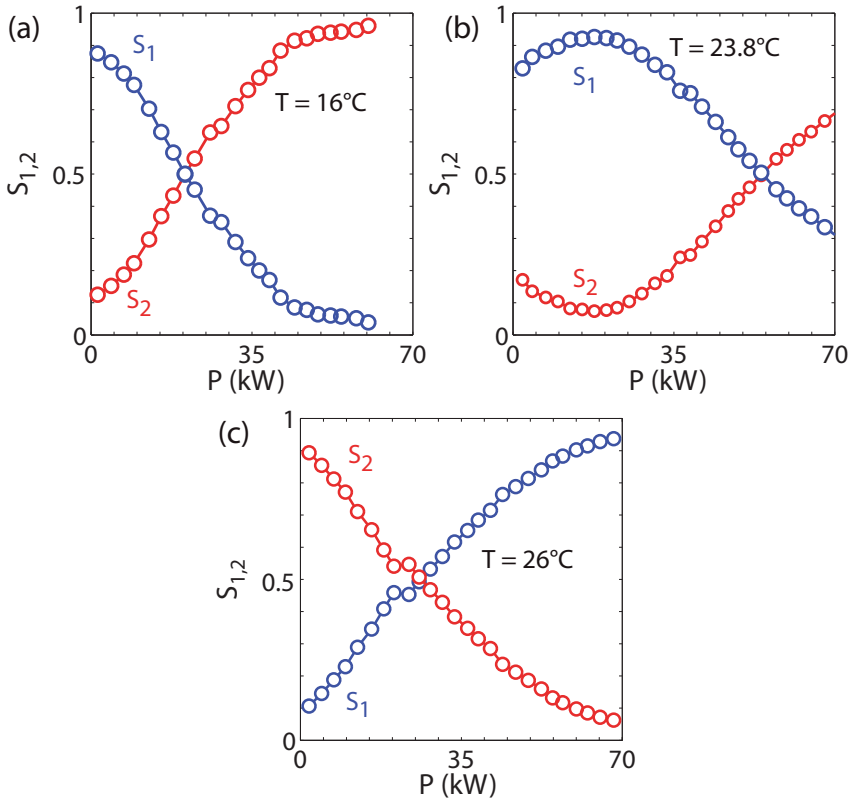

Figure 8.6.: Experimentally measured power distribution between output channels S_1 and S_2 versus input power at (a) T = 16 °C, (b) T = 23.8 °C, and (c) T = 26 °C for the same nonlinear optofluidic coupler.

tuning the coupling strength with the temperature.

In conclusion the current chapter presents a thermo-optic as well as a nonlinear application of a selectively fluid-filled PCF. The optofluidic ultrafast nonlinear coupler built consists of two liquid strands embedded in a PCF. Due to the high nonlinearity of the liquid CCl_4, nonlinear switching can be observed in this system and the output can be controlled by the incoupled light. The underlying process for this nonlinearity is the ultrafast Kerr-effect. Therefore, this device can be used as an ultrafast all-optical switch with switching times below 1 ps, which benefits from the enhanced nonlinear properties of the liquid. Furthermore, the thermo-optic properties of the liquid allow it to tune

the coupling strength and, therefore, the dynamics of the optofluidic nonlinear coupler over a broad region.

9. Spatial solitons in fluid-filled fibers

Starting from the coupler in the previous chapter, more waveguides are added to the system on the way from simple to complex systems. At first couplers with more than two waveguides were investigated [101, 122, 125, 199]. Every time these steps were accompanied by nonlinear effects and influences on the propagation in the multiple waveguide systems [107, 200–202].

In 1988 the term "discrete optics" was introduced by Christodulides and co-workers [44, 45] dealing with all devices with more than two coupled waveguides [203], which were mostly linearly arranged. A new field was established with several new effects like discrete diffraction [46, 47].

With including nonlinearity into the system, numerous new properties and effects came up, such as light localization [44, 48–51, 133], self-trapping [126, 204], beam steering [52, 55], and the optical analog of Bloch waves [53, 54]. Defocusing nonlinearity enriched the field even further [205].

All these effects are, in principle, also accessible in the optofluidic system presented here. Nevertheless, the following experiments and descriptions are restricted to the simple case of light self-localization analogous to [44, 49, 50]. This effect is also known as spatial solitons.

Up to now ultrafast experiments were only performed in solid structures [51, 206] which are easy to fabricate by etching the waveguides into a substrate. However, these structures are restricted to linear one-dimensional arrays. With the 2D photonic structure of the photonic crystal fibers, this limitation can be resolved and two-dimensional spatial solitons can be generated in these devices.

Complete filled fibers with thermal and slow defocusing nonlinearity were already used to demonstrate spatial effects [56–58, 159]. The

following description shows the first realization of spatial solitons in an optofluidic system given by the selectively fluid-filled fibers relying on the ultrafast Kerr nonlinearity of highly nonlinear liquids [4].

9.1. Realization

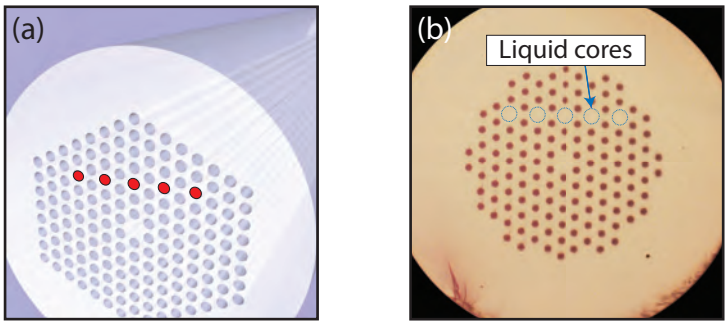

Figure 9.1.: (a) Illustration of an optofluidic waveguide array scaffolded by a photonic crystal fiber. (b) Microscopic image of a fluid-filled photonic crystal fiber with five CCl_4 strands acting as a nonlinear waveguide array.

The system used to observe the effect of light self-localization or spatial solitons is schematically shown in Fig. 9.1(a). A microscopic image of an optofluidic waveguide array scaffolded by a PCF is presented in Fig. 9.1(b). These samples are produced by the methods described in Chapter 5. As basis the LMA-8 fiber is used. Hence, the cores have a diameter of 2.7 μm and analogous to Chapter 8 about the nonlinear coupler, the coupling strength of the waveguides is roughly controlled by the position of the infiltrated strands within the photonic structure of the fiber. A distance of $\sqrt{3}\Lambda = 9.6\,\mu$m is achieved by separating the waveguides by an additional row. The finer adjustment of the coupling strength is done by the temperature tuning. In all following experiments CCl_4 is the liquid used to form the waveguide cores. With this combination of liquid and fiber, the pump wavelength of 1040 nm lies in the normal dispersion regime. Hence no temporal solitons will form in the experiments.

The setup used for surveying these effects is described in Chapter 6. The investigated structure consists of an array of five coupled liquid waveguides. In the first step the linear and nonlinear behavior will be simulated. In the subsequent section experimental results will be presented and compared to the simulation data.

9.2. Simulation

For the simulation the Eq. (3.13) was solved numerically by the method described in Section 3.4. The MatLab code is listed in Appendix B. The central waveguide was excited in the simulation.

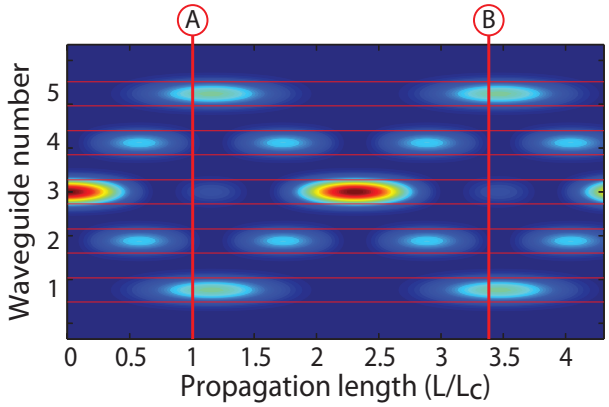

Figure 9.2.: Simulation of the intensity distribution in the linear regime of the optofluidic waveguide array with five waveguides over the propagation distance. The letters "A" and "B" indicate the length of the measured samples below in units of the coupling length.

In Fig. 9.2 the linear propagation of the five waveguide array filled with CCl_4 is depicted as an intensity plot. The length is given in units of the coupling length L_c. Two different positions are chosen marked with the letters "A" and "B". Both devices have a length of 3 cm but are measured at different temperatures of 6 °C for sample "A" and 16 °C for sample "B". Thus the coupling length is changed to the different values of $L_c = L$ and $3.4 \cdot L_c = L$, respectively.

Fig. 9.3 shows the numerical results if nonlinearity is included. The

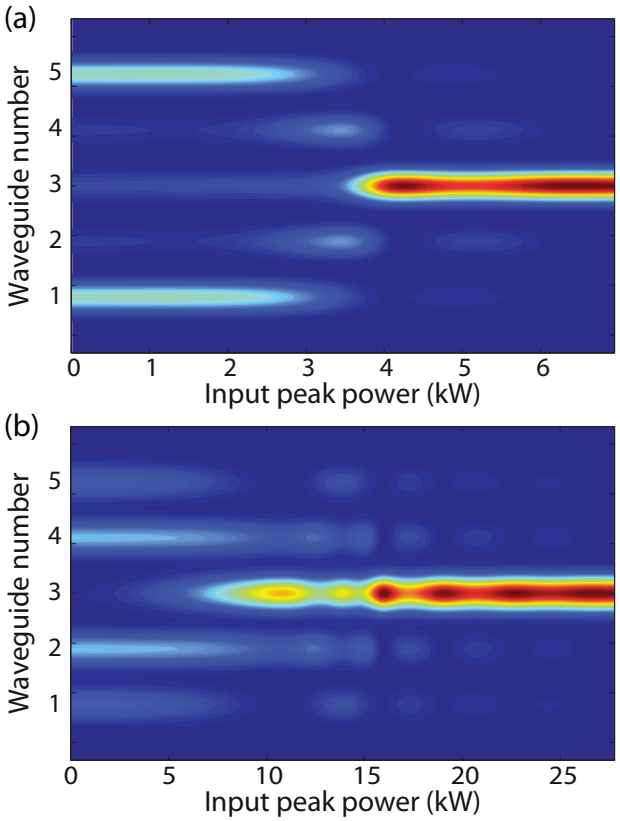

Figure 9.3.: Simulation of the intensity distribution of the optofluidic waveguide array with five waveguides over the incoupled input peak power - (a) For a temperature of 6 °C. (b) for a temperature of 16 °C.

intensity is plotted for increasing input power in the central waveguide. Fig. 9.3(a) shows the simulation for 6 °C with a calculated coupling strength of $60\,\mathrm{m}^{-1}$. Fig. 9.3(b) is the corresponding simulation result for 16 °C with a calculated coupling strength of $160\,\mathrm{m}^{-1}$ between each adjacent waveguide pair. In both cases light localization is clearly visible. Above a certain threshold most of the light is confined inside the central waveguide. This is a stable situation that does not change for an increased input power. A spatial soliton has formed. Apparent here are the different power scales. This is similar to the linear dependence of P_c on the temperature as described in Chapter 8. It is of course not exactly the same situation since the inner waveguides have two options

to couple their light.
The modes in the following sections are extracted from this simulation. A Gaussian intensity distribution is assumed to approximate their shape [81]. The patterns are normalized to the integral of the intensity.

9.3. Results

For the measurement of the nonlinear light localization inside a selectively fluid-filled PCF, the same setup is used as described in Chapter 6. As pump laser source the Yb:Glass oscillator is used at a wavelength of 1040 nm, a repetition rate of 20 MHz, and a pulse width of 180 fs [179]. The laser light is coupled into the central liquid core focused with a microscope objective (60x with NA $= 0.65$). The incoupling condition is observed by a CCD camera to make sure that the laser light is coupled only to one liquid core.
The output is recorded by another CCD camera. In order to measure the amplitudes in each waveguide a Gaussian function is fitted to the mode image and the amplitudes have been extracted from this fit.
During the measurement the temperature is kept constant by water cooling and the Peltier-element of the setup.
Fig. 9.4 shows the experimental result for the five core structure filled with CCl_4 for different input powers. In the linear case most of the light is in the outer waveguides as well as in the central core. For increasing input power the mode changes. In the intermediate power regime an asymmetric mode forms out. If the power is increased further, all the light localizes in the central core. This situation starts at about 45 kW and stays constant till the power limit of the used laser system.
Also shown in Fig. 9.4 is a comparison of the experimental recorded mode with the simulated modes from Section 9.2 given for the dimensionless power U (acc. to Eq. (8.1)). For the liner case as well as for the spatial soliton, a rather good agreement is achieved. The deviation in the intermediated regime results from slight inhomogeneities of the fluid-filled fiber between the different cores. This results in a preference of the light since it accumulates in the waveguide with the

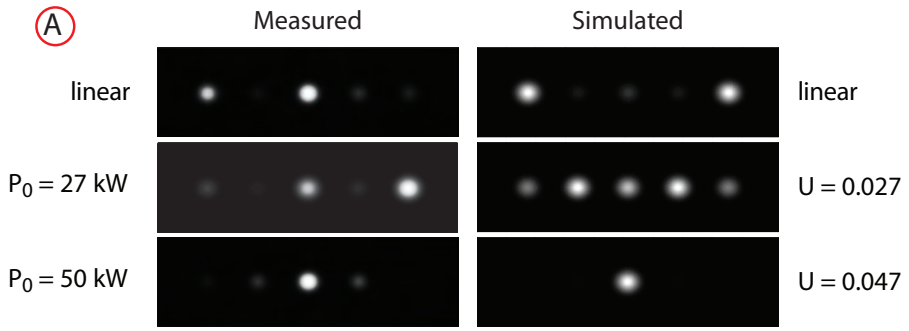

Figure 9.4.: Experimentally measured modes for three different input peak powers starting from the linear up to the nonlinear dominated regime above 45 kW in comparison with the simulated modes at the corresponding power given in the dimensionless peak power U. Both, measurement and simulation, are carried out for a temperature of 6 °C and a device length of 3 cm.

highest refractive index [52, 53]. Hence the inhomogeneity has to be overcome by the nonlinear effects to form a spatial soliton regardless of these inhomogeneities. This is an additional reason for the power difference between simulation and experiment, besides all kinds of losses stemming from incoupling, confinement and material losses.

The power dependent evolution of the mode is visualized in Fig. 9.5. From this one can see the formation of the spatial soliton starting at an input peak power of 45 kW and being stable over the complete measurement region up to 71 kW. Clearly visible from the intensity map are also the asymmetric modes in the intermediate power region below 40 kW. As described above, this is a consequence of the waveguide inhomogeneities.

In a second experiment, the same structure as described above is used with only the temperature changed to 16 °C. Thus the array has a length of about 3.4 times the coupling length L_c (marked with a "B" in Fig. 9.2). This also increases the required power for the formation of a spatial soliton. The measured modes for selected values of the input peak power are depicted in Fig. 9.6 and also compared with the simulated ones at the corresponding power value. Indeed, for an increased power the modes start to change in the intermediate power regime. For the

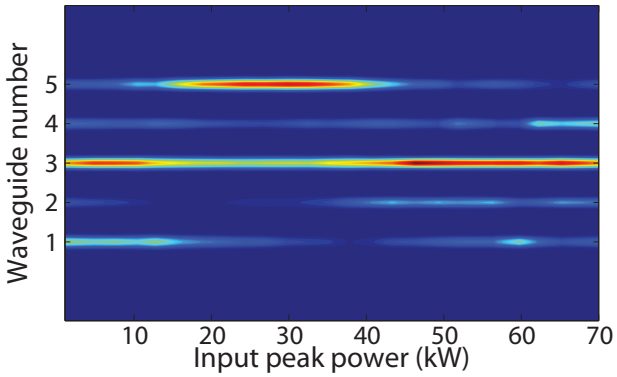

Figure 9.5.: Intensity map of a liquid waveguide array within an LMA-8 fiber filled with CCl_4 consisting of five waveguides. The intensity distribution is plotted here over the incoupled input peak power. This experiment is performed at a temperature of 6 °C.

highest possible power of the used laser system of 71 kW the mode clearly starts to symmetrize and the onset of light localization is clearly visible.

As a last experiment an array with six waveguides is fabricated with a length of 3 cm. Thus the incoupling condition is *a priori* asymmetric. The linear mode is pictured in Fig. 9.7. The same laser is used as in the experiment before at a wavelength of 1040 nm. During the measurement the device is constantly cooled down to a temperature of 6 °C. The waveguide to which the light is coupled, is marked in Fig. 9.7.

To generate a spatial soliton inside this structure and observe light localization, the power is increased. Here it is expected to get asymmetric modes. For an input peak power above 60 kW the light localizes in the incoupling waveguide due to the induced nonlinear effects and a spatial soliton forms. This observation proves that the final mode depends only on the incoupling condition. In each case the light is mainly confined inside the incoupling waveguide.

These observations allow the conclusion that the optofluidic fluid-filled fiber arrays presented here provide the platform to observe spatial solitons with the ultrafast focusing Kerr nonlinearity. This opens the gate to the field of discrete optics and marries it to the field of optoflu-

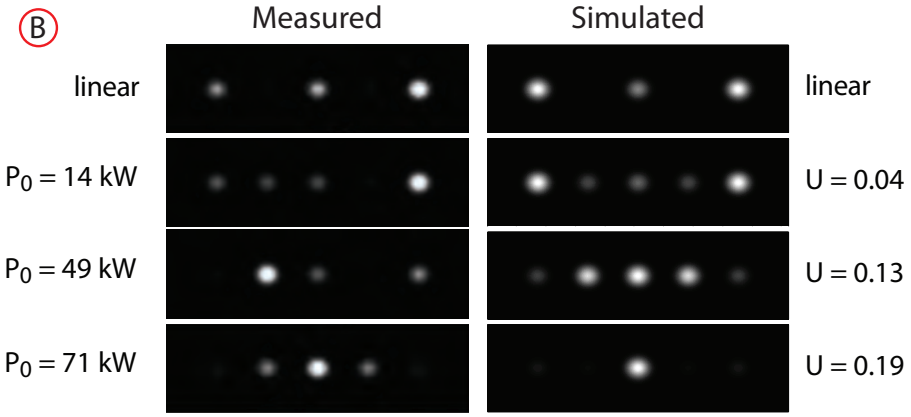

Figure 9.6.: Experimentally measured modes of a 3 cm long optofluidic waveguide array consisting of five waveguides at a temperature of 16.5 °C with increasing input peak power showing nonlinear light localization in the central waveguide. The measured modes are compared to simulated modes at the corresponding power given in the dimensionless unit U.

idics [207, 208].

So far everything presented here is limited to one dimension. A linearly distributed array of liquid waveguides was used to achieve these results. Up to now it was very hard or even impossible to tailor the spatial arrangement of waveguides in two dimensions without fabricating special kinds of optical fibers from scratch. The combination of the direct laser writing fabrication technique together with standard PCFs provides the possibilities to overcome these limitations. Furthermore, liquids offer a high degree of freedom to tailor their properties to the demands of the experiment. Therefore, they altogether provide an easy to implement way for the generation of 2D spatial solitons. Additionally, due to the reorientational molecular nonlinearity and their temporally retarded response, new effects become feasible and benefit from the unique properties of all kinds of liquids.

Tailoring the temporal dispersion accordingly to Chapter 7, complete control of temporal and spatial properties is ensured. The generation of three-dimensional spatial-temporal solitons (2D spatial + 1D temporal) [59, 209] becomes feasible in this optofluidic system [57–61], which

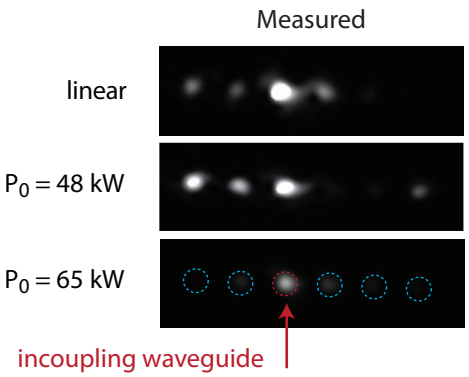

Figure 9.7.: Asymmetric conditions inside a six waveguides containing array at 6 °C also with a clear nonlinear light localization at the incoupling waveguide due to increased input power.

underpins the versatility of the selectively fluid-filled fiber even more.

10. Summary

In summary, in this thesis a novel and versatile optical device was presented, the selectively fluid-filled photonic crystal fiber. This device consists of a photonic crystal fiber with several selectively infiltrated holes in the fiber's holey region. The liquid strands act as waveguides with enhanced nonlinear properties by the liquids. The work is fundamentally important for the field of nonlinear optics as it provides a new platform for investigations of spatially and temporally nonlinear effects, and underpins new applications in ultrafast optical communication and future photonic circuits.

In the first part of this thesis the setup for the fabrication of the fluid-filled fibers was realized and demonstrated. This setup applies the direct laser writing technique to fibers and is able to selectively close single holes of the photonic crystal fiber on demand. This technique is neither limited by the desired patterns nor by the fiber used. The fibers were subsequently filled by the capillary force.

Applications of selectively fluid filled fibers were demonstrated experimentally. The description started with the single strand structure. Special care was taken of the dispersion properties to maintain propagation in the anomalous dispersion regime which is mandatory for the generation of temporal solitons. Together with the enhanced nonlinearity by the liquid, a 600 nm wide supercontinuum could be generated with very little input power. These results were accompanied and confirmed by the numerical solution of the nonlinear Schrödinger equation.

Spatial nonlinear effects were also observable in another kind of selectively fluid-filled fiber. Two coupled strands can form a nonlinear coupler device. Light was switched by the input power between these two waveguides with a discrimination of about 90%. Due to the Kerr type of the nonlinearity, switching times below 1 ps can be achieved. Furthermore, the huge thermo-optical effect in liquids allows for tuning the switching characteristics of the nonlinear coupler at will and build

an externally controllable nonlinear coupler device.

These experiments were confirmed by simulations. For the simulation, the amplitude model was developed in this thesis for solving the discrete nonlinear Schrödinger equation. This model is very fast and accurate, but only provides access to the mode amplitudes and not to the modes themselves. As comparison, the full 2D model was solved which takes the complete structure of the device into account. This method also gives information about the mode profile. Nevertheless, it is very computationally intensive and memory consumptive. The very good agreement of both models justified the usage of the simpler analytical amplitude model.

The last part concerns the young field of discrete optofluidics. Five waveguides filled with the highly nonlinear liquid CCl_4, coupled together inside a single photonic crystal fiber, are utilized to elucidate the nature of discrete optofluidics. Exploiting the nonlinearity of the liquid again, nonlinear light localization in a discrete system and the formation of a spatial soliton could be demonstrated. Here the required input power for the formation and thus the characteristics of the spatial soliton in general could be manipulated by the strong thermo-optical effect of the liquids. This was further proven by a six waveguide array which also showed the formation of a spatial soliton.

In general, the concept of selectively fluid-filled fibers offers complete control of all important optical properties. Dispersion management, adjustable coupling strength, spatial arrangement of waveguides, and specified nonlinearity by the liquid in the photonic structure of the fiber were demonstrated in this thesis and could be adjusted to the requirements of the experiments. This leads to the control of the spatial as well as temporal behavior of light inside these devices.

By arranging several waveguides inside one photonic crystal fiber an optofluidic discrete system can be built which is further enhanced by the possibilities which come along with the selectively fluid-filled fiber. The field of discrete optofluidics which combines photonic crystal fibers with highly nonlinear liquids opens the gate to new and versatile devices. This not only provides deeper insight into the soliton dynamics by the adjustment of the response of the nonlinear material, it also

means real world application in future photonic circuits become feasible, such as ultrafast and tunable switching and routing devices with unprecedented properties.

11. Outlook

This thesis can serve as a starting point for the field of discrete linear and nonlinear optofluidics. It provides the techniques to fabricate the necessary structures and has already shown some examples of application. However, improvements of the experiments shown in this thesis as well as numerous completely different applications are possible; alternative filling media or new effects of complex nonlinear landscapes become able by exploiting the versatility of the selectively fluid-filled structures.

In all experiments of this thesis the use of liquids such as CS_2 would reduce the demands on the laser source further. Of course one has to deal with the toxicity and with a decreased structure size to maintain the dispersion properties. However, this is not a general argument against the use of CS_2.

For the supercontinuum generation the enhanced nonlinearity would lead to the development of low power white light devices for application resulting in a fluid-filled fiber which could be pumped by a micro-chip laser to achieve a compact and cost efficient coherent white light source for microscopy and white light interferometry. Of course, further engineering has to be carried out to make such devices more stable and reliable. Especially the throughput has to be increased for future applications.

CS_2 would have another advantage. It is almost transparent up to a wavelength of $5\,\mu$m. Pumping a single strand fiber with an optical parametric amplifier at a wavelength in the IR at around $1.5\,\mu$m, the resulting supercontinuum would extend to regions where it is complicated to build light sources for.

The nonlinear optofluidic coupler presented in this thesis is able to switch at a THz rate. Temporal experiments should elucidate the switching behavior and the performance as all-optical gate. Different

liquids provide the ability to investigate the influence of the retarded response on the switching characteristics. Theoretical work has already been published [5], but the experimental confirmation of this theory is still pending.

The presented investigations in the field of discrete optofluidics are the first step towards new experiments and effects; a proof of principle that these structures offer the possibility for more sophisticated experiments and applications. Complex shapes of nonlinear landscapes become feasible together with the ability to control the coupling between the waveguides. The theory is at this point already, experiments should follow. Thus it is predicted that in these devices it should be possible to see ring modes [210] and more complex stable vortex states [211–213] of solitons. In order to achieve this, focusing and defocusing nonlinear media have to be arranged spatially. This arrangement of different types of liquids in one fiber is still a challenge.

Much easier to realize are purely nonlinear lattices, where waveguiding takes place only by the means of nonlinearity. A variety of publications predict novel effects in these nonlinear lattices which are summarized in [210]. Liquids offer here the striking possibility to adjust the linear as well as the nonlinear refractive index either by mixing or by tuning the temperature. Including the temperature dependence, beam steering and thus on-demand switching and steering inside a single photonic crystal fiber with several incorporated waveguides should become feasible.

All these experiments can benefit from the fact that the photonic crystal fiber easily offers a two-dimensional structure which can be exploited for all different kinds of discrete two-dimensional arrangements of nonlinear waveguides. Several liquid strands can be arranged freely inside the 2D photonic structure of the fiber and thus 2D coupled discrete optofluidic waveguide arrays can be built.

So far all suggestions only include either temporal effects or spatial effects separately. Combining the temporal control with the ability to tailor the spatial properties, the possibility arises to engineer a device which is capable of generating 3D optical bullets [57, 60].

Further, selectively closed fibers can easily be filled with all kinds of

different media. One is not limited to liquids. Filling with different materials has already been realized, broadening the wide field even further to which the techniques presented here are the key. For example, the fibers can be filled with metal to achieve a hybrid photonic-plasmonic system [214, 215]. Liquid crystals would offer all the abilities of e.g. switching, attenuation, and polarization control [177]. Sensing of very low concentration becomes feasible due to the long interaction length. This would also be possible in an evanescent sensing configuration. Fibers could be selectively filled with semiconductors [176], giving rise to the functionalities provided by these materials. The fibers can be filled with an active medium that can be pumped (also an evanescent configuration might be possible here) and thus these devices should be able to generate laser light [216].
Also, atomic gases such as Caesium or Rubidium could be filled into fibers and be used for atomic physics type experiments [217, 218].

This long list underpins once more the versatility of the techniques presented here.

In general, fluid-filled fibers and also selectively filled fibers will be the basis for new and versatile optical fiber devices with unprecedented performance revealing novel effects and applications with unique and remarkable properties.

A. Dispersion formula and absorption spectra

In this section, the dispersion relation of CCl_4 is presented together with its absorption spectrum. All data are measured data. More information about this can be found in [7,219].

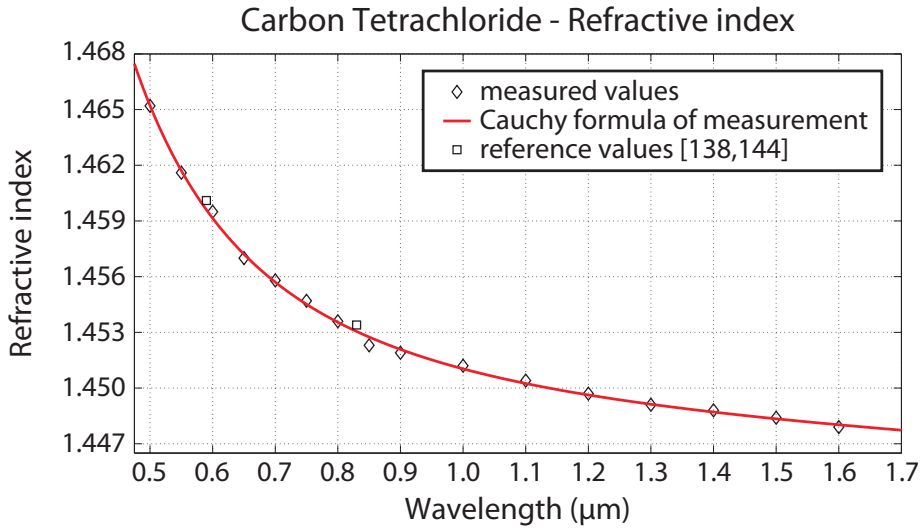

Figure A.1.: Refractive index measurement and reference values.

Fig. A.1 shows the refractive index plotted as a function of the wavelength. The diamonds are the measured data points. The red line is the fitted Cauchy function. This function is determined to be

$$n^2_{CCl_4}(\lambda) = (2.09503 \pm 0.00208) + (0.01102 \pm 0.00144)\frac{1}{\lambda^2} + \ldots \ldots (0.00050 \pm 0.00026)\frac{1}{\lambda^4} - (0.00102 \pm 0.00074)\lambda^2 \quad \text{(A.1)}$$

with the wavelength λ given in micrometers. The measurement is in very good agreement to the two references [140,146], plotted in Fig. A.1 as squares. The measurements are performed at room temperature.

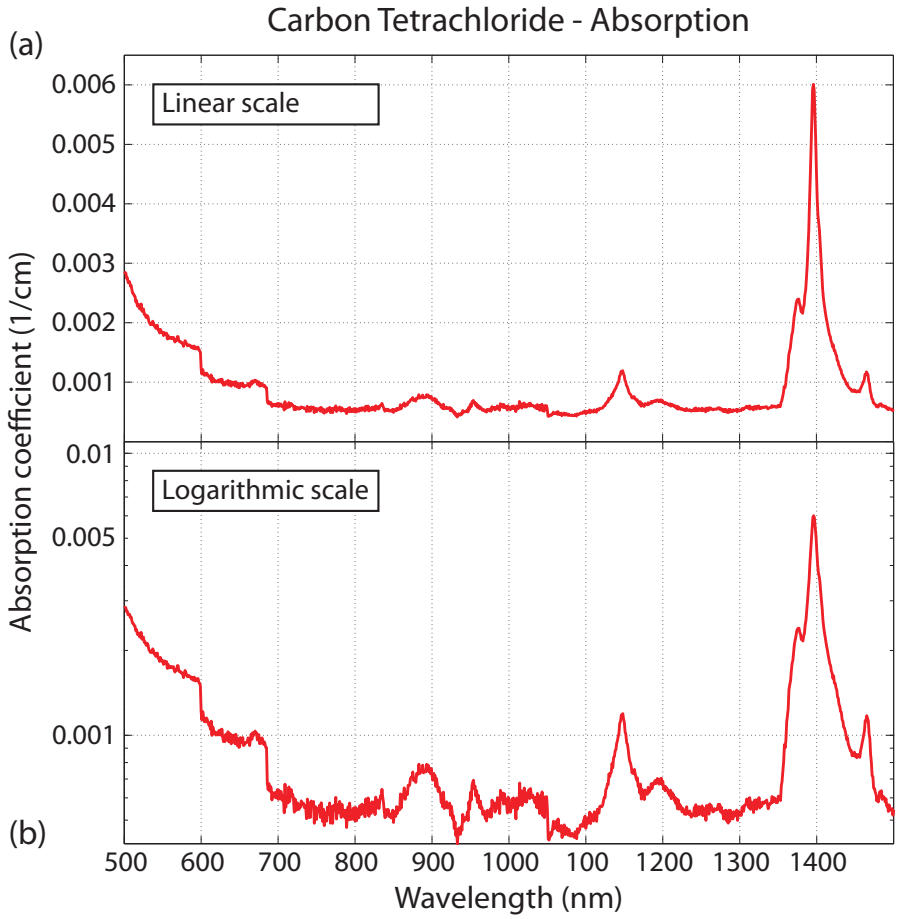

Figure A.2.: Absorption measurement of CCl_4 - (a) The measurement plotted on a linear scale. (b) The same measurement as in (a) just plotted logarithmically.

In Fig. A.2 the measured absorption of CCl_4 is plotted in the wavelength range starting from 500 nm up to 1500 nm. The upper plot is the linear representation and the same measurement plotted logarithmically below. Over almost the complete wavelength range the absorption of CCl_4 is very low and, except at some single adsorption peaks, it does not exceed $1{\cdot}10^{-3}\text{cm}^{-1}$. At around 1400 nm a small peak arises.

Nevertheless, it does not influence the results of this thesis; only for the supercontinuum generation it might play a minor role.

B. MatLab source code

This section provides the code to calculate a nonlinear waveguide array. The following program is written in MatLab and solves numerically the Eq. (3.13) for the situation of a selectively fluid-filled array. For a comprehensive program structure, parts of the calculation are programmed by functions such as the calculation of the effective refractive index of the photonic structure or the propagation constant. Most of them are not listed here, except the function B.2 which solves the differential equation system itself.

The length, pitch, and hole diameter of the fiber are parameters needed as input for the program. The parameters describing the pump source are the average pump power, wavelength, pulse length, and repetition rate. Together with the number of waveguides and the material of the waveguide array, the program calculates the amplitudes in each waveguide for each pump power. At last the output for a certain length is plotted for increasing peak power.

Listing B.1: NLWGArray.m

```
clear all;

%%=========================%%
%%====== Input section ======%%
%%=========================%%

% ------------------------------------------------
% Simulation Parameter
% ------------------------------------------------

T = 6;                          % Temperature [°C]
N = 5;                          % number of Waveguides
ex = 3;                         % number of excited WG

% ------------------------------------------------
% Laser Parameter
% ------------------------------------------------

wavelength = 1.040e-6;          % Central wavelength [m]
R = 20e6;                       % Repetition rate [Hz]
```

```
21 tau0 = 180e-15;              % FWHM of pulse duration [s]
22 Pavg_start = 0:0.0005:0.1;% Incoupled average power [W]
23
24 % ------------------------------------------------
25 % Fiber Parameter
26 % ------------------------------------------------
27
28 L = 0.030;                   % Fiber length [m]
29 pitch = 5.6e-6;              % Fiber pitch [m]
30 dd = 2.74e-6;                % Core of the liquid strand Fibre  [m]
31
32 % Medium filled in central hole
33 % 1 : CS2
34 % 2 : Nitrobenzene
35 % 3 : Fused silica
36 % 4 : Benzene
37 % 5 : Toluol
38 % 6 : CCl4
39 % 7 : Chloroform
40 % 8 : Methanol
41 % 9 : Ethanol
42 %10 : Air
43 medium = 6;
44
45 %%==============================%%
46 %%====== Loop Preparation ======%%
47 %%==============================%%
48
49 % ------------------------------------------------
50 % Coupler Parameter
51 % ------------------------------------------------
52
53 % Coupling strength
54 % Interpolated from Comsol-Simulation results
55 Temp = [0 2.5 5 7.5 10 12.5 15 17.5 20...
56       21 22.5 25 27.5 30 32.5 35 40 50];
57 kappa = [34.68 45.71 60.42 78.54 96.66 117.81 145 175.2 202.39...
58       211.45 229.45 259.79 289.99 317.18 341.35 368.53 410.82 483.32];
59 kk = interp1(Temp,kappa,T);
60
61 % ------------------------------------------------
62 % Numerical parameter
63 % ------------------------------------------------
64 precision = 1e-300;          % Numerical precision for root finding
65 deltaz = 100e-6;             % Simulational step width [m]
66
67 z = 0:deltaz:L;              % Generation of the mesh
68 m = 1;                       % Fundamental mode
69
70 %%========================%%
71 %%====== Calculation ======%%
72 %%========================%%
73
74 % Core refractive index
```

```
nCore = IOR(medium,wavelength)+(T-20)*(-5.5e-4);
% Effective refravtive index of the fiber caldding
neff = find_PCF_index(m,wavelength,dd/2,pitch/2,1,...
                      IOR('Glas',wavelength),precision);
% Propagation constant
beta = find_beta(m,wavelength,dd/2,nCore,neff,precision);
% Wavenumber
k0 = 2*pi/wavelength;
% Diameter of the effective mode area
w0 = sqrt(2)*dd/2/(sqrt(log(dd^2/4*k0^2*(nCore^2-neff^2))));
% Effective mode area
Aeff = pi*w0^2;
% Nonlinearity
gamma = NLIOR(medium)*2*pi/(Aeff*wavelength);

%%=======================%%
%%====== Main Loop ======%%
%%=======================%%
waiter = waitbar(0,'Please wait...');

% Loop for each power value
for p = 1:length(Pavg_start)
  A = zeros(length(z),N);
  A(1,ex) = sqrt(Pavg_start(p)/(2*R*tau0));

% Loop for each spatial step
    for j = 1:length(z)-1
      gg = gamma*abs(A(j,:)).^2;

% Generation of the coupler matrix for a linear array
      C = zeros(N,N);
      for h = 1:N
        for m =1:N
          if h == m
            C(h,m) = beta + gg(h);
          end
          if h == m+1 || h == m-1
            C(h,m) = kk;
          end
        end
      end

% Solving the differential equation system
      A(j+1,:) = DGL_sol(A(j,:),0,kk,deltaz,N,C);
    end

  AA_full(p,:,:) = A;
  AA(p,:) = A(end,:);
  AA_result (p,:) = AA(p,:)/A(1,ex);


  waitbar(p / length(Pavg_start));
end

```

```
129
130 %%================================%%
131 %%====== Output Preparation ======%%
132 %%================================%%
133
134 ww = w0*1e6/2;
135 pp = pitch*1e6;
136 x_pos = -pp*(N-1)/2:pp:pp*(N-1)/2;
137
138 x_steps = 128;
139 x = linspace(-(N+1)/2*pp,(N+1)/2*pp,x_steps);
140
141 % Loop for each power value
142 for k = 1:length(Pavg_start)
143
144   % Adding Gaussian functions
145   for m = 1:length(x_pos)
146     B(:,m) = abs(AA_result(k,m))^2*exp(-(x-x_pos(m)).^2./(2*ww));
147   end
148
149   BB(:,k) = sum(B,2)/N;
150
151 end
152
153 close(waiter);
154
155 %%====================%%
156 %%====== Output ======%%
157 %%====================%%
158
159 figure;
160 contourf(x,Pavg_start*1e-6/(2*tau0*R),BB',30,'LineStyle','none');
```

Listing B.2: DGLsolution.m

```
1 % calculates the amplitudes of a WG array -
2 % geometry given by matrix C
3 %
4 % a0 = initial values (array)
5 % bb = propagation constant (array)
6 % kk = linear coupling constant
7 % z  = propagation length
8 % N  = number of WG
9 % C  = coupling matrix NxN
10
11 function aa = DGL_sol(a0,bb,kk,z,N,C)
12
13 [eigvec,eigval] = eig(C);
14
15 CC = inv(eigvec)*a0.';
16
17 aa = zeros(1,N);
18
19 for h=1:N
```

```
20      for m = 1:N
21          aa(h) = aa(h) + CC(m)*exp(1i*eigval(m,m)*z)*eigvec(h,m);
22      end
23  end
```

Bibliography

[1] M. Vieweg, T. Gissibl, S. Pricking, B. T. Kuhlmey, D. C. Wu, B. J. Eggleton, and H. Giessen, "Ultrafast nonlinear optofluidics in selectively liquid-filled photonic crystal fibers," Optics Express **18,** 25232 (2010).

[2] M. Vieweg, T. Gissibl, and H. Giessen, "Photonic-crystal fibers are selectively filled with nonlinear liquids," Laser Focus World **47,** 53 (2011).

[3] M. Vieweg, S. Pricking, T. Gissibl, Y. Kartashov, L. Torner, and H. Giessen, "Tunable ultrafast nonlinear optofluidic coupler," Optics Letters **37,** 1058 (2012).

[4] M. Vieweg, T. Gissibl, Y. Kartashov, L. Torner, and H. Giessen, "Spatial solitons in 1D optofluidic waveguide arrays with ultrafast Kerr nonlinearity," Optics Letters **37,** 2454 (2012).

[5] S. Pricking, M. Vieweg, and H. Giessen, "Influence of the retarded response on an ultrafast nonlinear optofluidic fiber coupler," Optics Express **19,** 21673 (2011).

[6] T. Gissibl, M. Vieweg, M. M. Vogel, M. Aboud Ahmed, T. Graf, and H. Giessen, "Preparation and characterization of a large mode area liquid-filled photonic crystal fiber: transition from isolated to coupled spatial modes," Applied Physics B **106,** 521 (2012).

[7] S. Kedenburg, M. Vieweg, T. Gissibl, and H. Giessen, "Linear refractive index and absorption of nonlinear optical liquids," Optical Materials Express , submitted (2012).

[8] J. Armstrong, N. Bloembergen, J. Ducuing, and P. Pershan, "Interactions between Light Waves in a Nonlinear Dielectric," Physical Review **127,** 1918 (1962).

[9] P. Franken, A. Hill, C. Peters, and G. Weinreich, "Generation of Optical Harmonics," Physical Review Letters **7,** 118 (1961).

[10] F. Shimizu, "Frequency Broadening in Liquids by a Short Light Pulse," Physical Review Letters **19,** 1097 (1967).

[11] R. R. Alfano and S. L. Shapiro, "Observation of Self-Phase Modulation and Small-Scale Filaments in Crystals and Glasses," Physical Review Letters **24,** 592 (1970).

[12] H. Haus, "Theory of mode locking with a slow saturable absorber," IEEE Journal of Quantum Electronics **11,** 736 (1975).

[13] M. DiDomenico, "Generation of Ultrashort Optical Pulses by Mode Locking the YAIG:Nd Laser," Applied Physics Letters **8,** 180 (1966).

[14] G. P. Agrawal, *Nonlinear Fiber Optics* (Academic, San Diego, Calif., 2007).

[15] C. Lin and R. H. Stolen, "Self-phase-modulation in silica optical fibers," Physical Review A **17,** 1448 (1978).

[16] R. Stolen and J. Bjorkholm, "Parametric amplification and frequency conversion in optical fibers," IEEE Journal of Quantum Electronics **18,** 1062 (1982).

[17] R. H. Stolen, J. E. Bjorkholm, and A. Ashkin, "Phase-matched three-wave mixing in silica fiber optical waveguides," Applied Physics Letters **24,** 308 (1974).

[18] R. Stolen, "Phase-matched-stimulated four-photon mixing in silica-fiber waveguides," IEEE Journal of Quantum Electronics **11,** 100 (1975).

[19] L. F. Mollenauer, R. H. Stolen, and J. P. Gordon, "Experimental observation of picosecond pulse narrowing and solitons in optical fibers," Physical Review Letters **45,** 1095 (1980).

[20] J. M. Dudley, "Supercontinuum generation in photonic crystal fiber," Reviews of Modern Physics **78,** 1135 (2006).

[21] A. V. Husakou and J. Herrmann, "Supercontinuum Generation of Higher-Order Solitons by Fission in Photonic Crystal Fibers," Physical Review Letters **87,** 203901 (2001).

[22] F. M. Mitschke and L. F. Mollenauer, "Discovery of the soliton self-frequency shift," Optics Letters **11,** 659 (1986).

[23] J. P. Gordon, "Theory of the soliton self-frequency shift," Optics

Letters **11,** 662 (1986).

[24] R. R. Alfano, *The Supercontinuum Laser Source* (Springer, Berlin, 2006).

[25] *Supercontinuum Generation*, J. M. Dudley and J. R. Taylor, eds., (Cambridge, Cambridge, 2010).

[26] J. C. Knight, T. A. Birks, P. S. J. Russell, and D. M. Atkin, "All-silica single-mode optical fiber with photonic crystal cladding," Optics Letters **21,** 1547 (1996).

[27] J. C. Knight, "Photonic crystal fibres," Nature **424,** 847 (2003).

[28] T. A. Birks, J. C. Knight, and P. S. J. Russell, "Endlessly single-mode photonic crystal fiber," Optics Letters **22,** 961 (1997).

[29] J. C. Knight, "Photonic Band Gap Guidance in Optical Fibers," Science **282,** 1476 (1998).

[30] P. S. J. Russell, "Photonic crystal fibers," Science **299,** 358 (2003).

[31] T. Birks, P. Roberts, P. Russell, D. Atkin, and T. Shepherd, "Full 2-D photonic bandgaps in silica/air structures," Electronics Letters **31,** 1941 (1995).

[32] R. F. Cregan, "Single-Mode Photonic Band Gap Guidance of Light in Air," Science **285,** 1537 (1999).

[33] N. A. Mortensen, "Effective area of photonic crystal fibers," Optics Express **10,** 341 (2002).

[34] J. K. Ranka, R. S. Windeler, and A. J. Stentz, "Visible continuum generation in air-silica microstructure optical fibers with anomalous dispersion at 800 nm," Optics Letters **25,** 25 (2000).

[35] A. Fedotov, A. Zheltikov, L. Melnikov, V. Beloglazov, and Y. Skibina, "Tuning the photonic band gap of sub-500 nm pitch holey fibers in 930-1030 nm range," Laser Physics **10,** 1086 (2000).

[36] P. Mach, M. Dolinski, K. W. Baldwin, J. A. Rogers, C. Kerbage, R. S. Windeler, and B. J. Eggleton, "Tunable microfluidic optical fiber," Applied Physics Letters **80,** 4294 (2002).

[37] C. Kerbage, P. Steinvurzel, P. Reyes, P. S. Westbrook, R. S. Windeler, A. Hale, and B. J. Eggleton, "Highly tunable birefringent microstructured optical fiber," Optics Letters **27,** 842 (2002).

[38] R. Zhang, J. Teipel, and H. Giessen, "Theoretical design of a

liquid-core photonic crystal fiber for supercontinuum generation," Optics Express **14,** 6800 (2006).

[39] L. Xiao, W. Jin, M. S. Demokan, H. L. Ho, Y. L. Hoo, and C. Zhao, "Fabrication of selective injection microstructured optical fibers with a conventional fusion splicer," Optics Express **13,** 9014 (2005).

[40] A. Witkowska, K. Lai, S. G. Leon-Saval, W. J. Wadsworth, and T. A. Birks, "All-fiber anamorphic core-shape transitions," Optics Letters **31,** 2672 (2006).

[41] S. Maruo, O. Nakamura, and S. Kawata, "Three-dimensional microfabrication with two-photon-absorbed photopolymerization," Optics Letters **22,** 132 (1997).

[42] J. H. Strickler and W. W. Webb, "Three-dimensional optical data storage in refractive media by two-photon point excitation," Optics Letters **16,** 1780 (1991).

[43] D. A. Parthenopoulos and P. M. Rentzepis, "Three-Dimensional Optical Storage Memory," Science **245,** 843 (1989).

[44] D. N. Christodoulides and R. I. Joseph, "Discrete self-focusing in nonlinear arrays of coupled waveguides," Optics Letters **13,** 794 (1988).

[45] D. N. Christodoulides, F. Lederer, and Y. Silberberg, "Discretizing light behaviour in linear and nonlinear waveguide lattices," Nature **424,** 817 (2003).

[46] H. S. Eisenberg and Y. Silberberg, "Diffraction Management," Physical Review Letters **85,** 1863 (2000).

[47] T. Pertsch, T. Zentgraf, U. Peschel, A. Bräuer, and F. Lederer, "Anomalous Refraction and Diffraction in Discrete Optical Systems," Physical Review Letters **88,** 93901 (2002).

[48] H. S. Eisenberg and Y. Silberberg, "Discrete Spatial Optical Solitons in Waveguide Arrays," Physical Review Letters **81,** 3383 (1998).

[49] G. I. A. Stegeman, D. N. Christodoulides, and M. Segev, "Optical Spatial Solitons : Historical Perspectives," IEEE Journal of Selected Topics in Quantum Electronics **6,** 1419 (2000).

[50] G. I. Stegeman, "Optical Spatial Solitons and Their Interactions: Universality and Diversity," Science **286,** 1518 (1999).

[51] A. A. Sukhorukov, Y. S. Kivshar, H. S. Eisenberg, and Y. Silberberg, "Spatial Optical Solitons in Waveguide Arrays," Quantum **39,** 31 (2003).

[52] T. Pertsch, T. Zentgraf, U. Peschel, A. Bräuer, and F. Lederer, "Beam steering in waveguide arrays," Applied Physics Letters **80,** 3247 (2002).

[53] T. Pertsch, P. Dannberg, W. Elflein, A. Bräuer, and F. Lederer, "Optical Bloch Oscillations in Temperature Tuned Waveguide Arrays," Physical Review Letters **83,** 4752 (1999).

[54] U. Peschel, T. Pertsch, and F. Lederer, "Optical Bloch oscillations in waveguide arrays," Optics Letters **23,** 1701 (1998).

[55] D. Christodoulides and E. Eugenieva, "Blocking and Routing Discrete Solitons in Two-Dimensional Networks of Nonlinear Waveguide Arrays," Physical Review Letters **87,** 233901 (2001).

[56] P. D. Rasmussen, F. H. Bennet, D. N. Neshev, A. A. Sukhorukov, C. R. Rosberg, W. Krolikowski, O. Bang, and Y. S. Kivshar, "Observation of two-dimensional nonlocal gap solitons," Optics Letters **34,** 295 (2009).

[57] P. D. Rasmussen, A. S. Sukhorukov, D. N. Neshev, W. Krolikowski, O. Bang, J. Lægsgaard, and Y. S. Kivshar, "Spatiotemporal control of light by Bloch-mode dispersion in multi-core fibers," Optics Express **16,** 5878 (2008).

[58] C. R. Rosberg, F. H. Bennet, D. N. Neshev, P. D. Rasmussen, O. Bang, W. Krolikowski, A. Bjarklev, and Y. S. Kivshar, "Tunable diffraction and self-defocusing in liquid-filled photonic crystal fibers.," Optics Express **15,** 12145 (2007).

[59] Y. Silberberg, "Collapse of optical pulses," Optics Letters **15,** 1282 (1990).

[60] S. Minardi *et al.*, "Three-Dimensional Light Bullets in Arrays of Waveguides," Physical Review Letters **105,** 263901 (2010).

[61] F. Ye, Y. V. Kartashov, B. Hu, and L. Torner, "Light bullets in Bessel optical lattices with spatially modulated nonlinearity," Optics

Express **17,** 11328 (2009).

[62] R. W. Boyd, *Nonlinear Optics* (Academic, San Diego, Calif., 2003).

[63] A. B. Fallahkhair, K. S. Li, and T. E. Murphy, "Vector Finite Difference Modesolver for Anisotropic Dielectric Waveguides," Journal of Lightwave Technology **26,** 1423 (2008).

[64] J. Crank and P. Nicolson, "A practical method for numerical evaluation of solutions of partial differential equations of the heat-conduction type," Advances in Computational Mathematics **6,** 207 (1996).

[65] M. Szpulak, W. Urbanczyk, E. Serebryannikov, A. M. Zheltikov, A. Hochman, Y. Leviatan, R. Kotynski, and K. Panajotov, "Comparison of different methods for rigorous modeling of photonic crystal fibers," Optics Express **14,** 5699 (2006).

[66] K. Saitoh and M. Koshiba, "Numerical modeling of photonic crystal fibers," Journal of Lightwave Technology **23,** 3580 (2005).

[67] P. S. J. Russell, "Photonic-Crystal Fibers," Journal of Lightwave Technology **24,** 4729 (2006).

[68] D. W. Garvey *et al.*, "Single-mode nonlinear-optical polymer fibers," Journal of the Optical Society of America B **13,** 2017 (1996).

[69] A. Argyros, F. M. Cox, and M. C. J. Large, "Liquid-filled hollow core microstructured polymer optical fiber," Optics Express **14,** 4135 (2006).

[70] M. Liao, C. Chaudhari, G. Qin, X. Yan, T. Suzuki, and Y. Ohishi, "Tellurite microstructure fibers with small hexagonal core for supercontinuum generation," Optics Express **17,** 12174 (2009).

[71] H. Hundertmark, S. Rammler, T. Wilken, R. Holzwarth, T. W. Hänsch, and P. S. Russell, "Octave-spanning supercontinuum generated in SF6-glass PCF by a 1060 nm mode-locked fibre laser delivering 20 pJ per pulse," Optics Express **17,** 1919 (2009).

[72] F. Luan, A. K. George, T. D. Hedley, G. J. Pearce, D. M. Bird, J. C. Knight, and P. S. J. Russell, "All-solid photonic bandgap fiber," Optics Letters **29,** 2369 (2004).

[73] T. A. Birks, J. C. Knight, D. Mogilevtsev, P. S. J. Russell, P. J.

Roberts, J. Broeng, J. A. West, D. C. Allan, and J. C. Fajardo, *OFC/IOOC . Technical Digest. Optical Fiber Communication Conference, 1999, and the International Conference on Integrated Optics and Optical Fiber Communication* (IEEE, 1999), Vol. 4, pp. 114–116.

[74] M. Koshiba and K. Saitoh, "Applicability of classical optical fiber theories to holey fibers.," Optics Letters **29,** 1739 (2004).

[75] M. P. Singh, M. Midrio, and C. G. Someda, "The space filling mode of holey fibers: an analytical vectorial solution," Journal of Lightwave Technology **18,** 1031 (2000).

[76] Y. Li, C. Wang, and M. Hu, "A fully vectorial effective index method for photonic crystal fibers: application to dispersion calculation," Optics Communications **238,** 29 (2004).

[77] Y. Li, Y. Yao, M. Hu, L. Chai, and C. Wang, "Improved fully vectorial effective index method for photonic crystal fibers: evaluation and enhancement," Applied Optics **47,** 399 (2008).

[78] N. A. Mortensen, J. R. Folkenberg, M. D. Nielsen, and K. P. Hansen, "Modal cutoff and the V parameter in photonic crystal fibers," Optics Letters **28,** 1879 (2003).

[79] M. Koshiba and K. Saitoh, "Structural dependence of effective area and mode field diameter for holey fibers," Optics Express **11,** 1746 (2003).

[80] A. W. Snyder and W. R. Young, "Modes of optical waveguides," Journal of the Optical Society of America **68,** 297 (1978).

[81] D. Marcuse, "Gaussian approximation of the fundamental modes of graded-index fibers," Journal of the Optical Society of America **68,** 103 (1978).

[82] K. Itoh, Y. Toda, R. Morita, and M. Yamashita, "Coherent Optical Control of Molecular Motion Using Polarized Sequential Pulses," Japanese Journal of Applied Physics **43,** 6448 (2004).

[83] I. A. Heisler, R. R. B. Correia, T. Buckup, S. L. S. Cunha, and N. P. da Silveira, "Time-resolved optical Kerr-effect investigation on CS_2/polystyrene mixtures," The Journal of Chemical Physics **123,** 054509 (2005).

[84] P. Wiewior and C. Radzewicz, "Dynamics of molecular liquids

studied by femtosecond optical Kerr effect," Optica Applicata **30,** 103 (2000).

[85] S. Pricking, PhD Thesis, University of Stuttgart, 2011.

[86] J. Herrmann, U. Griebner, N. Zhavoronkov, A. Husakou, D. Nickel, J. C. Knight, W. J. Wadsworth, P. S. J. Russell, and G. Korn, "Experimental Evidence for Supercontinuum Generation by Fission of Higher-Order Solitons in Photonic Fibers," Physical Review Letters **88,** 173901 (2002).

[87] N. Akhmediev and M. Karlsson, "Cherenkov radiation emitted by solitons in optical fibers," Physical Review A **51,** 2602 (1995).

[88] R. Trebino, K. W. DeLong, D. N. Fittinghoff, J. N. Sweetser, M. A. Krumbügel, B. A. Richman, and D. J. Kane, "Measuring ultrashort laser pulses in the time-frequency domain using frequency-resolved optical gating," Review of Scientific Instruments **68,** 3277 (1997).

[89] S. Linden, H. Giessen, and J. Kuhl, "XFROG – A New Method for Amplitude and Phase Characterization of Weak Ultrashort Pulses," Physica Status Solidi B **206,** 119 (1998).

[90] R. Hellwarth, "Third-order optical susceptibilities of liquids and solids," Progress in Quantum Electronics **5,** 1 (1979).

[91] R. Hellwarth, "Origin of the Nonlinear Refractive Index of Liquid CCl_4," Physical Review A **30,** 2342 (1971).

[92] K. Blow and D. Wood, "Theoretical description of transient stimulated Raman scattering in optical fibers," IEEE Journal of Quantum Electronics **25,** 2665 (1989).

[93] R. L. Sutherland, *Handbook of Nonlinear Optics* (Marcel Dekker Inc., New York, 2003), pp. 350–355.

[94] Y. Shen, *The Principles of Nonlinear Optics* (Wiley & Sons, New York, 1984).

[95] D. McMorrow, W. T. Lotshaw, and G. A. Kenney-Wallace, "Femtosecond optical Kerr studies on the origin of the nonlinear responses in simple liquids," IEEE Journal of Quantum Electronics **24,** 443 (1988).

[96] B. F. Levine and C. G. Bethea, "Second and third order hyper-

polarizabilities of organic molecules," The Journal of Chemical Physics **63,** 2666 (1975).

[97] G. S. He and P. N. Prasad, "Stimulated Kerr scattering and reorientation work of molecules in liquid CS_2," Physical Review A **41,** 2687 (1990).

[98] F. Kajzar and J. Messier, "Third-harmonic generation in liquids," Physical Review A **32,** 2352 (1985).

[99] S. Pricking and H. Giessen, "Generalized retarded response of nonlinear media and its influence on soliton dynamics," Optics Express **19,** 2895 (2011).

[100] S. Somekh, E. Garmire, A. Yariv, H. L. Garvin, and R. G. Hunsperger, "Channel Optical Waveguides and Directional Couplers in GaAs - lmbedded and Ridged," Applied Optics **13,** 327 (1974).

[101] S. Somekh, E. Garmire, A. Yariv, H. Garvin, and R. Hunsperger, "Channel optical waveguide directional couplers," Applied Physics Letters **22,** 46 (1973).

[102] A. Hardy and W. Streifer, "Coupled mode theory of parallel waveguides," Journal of Lightwave Technology **3,** 1135 (1985).

[103] A. Snyder, "Coupled-Mode Theory for Optical Fibers," Journal of the Optical Society of America **62,** 1267 (1972).

[104] A. Yariv, "Coupled-Mode Theory for Guided-Wave Optics," IEEE Journal of Quantum Electronics **QE-9,** 919 (1973).

[105] H. Haus and W. Huang, "Coupled-mode theory," Proceedings of the IEEE **79,** 1505 (1991).

[106] C. Vassallo, "About coupled-mode theories for dielectric waveguides," Journal of Lightwave Technology **6,** 294 (1988).

[107] S. M. Jensen, "The nonlinear coherent coupler," IEEE Journal of Quantum Electronics **18,** 1580 (1982).

[108] S. Trillo, S. Wabnitz, E. M. Wright, and G. I. Stegeman, "Soliton switching in fiber nonlinear directional couplers," Optics Letters **13,** 672 (1988).

[109] S. R. Friberg, Y. Silberberg, M. K. Oliver, M. J. Andrejco, M. A. Saifi, and P. W. Smith, "Ultrafast all-optical switching in a dual-core fiber nonlinear coupler," Applied Physics Letters **51,** 1135

(1987).

[110] S. R. Friberg, A. M. Weiner, Y. Silberberg, B. G. Sfez, and P. S. Smith, "Femotosecond switching in a dual-core-fiber nonlinear coupler," Optics Letters **13,** 904 (1988).

[111] Y. Silberberg and G. I. Stegeman, "Nonlinear coupling of waveguide modes," Applied Physics Letters **50,** 801 (1987).

[112] H. Haus and L. Molter-Orr, "Coupled multiple waveguide systems," IEEE Journal of Quantum Electronics **19,** 840 (1983).

[113] D. Marcuse, *Theory of Dielectric Optical Waveguides (Optics and Photonics Series)* (Academic, San Diego, Calif., 1991).

[114] K. Okamoto, *Fundamentals of Optical Waveguides* (Academic, San Diego, Calif., 2006).

[115] G. P. Agrawal, *Lightwave Technology* (Wiley & Sons, New York, 2004).

[116] *Handbook of Mathematical Functions*, 2 ed., M. Abramowitz and I. A. Stegun, eds., (National Bureau of Standards, Washington, D.C., 1971).

[117] F. H. Bennet and M. I. Molina, "Nonlinear light localization around the core of a 'holey' fiber," arXiv:1103.3162v1 (2011).

[118] Y. Wang and W. Wang, "Nonlinear optical pulse coupling dynamics," Journal of Lightwave Technology **24,** 2458 (2006).

[119] W. Krolikowski, U. Trutschel, M. Cronin-Golomb, and C. Schmidt-Hattenberger, "Solitonlike optical switching in a circular fiber array," Optics Letters **19,** 320 (1994).

[120] M. Romagnoli, S. Trillo, and S. Wabnitz, "Soliton switching in nonlinear couplers," Optical and Quantum Electronics **24,** 1237 (1992).

[121] Y. Wang and W. Wang, "Study of ultrafast pulse coupling dynamics considering retarded nonlinear response and self-steepening effects," Journal of Lightwave Technology **24,** 1041 (2006).

[122] C. Guan, L. Yuan, Q. Dai, and F. Tian, "Supermodes Analysis for Linear-Core-Array Microstructured Fiber," Journal of Lightwave Technology **27,** 1741 (2009).

[123] C. Guan and L. Yuan, *2009 Symposium on Photonics and Optoelec-*

tronics (IEEE eXpress Conference Publishing, 2009).

[124] N. Kishi, E. Yamashita, and H. Kawabata, "Modal and coupling-field analysis of optical fibers with linearly distributed multiple cores," Journal of Lightwave Technology **7,** 902 (1989).

[125] N. Kishi and E. Yamashita, "A simple coupled-mode analysis method for multiple-core optical fiber and coupled dielectric waveguide structures," IEEE Transactions on Microwave Theory and Techniques **36,** 1861 (1988).

[126] R. Morandotti, H. Eisenberg, Y. Silberberg, M. Sorel, and J. Aitchison, "Self-Focusing and Defocusing in Waveguide Arrays," Physical Review Letters **86,** 3296 (2001).

[127] P. G. Kevrekidis, *The Discrete Nonlinear Schrödinger Equation*, Vol. 232 of *Springer Tracts in Modern Physics* (Springer, Berlin, Heidelberg, 2009).

[128] P. G. Kevrekidis, K. O. Rasmussen, and A. R. Bishop, "The discrete nonlinear Schrödinger equation: A survey of recent results," Journal of Modern Physics B **15,** 2833 (2001).

[129] F. Lederer, G. I. Stegeman, D. N. Christodoulides, G. Assanto, M. Segev, and Y. Silberberg, "Discrete solitons in optics," Physics Reports **463,** 1 (2008).

[130] Y. V. Kartashov, B. A. Malomed, V. A. Vysloukh, and L. Torner, "Two-dimensional solitons in nonlinear lattices," Optics Letters **34,** 770 (2009).

[131] R. Fischer, D. Träger, D. N. Neshev, A. A. Sukhorukov, W. Krolikowski, C. Denz, and Y. S. Kivshar, "Reduced-Symmetry Two-Dimensional Solitons in Photonic Lattices," Physical Review Letters **96,** 23905 (2006).

[132] F. Eilenberger, A. Szameit, and T. Pertsch, "Transition from discrete to continuous Townes solitons in periodic media," Physical Review A **82,** 43802 (2010).

[133] A. Ferrando, M. Zacares, P. F. De Cordoba, D. Binosi, and J. Monsoriu, "Spatial soliton formation in photonic crystal fibers," Optics Express **11,** 452 (2003).

[134] J. W. Fleischer, M. Segev, N. K. Efremidis, and D. N.

Christodoulides, "Observation of two-dimensional discrete solitons in optically induced nonlinear photonic lattices," Nature **422,** 147 (2003).

[135] R. Zhang, PhD Thesis, University of Stuttgart, 2006.

[136] R. Zhang, X. Zhang, D. Meiser, and H. Giessen, "Mode and group velocity dispersion evolution in the tapered region of a single-mode tapered fiber," Optics Express **12,** 5840 (2004).

[137] NKT Photonics, http://www.nktphotonics.com/files/files/NL-23-790.pdf.

[138] T. P. White, R. C. McPhedran, C. M. de Sterke, L. C. Botten, and M. J. Steel, "Confinement losses in microstructured optical fibers," Optics Letters **26,** 1660 (2001).

[139] NKT Photonics, http://www.nktphotonics.com/files/files/LMA-8-111222.pdf.

[140] M. J. Weber, *Handbook of Optical Materials* (CRC, Boca Raton, Florida, 2003).

[141] P. P. Ho and R. R. Alfano, "Optical Kerr effect in liquids," Physical Review A **20,** 2170 (1979).

[142] J. Ellis, "The Near Infra-Red Absorption Spectra of Some Organic Liquids," Physical Review **23,** 48 (1924).

[143] P. Brocos, A. Piñeiro, R. Bravo, and A. Amigo, "Refractive indices, molar volumes and molar refractions of binary liquid mixtures: concepts and correlations," Physical Chemistry Chemical Physics **5,** 550 (2003).

[144] W. Heller, "Remarks on refractive index mixture rules," The Journal of Physical Chemistry **69,** 1123 (1965).

[145] G. M. Hale and M. R. Querry, "Optical Constants of Water in the 200 nm to 200 μm Wavelength Region," Applied Optics **12,** 555 (1973).

[146] J. Rheims, J. Köser, and T. Wriedt, "Refractive-index measurements in the near-IR using an Abbe refractometer," Measeasurement Science and Technology **8,** 601 (1997).

[147] A. Samoc, "Dispersion of refractive properties of solvents: Chloroform, toluene, benzene, and carbon disulfide in ultraviolet,

visible, and near-infrared," Journal of Applied Physics **94,** 6167 (2003).

[148] S. Couris, "An experimental investigation of the nonlinear refractive index (n_2) of carbon disulfide and toluene by spectral shearing interferometry and z-scan techniques," Chemical Physics Letters **369,** 318 (2003).

[149] H. H. Marvin, "The Selective Transmission and the Dispersion of the Liquid Chlorides," Physical Review **34,** 161 (1912).

[150] S. Ghosal, J. Ebert, and S. Self, "The infrared refractive indices of $CHBr_3$, CCl_4 and CS_2," Infrared Physics **34,** 621 (1993).

[151] I. H. Malitson, "Interspecimen Comparison of the Refractive Index of Fused Silica," Journal of the Optical Society of America **55,** 1205 (1965).

[152] W. L. Smith, in *Handbook of Laser Science and Technology*, M. J. Weber, ed., (CRC, Boca Raton, Florida, 1986), Vol. 3, pp. 259–281.

[153] M. Vieweg, Diploma Thesis, University of Bonn, 2008.

[154] T. Gissibl, Diploma Thesis, University of Stuttgart, 2010.

[155] A. Fuerbach, P. Steinvurzel, J. A. Bolger, A. Nulsen, and B. J. Eggleton, "Nonlinear propagation effects in antiresonant high-index inclusion photonic crystal fibers," Optics Letters **30,** 830 (2005).

[156] P. Domachuk, H. Nguyen, and B. Eggleton, "Transverse Probed Microfluidic Switchable Photonic Crystal Fiber Devices," IEEE Photonics Technology Letters **16,** 1900 (2004).

[157] B. T. Kuhlmey, B. J. Eggleton, and D. K. C. Wu, "Fluid-Filled Solid-Core Photonic Bandgap Fibers," Lightwave **27,** 1617 (2009).

[158] J. S. Y. Chen, T. G. Euser, N. J. Farrer, P. J. Sadler, M. Scharrer, and P. S. J. Russell, "Photochemistry in photonic crystal fiber nanoreactors," Chemistry **16,** 5607 (2010).

[159] F. H. Bennet, I. A. Amuli, A. A. Sukhorukov, W. Krolikowski, D. N. Neshev, and Y. S. Kivshar, "Focusing-to-defocusing crossover in nonlinear periodic structures," Optics Letters **35,** 3213 (2010).

[160] Y. Wang, S. Liu, X. Tan, and W. Jin, "Selective-Fluid-Filling Technique of Microstructured Optical Fibers," Journal of Lightwave

Technology **28,** 3193 (2010).

[161] C. M. B. Cordeiro, E. M. dos Santos, C. H. Brito Cruz, C. J. de Matos, and D. S. Ferreiira, "Lateral access to the holes of photonic crystal fibers - selective filling and sensing applications," Optics Express **14,** 8403 (2006).

[162] W. H. Teh, U. Dürig, U. Drechsler, C. G. Smith, and H.-J. Güntherodt, "Effect of low numerical-aperture femtosecond two-photon absorption on (SU-8) resist for ultrahigh-aspect-ratio microstereolithography," Journal of Applied Physics **97,** 054907 (2005).

[163] T. Ergin, N. Stenger, P. Brenner, J. B. Pendry, and M. Wegener, "Three-dimensional invisibility cloak at optical wavelengths," Science **328,** 337 (2010).

[164] J. K. Gansel, M. Thiel, M. S. Rill, M. Decker, K. Bade, V. Saile, G. von Freymann, S. Linden, and M. Wegener, "Gold helix photonic metamaterial as broadband circular polarizer," Science **325,** 1513 (2009).

[165] Coherent Inc., http://www.coherent.com/products/?1852/Verdi-V-Series.

[166] Newport Corporation, http://www.newport.com/Tsunami-Ultrafast-Lasers/368126/1033/info.aspx.

[167] Microchemicals, http://www.microchem.com/pdf/SU-82000DataSheet2000_5thru2015Ver4.pdf.

[168] D. K. C. Wu, Diploma Thesis, University of Sydney, Australia, 2007.

[169] K. Nielsen, D. Noordegraaf, T. Sørensen, A. Bjarklev, and T. P. Hansen, "Selective filling of photonic crystal fibres," Journal of Optics A: Pure and Applied Optics **7,** L13 (2005).

[170] J. Ju, H. F. Xuan, W. Jin, S. Liu, and H. L. Ho, "Selective opening of airholes in photonic crystal fiber," Optics Letters **35,** 3886 (2010).

[171] Y. Wang, C. R. Liao, and D. N. Wang, "Femtosecond laser-assisted selective infiltration of microstructured optical fibers," Optics Express **18,** 18056 (2010).

[172] J. R. Sparks, J. L. Esbenshade, R. He, N. Healy, T. D. Day, D. W.

Keefer, P. J. A. Sazio, A. C. Peacock, and J. V. Badding, "Selective semiconductor filling of microstructured optical fibers," Journal of Lightwave Technology **29,** 2005 (2011).

[173] F. Wang, W. Yuan, O. Hansen, and O. Bang, "Selective filling of photonic crystal fibers using focused ion beam milled microchannels," Optics Express **19,** 17585 (2011).

[174] F. Benabid, J. C. Knight, G. Antonopoulos, and P. S. J. Russell, "Stimulated Raman scattering in hydrogen-filled hollow-core photonic crystal fiber," Science **298,** 399 (2002).

[175] J. C. Travers, W. Chang, J. Nold, N. Y. Joly, and P. St. J. Russell, "Ultrafast nonlinear optics in gas-filled hollow-core photonic crystal fibers [Invited]," Journal of the Optical Society of America B **28,** A11 (2011).

[176] P. J. A. Sazio *et al.*, "Microstructured optical fibers as high-pressure microfluidic reactors," Science **311,** 1583 (2006).

[177] T. Larsen, A. Bjarklev, D. S. Hermann, and J. Broeng, "Optical devices based on liquid crystal photonic bandgap fibres," Optics Express **11,** 2589 (2003).

[178] T. T. Alkeskjold, J. Lægsgaard, A. Bjarklev, D. S. Hermann, A. Anawati, J. Broeng, J. Li, and S.-T. Wu, "All-optical modulation in dye-doped nematic liquid crystal photonic bandgap fibers," Optics Express **12,** 5857 (2004).

[179] F. Hoos, S. Pricking, and H. Giessen, "Compact portable 20 MHz solid-state femtosecond whitelight-laser," Optics Express **14,** 10913 (2006).

[180] F. Hoos, S. Li, T. P. Meyrath, B. Braun, and H. Giessen, "Thermal lensing in an end-pumped Yb:KGW slab laser with high power single emitter diodes," Optics Express **16,** 6041 (2008).

[181] Elliot Scientific Ltd., http://www.elliotscientific.com/171-1-207-270/Elliot-Gold\%E2\%84\%A2-Series-Fibre-Launch-System-with-High-Precision-Adjusters/.

[182] F. Dai, Y. Xu, and X. Chen, "Enhanced and broadened SRS spectra of toluene mixed with chloroform in liquid-core fiber," Optics Express **17,** 19882 (2009).

[183] J. Bethge, A. Husakou, F. M. Mitschke, F. Noack, U. Griebner, G. Steinmeyer, and J. Herrmann, "Two-octave supercontinuum generation in a water-filled photonic crystal fiber," Optics Express **18,** 6230 (2010).

[184] A. Bozolan, C. J. de Matos, C. M. B. Cordeiro, E. M. dos Santos, and J. Travers, "Supercontinuum generation in a water-core photonic crystal fiber," Optics Express **16,** 9671 (2008).

[185] K. Porsezian and R. Vasantha Jayakantha Raja, "Soliton-induced supercontinuum generation in liquid-filled photonic crystal fibre," Pramana **77,** 1 (2011).

[186] H. Zhang, S. Chang, J. Yuan, and D. Huang, "Supercontinuum generation in chloroform-filled photonic crystal fibers," Optik - International Journal for Light and Electron Optics **121,** 783 (2010).

[187] R. Vasantha Jayakantha Raja, A. Husakou, J. Hermann, and K. Porsezian, "Supercontinuum generation in liquid-filled photonic crystal fiber with slow nonlinear response," Journal of the Optical Society of America B **27,** 1763 (2010).

[188] C. Conti, M. Schmidt, P. Russell, and F. Biancalana, "Highly Noninstantaneous Solitons in Liquid-Core Photonic Crystal Fibers," Physical Review Letters **105,** 263902 (2010).

[189] A. A. Voronin, V. P. Mitrokhin, A. A. Ivanov, A. B. Fedotov, D. A. Sidorov-Biryukov, V. I. Beloglazov, M. V. Alfimov, H. Ludvigsen, and A. M. Zheltikov, "Understanding the nonlinear-optical response of a liquid-core photonic-crystal fiber," Laser Physics Letters **7,** 46 (2010).

[190] H. W. Lee, M. A. Schmidt, P. Uebel, H. Tyagi, N. Y. Joly, M. Scharrer, and P. S. J. Russell, "Optofluidic refractive-index sensor in step-index fiber with parallel hollow micro-channel," Optics Express **19,** 8200 (2011).

[191] N. A. Mortensen, J. R. Folken, P. M. W. Skovgaard, and J. Broeng, "Numerical aperture of single-mode photonic crystal fibers," IEEE Photonics Technology Letters **14,** 1094 (2002).

[192] M. Nielsen and N. A. Mortensen, "Photonic crystal fiber design based on the V-parameter," Optics Express **11,** 2762 (2003).

[193] D. K. C. Wu, B. T. Kuhlmey, and B. J. Eggleton, "Ultrasensitive photonic crystal fiber refractive index sensor," Optics Letters **34,** 322 (2009).

[194] J. Lægsgaard, "Directional coupling in twin-core photonic bandgap fibers," Optics Letters **30,** 3281 (2005).

[195] Z. Wang, T. Taru, T. A. Birks, J. C. Knight, Y. Liu, and J. Du, "Coupling in dual-core photonic bandgap fibers: theory and experiment," Optics Express **15,** 4795 (2007).

[196] P. Di Bin and N. Mothe, "Numerical analysis of directional coupling in dual-core microstructured optical fibers," Optics Express **17,** 15778 (2009).

[197] A. W. Snyder and D. R. Rowland, "Low power fibre coupler devices: few- versus many-period operation," Optical and Quantum Electronics **24,** 31 (1992).

[198] S.-H. Gong and A. Penzkofer, "Two-photon absorption and two-photon induced absorption of liquid toluene at 347.15 nm," Optical and Quantum Electronics **31,** 1145 (1999).

[199] N. Kishi, E. Yamashita, and K. Atsuki, "Modal and coupling field analysis of optical fibers with circularly distributed multiple cores and a central core," Journal of Lightwave Technology **4,** 991 (1986).

[200] N. Finlayson and G. I. Stegeman, "Spatial switching, instabilities, and chaos in a three-waveguide nonlinear directional coupler," Applied Physics Letters **56,** 2276 (1990).

[201] C. Schmidt-Hattenberger, U. Trutschel, and F. Lederer, "Nonlinear switching in multiple-core couplers," Optics Letters **16,** 294 (1991).

[202] C. Schmidt-Hattenberger, R. Muschall, U. Trutschel, and F. Lederer, "Nonlinear eigenmodes of a three-core fibre coupler," Optical and Quantum Electronics **24,** 691 (1992).

[203] A. C. Scott and L. Macneil, "Binding energy versus nonlinearity for a "small" stationary soliton," Physics Letters **98,** 87 (1983).

[204] A. B. Aceves, C. De Angelis, S. Trillo, and S. Wabnitz, "Storage and steering of self-trapped discrete solitons in nonlinear waveguide arrays," Optics Letters **19,** 332 (1994).

[205] Y. S. Kivshar, "Self-localization in arrays of defocusing waveguides," Optics Letters **18,** 1147 (1993).

[206] P. Millar, J. S. Aitchison, J. U. Kang, G. I. Stegeman, A. Villeneuve, G. T. Kennedy, and W. Sibbett, "Nonlinear waveguide arrays in AlGaAs," Journal of the Optical Society of America B **14,** 3224 (1997).

[207] D. Psaltis, S. R. Quake, and C. Yang, "Developing optofluidic technology through the fusion of microfluidics and optics," Nature **442,** 381 (2006).

[208] C. Monat, P. Domachuk, and B. J. Eggleton, "Integrated optofluidics: A new river of light," Nature Photonics **1,** 106 (2007).

[209] B. A. Malomed, D. Mihalache, F. Wise, and L. Torner, "Spatiotemporal optical solitons," Journal of Optics B: Quantum and Semiclassical Optics **7,** R53 (2005).

[210] Y. Kartashov, B. Malomed, and L. Torner, "Solitons in nonlinear lattices," Review of Modern Physics **83,** 247 (2011).

[211] D. Leykam and A. S. Desyatnikov, "Discrete multivortex solitons," Optics Letters **36,** 4806 (2011).

[212] V. E. Lobanov, O. V. Borovkova, Y. V. Kartashov, B. A. Malomed, and L. Torner, "Stable brigth and vortex solitons in photonic crystal fibers with inhomognenous defocusing nonlinearity," Optics Letters, in preparation (2012).

[213] J. R. Salgueiro, Y. S. Kivshar, D. E. Pelinovsky, V. Simon, and H. Michinel, "Spatial Vector Solitons in Nonlinear Photonic Crystal Fibers," Studies in Applied Mathematics **115,** 157 (2005).

[214] H. W. Lee, M. A. Schmidt, H. K. Tyagi, L. P. Sempere, and P. S. J. Russell, "Polarization-dependent coupling to plasmon modes on submicron gold wire in photonic crystal fiber," Applied Physics Letters **93,** 111102 (2008).

[215] M. A. Schmidt, L. N. Prill Sempere, H. K. Tyagi, C. G. Poulton, and P. S. J. Russell, "Waveguiding and plasmon resonances in two-dimensional photonic lattices of gold and silver nanowires," Physical Review B **77,** 13 (2008).

[216] A. M. Stolyarov, L. Wei, O. Shapira, F. Sorin, S. L. Chua, J. D.

Joannopoulos, and Y. Fink, "Microfluidic directional emission control of an azimuthally polarized radial fibre laser," Nature Photonics **6,** 229 (2012).

[217] S. Ghosh, A. R. Bhagwat, C. K. Renshaw, S. Goh, A. L. Gaeta, and B. J. Kirby, "Low-Light-Level Optical Interactions with Rubidium Vapor in a Photonic Band-Gap Fiber," Physical Review Letters **97,** 23603 (2006).

[218] P. Londero, V. Venkataraman, A. R. Bhagwat, A. D. Slepkov, and A. L. Gaeta, "Ultralow-Power Four-Wave Mixing with Rb in a Hollow-Core Photonic Band-Gap Fiber," Physical Review Letters **103,** 43602 (2009).

[219] S. Kedenburg, Bachelor Thesis, University of Stuttgart, 2011.

Acknowledgements

Experimental physics is a team sport. This thesis would be impossible without other people. Therefore at the end of my thesis I want thank all these people, who supported me during my time as a Ph.D. student and gave me help and advices.

- Thanks to Prof. Dr. Giessen for giving me the opportunity to work in his group and in the field of nonlinear optics. I especially appreciated the opportunity for the self dependent research and work. Nevertheless, he always gave me the help and advices to follow the emerging ideas and to bring me forward.
- Thanks to Prof. Dr. Graf for being the second corrector of my thesis.
- Thanks to my work colleagues of the laser part of the group for valuable discussions, hints, ideas and always the willingness to help. Here I especially have to thank my former diploma student Timo Gissibl, my office mate Bernd Metzger, our post-doc Andy Steinmann, and Sebastian Pricking.
- Thanks to Mario Hentschel and Daniel Drégely for being my sports colleagues for swimming, hiking, cycling and running as stress-balance with discussions about physics and everything beyond. It was always a a lot of fun and support.
- Thanks to all current and former members of the 4th Physics Institute for many shared hours of work in the lab and in the office, and in valuable discussion about physics. Apart from science, I also enjoyed the time in the Kaffeeecke with cookies and all kinds of after-work activities. It was a nice and very good atmosphere.
- Thanks to my parents and my family who helped me throughout my studies and research wherever they could.
- Thanks to my girlfriend and fiancée Laura Sophie Kunz who has

accompanied and supported me during my time in Stuttgart and with whom I could share all the highs and lows of my Ph.D.

Curriculum Vitae

Personal Data

Name:	Marius Vieweg
Date of birth:	September 28th, 1983
Place of birth:	Siegburg
Citizenship:	Germany
Email address:	m.vieweg@physik.uni-stuttgart.de
Current institute:	4th Physics Institute, University of Stuttgart, Germany

School

1994 – 2003	Visit of the Collegium Josephinum Bonn
2003	Abitur (major subjects: Physics, Mathematics, German, History)

Academic Studies

10.2003 – 12.2008	Rheinische Friedrich-Wilhelms-Universität Bonn Diplomstudiengang Physik
12.2007	Vordiplom, minor subject: Chemistry
12.2007 – 12.2008	Diploma thesis in Physics at the University of Bonn externally at the 4th Physics Institute, University of Stuttgart Supervisor: Prof. Dr. Harald Giessen
12.2008	Diploma degree, minor subject: Geophysics
01.2009 – present	Ph.D. student at the 4th Physics Institute, University of Stuttgart Supervisor: Prof. Dr. Harald Giessen

Teaching

2008	Organization of the Tutorium Kernphysik
2009	Tutor for Umweltphysik
2010	Tutor for Umweltphysik
2010	Tutor for Experimental Physics I (Mechanics)
2011	Tutor for Experimental Physics II (Thermodynamics)
2011	Tutor for Experimental Physics III (Optics)